Institute of Ion Beam Physics and Materials Research

Annual Report 1998

FORSCHUNGSZENTRUM ROSSENDORF FZR
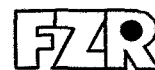
Annual Report 1998

Institut für Ionenstrahlphysik und Materialforschung

For further information on the research projects described in the present annual report, please address the director or one of the authors at the institute.

Front cover:
Non-destructive composition analysis of ceramic art objects at the Rossendorf external proton beam. The figure shows a tankard made from Böttger stoneware together with the corresponding PIXE spectrum of main elements. See p. 11.

Director: Prof. Dr. Wolfhard Möller

P. O. B. 51 01 19
D-01314 Dresden
Germany

Tel.: +49 351 260 2245
Fax: +49 351 260 3285
E-mail: w.moeller@fz-rossendorf.de

Preface

The Research Center Rossendorf (Forschungszentrum Rossendorf, FZR) represents the largest governmental research institution in the "new" states of the Federal Republic of Germany. Its presently about 600 employees, organized in five institutes, study problems of basic and applied science in the fields of materials science, biomedical and environmental research, and nuclear physics. The FZR is a member of the "Gottfried Wilhelm Leibniz Society" (WGL), with the federal government and the state of Saxony contributing 50 % of the basic funding each.
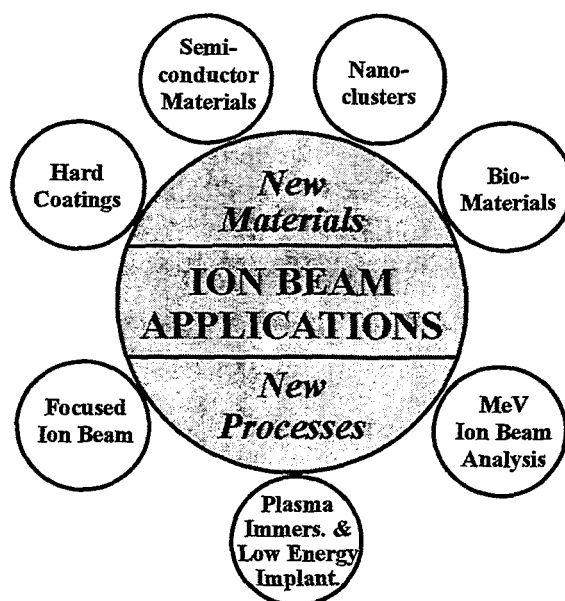
The Institute of Ion Beam Physics and Materials Research (IIM) has 76 permanent positions of scientists (32), technicians and engineers (42) and administration personnel (2). In average about 40 additional employees are funded from PhD student and PostDoc programs, guest funds, and governmental and industrial projects. The aim of the institute is to combine basic research and application-oriented studies in the fields of ion surface modification and ion beam surface analysis. According to the German Science Council, the institute shall represent a national ion beam center, which, in addition to its own scientific activities, offers services and transfers know-how on ion beam techniques to universities, other research institutes, and industry.

For these purposes, a broad range of ion-related equipment is available, delivering ion energies from about 10 eV (plasma treatment) to several 10 MeV (electrostatic accelerators). For the diagnostics of ion-treated surfaces, standard analytical techniques are available such as transmission electron microscopy, X-ray diffraction, Auger and photoelectron spectroscopy, and a number of chemical, optical, electrical, and mechanical diagnostics. Sample preparation is available for a large number of different materials including standard silicon processing.

As shown in the diagram on p. 4, the main R&D activities of the institute are subdivided into the areas of New Materials and New Processes. In the former, a new field of ion modification of biomaterials has been added in 1998 to the ion-assisted deposition of hard coatings, the ion beam modification of semiconductors materials and the ion-assisted generation of nanoclusters. New processes involve basic investigations and applications using a focused ion beam, plasma immersion and low-energy ion implantation, and the development of high-energy ion beam analysis tools.

It is the purpose of the present Annual Report to document the scientific progress of the institute in 1998 by a few selected extended contributions, numerous short contributions, and a statistical overview on its publications, conference contributions and lectures given by members of the institute. It also reports on the training of young scientists and the external and collaborative actions. We hope to demonstrate a very successful development in all of these areas.

A few important events and actions deserve special comments. Within the program of the European Commission to promote the Transfer and Mobility of Researchers (TMR), the institute was selected as a Large Scale Facility (LSF) entitled "Center for Application of Ion Beams in Materials Research" ("AIM"). From corresponding funds, travel support is now available for European users of the Rossendorf ion facilities, with the institute being funded to open about 15% of its experimental capacity for these actions.

Semi-conductor Materials

Nano-clusters

Hard Coatings

Bio-Materials

New Materials

ION BEAM APPLICATIONS

New Processes

Focused Ion Beam

MeV Ion Beam Analysis

Plasma Immers. & Low Energy Implant.

A significant step was completed in the course of locally joining and combining the different ion beam facilities of the institute. A new section was added to the accelerator building with an area of about 1500 m² on two floors, allowing to move equipment from formerly dispersed sites. In the lower floor, an analytical center including transmission and scanning electron microscopy, Auger electron and X-ray photoelectron spectroscopy, and Mössbauer spectroscopy was established and went into routine operation. On the upper floor, the 500 kV implanter was installed and commissioned. The 200 keV implanter will follow in 1999. The installation of the system of beam lines and experimental devices, which will combine the Tandem and Tandetron high-energy accelerators with the 500 keV implanter, has been commenced. In this area, a new clean room has been constructed and commissioned (A special contribution is given below).

With a ceremony in June 1998, the Rossendorf Beam Line (ROBL) at the European Synchrotron Radiation Facility (ESRF) in Grenoble (France) went officially into operation. The Grenoble team of the institute now contributes to several of the research projects with new and highly efficient diagnostics, and has opened new possibilities for international collaborations.

In 1998, three PhD students and one diploma student finished their thesis at the the institute and their examinations at the Technical University of Dresden. The second summer school "Nuclear Probes and Ion Beams" was organized in Bad Blankenburg (Thuringia) in cooperation with the Hahn-Meitner Institute, Berlin, whith increasing interest (45 students and 13 lecturers). This might contribute to a continuing interest of young scientists in our field. However, in accordance with the dramatically decreasing number of students in physics and engineering in Germany and other European countries, it has become increasingly difficult and time-consuming to recruit suitable PhD students and PostDocs. In two instances, PostDocs left the institute due to excellent offers from industry. Although this must be appreciated in principle and might promote in future a trend which is reverse to the abovementioned, it is presently detrimental to an efficient and continuous research also at our institute.

Technology transfer and ion beam service activities of the institute have again been significantly extended in 1998. Ion beam analysis services for universities and industry cover a wide range of materials such as metals, semiconductors, hard coatings, oxides, and perovskites, and are related to a broad spectrum of activities for mechanical and electronic applications in energy research, biomedicine, information technology, geology, and extraterrestrial research. A new beam line has been commissioned at the Tandem accelerator for industrial implantations of semiconductor wafers. Further ion implantation tests and service were performed in cooperation with about 40 partner institutions from research and industry, with particular emphasis on technological applications of plasma immersion implantation for automotive and machine components and different cutting tools.

The institute would like to thank all friends and organisations who supported its progress in 1998. Special thanks are due to the Executive Board of the Forschungszentrum Rossendorf, the Minister of Science and Arts of the Free State of Saxony, and the Minister of Education and Research of the Federal Government of Germany. Our partners from industry and other research institutes play an essential role for the Rossendorf ion beam center. Last but not least, the director would like to thank all members and guests of the institute for their active and often excellent contributions to a successful development in 1998.

Prof. Wolfhard Möller

Contents

Statistics

Highlights

„Böttger Stoneware" – Authentic or Not ?

C. Neelmeijer, M. Mäder, U. Pietsch*, H. Ulbricht* and H.-M. Walcha*
* Staatliche Kunstsammlungen Dresden, Pozellansammlung im Zwinger, D-01067 Dresden

In the early 18th century, on the track to the invention of the famous European hard porcelain, J. F. Böttger succeeded first in the production of „red porcelain" or „Jaspis porcelain". This so-called „Böttger stoneware" [1] represents an independent technological development. Even today, the perfection of the artificial design of objects made from Böttger stoneware shows the high level of art and technology which had been reached in Saxony already before the foundation of the "Porcelain Manufacture of Meißen" in 1710. In comparison to other ceramics Böttger stoneware is characterised by a high material density, consequently high hardness and the suitability for surface polishing. Böttger reached these excellent properties by using basic mass of very high quality and a special burning procedure.

The oldest objects made from tight ceramic material were produced in China about 4000 years ago [2]. During the development of hard burnt and tight ceramics in China the "Yixing-stoneware" was created as a by-product of porcelain. This type of stoneware was later copied in Europe, namely in the second half of 17th century in The Netherlands (Ary de Milde) and England (Elers Brothers, Wedgwood in the 19th century) but also in Meißen (Böttger stoneware) in the early 18th century. Parts of Böttger's "arcanum" were transferred from Saxony into the region of Berlin. This is the reason why Plaue (at river Havel) became a competitive place of manufacturing stoneware in Germany in the 18th century.

Today, a variety of objects made from Böttger stoneware are suspected on the international arts market to be modern fakes. In fact, the statement of the authenticity of Böttger stoneware and its differentiation from ceramic art objects of other provenance is the job of experts and art scientists. However, in the case of objects without signature their decisions are often controversial and subjectively modified. Hence, museums show growing interest to obtain objective criteria based on non-destructive methods of stoneware material analysis [3]. Concentration ratios of main and secondary elements are suggested to show characteristic "fingerprints" for the different provenance of stoneware. In the present work this possibility is tested by making use of ion beam analysis, using in particular PIXE at the external proton beam of the 5 MV Rossendorf Tandem accelerator.

As evident from the cover picture of the present annual report, positioning the stoneware object in front of the beam exit pipe [4] is very convenient. Working in a continuous helium gas stream on the non-vacuum side of the beam exit window reduces proton stopping as well as X-ray absorption and prevents the emission of interfering Ar K-radiation from air. A direct contact between the He gas and the Be detector window is prevented by means of a 5 µm thick Mylar foil. X-rays from chemical elements $Z>13$ are measured at 135° backward angle by means of a conventional Si(Li) detector (12 mm^2 active area). To minimise pulse pile-up and dead time the counting rate is limited to 10^3 counts/s by suitable combinations of diaphragms and filters in front of the detector. A diaphragm of 1.5 mm diameter and no additional absorber are used to detect the main elements of lower atomic numbers, i.e. Al to Fe. For analysis of the heavier trace elements $Z>26$ the diaphragm is opened to 2.4 mm diameter, and a 69 µm Al filter is inserted in order to absorb the intense X-radiation of the low-Z main elements. In comparison to more sensitive materials like varnish on paintings or paper backings [5] the proton beam intensity and irradiation time is less critical for non-destructive measurements of stoneware. Typical proton beam densities are 0.2 nA/mm^2. For good statistics in the peak areas of the "PIXE visible" main elements Al, Si, K, Ca, Ti and Fe

the irradiation times amount to 1-2 min. However, even a measuring time of 5 min is insufficient for reasonable statistics in the signals of trace elements. This is demonstrated in Fig. 1 which gives typical X-ray spectra as obtained from a brown unpolished Pilgrim bottle of Böttger stoneware. To limit the proton exposure of unique art objects the installation of a second Si(Li) detector of high efficiency (80 mm^2) is in preparation which allows the analysis of trace elements simultaneously to the main components. In the mean time we restrict our studies to the evaluation of material characteristic "fingerprints" for the main elements.
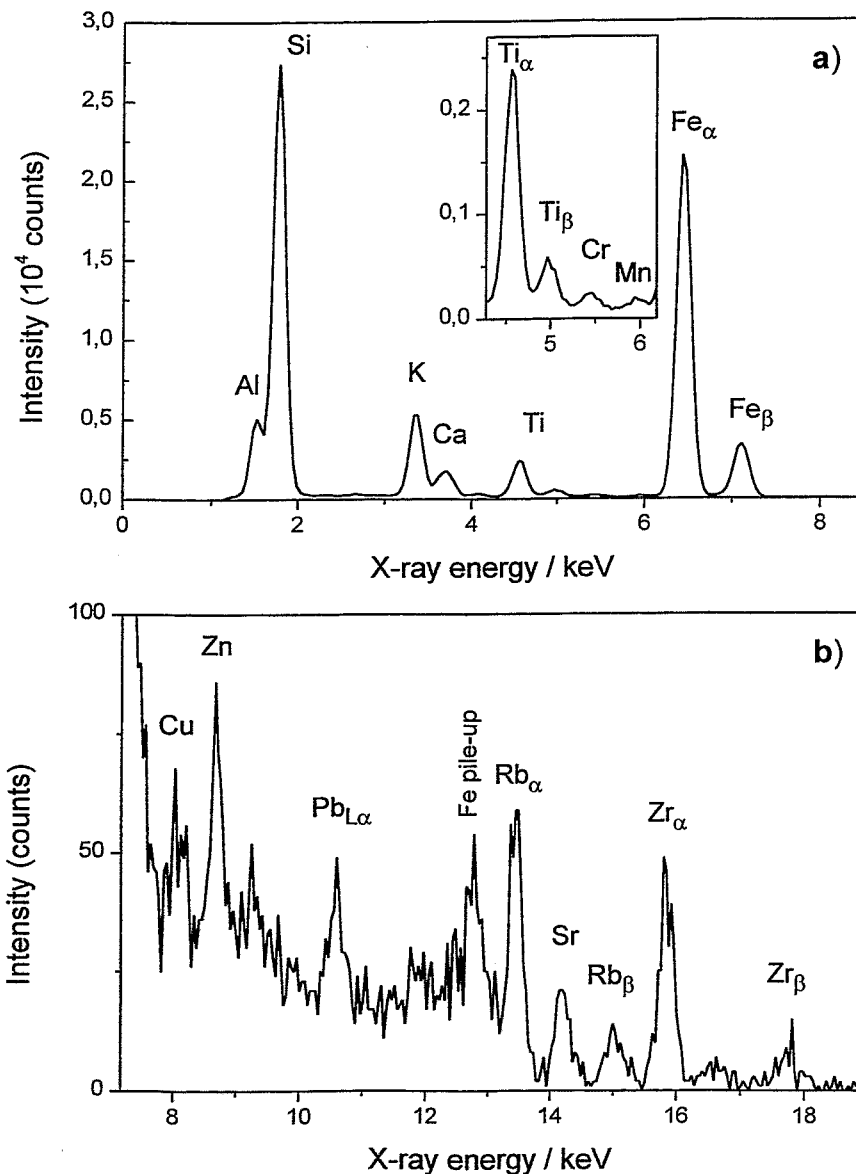
Fig. 1: PIXE spectra of Böttger stoneware obtained from the brown unpolished Pilgrim bottle PE 737 (Porzellansammlung im Zwinger Dresden). The measurements were taken non-destructively at the E_p=3.85 MeV external proton beam: a) main elements, b) trace elements (see text).

The reliability of "fingerprints" is a question of statistics. Hence, it is necessary (i) to guarantee representative composition data for a given object and (ii) to analyse a sufficient number of objects representative for a certain type of stoneware material. The present level of
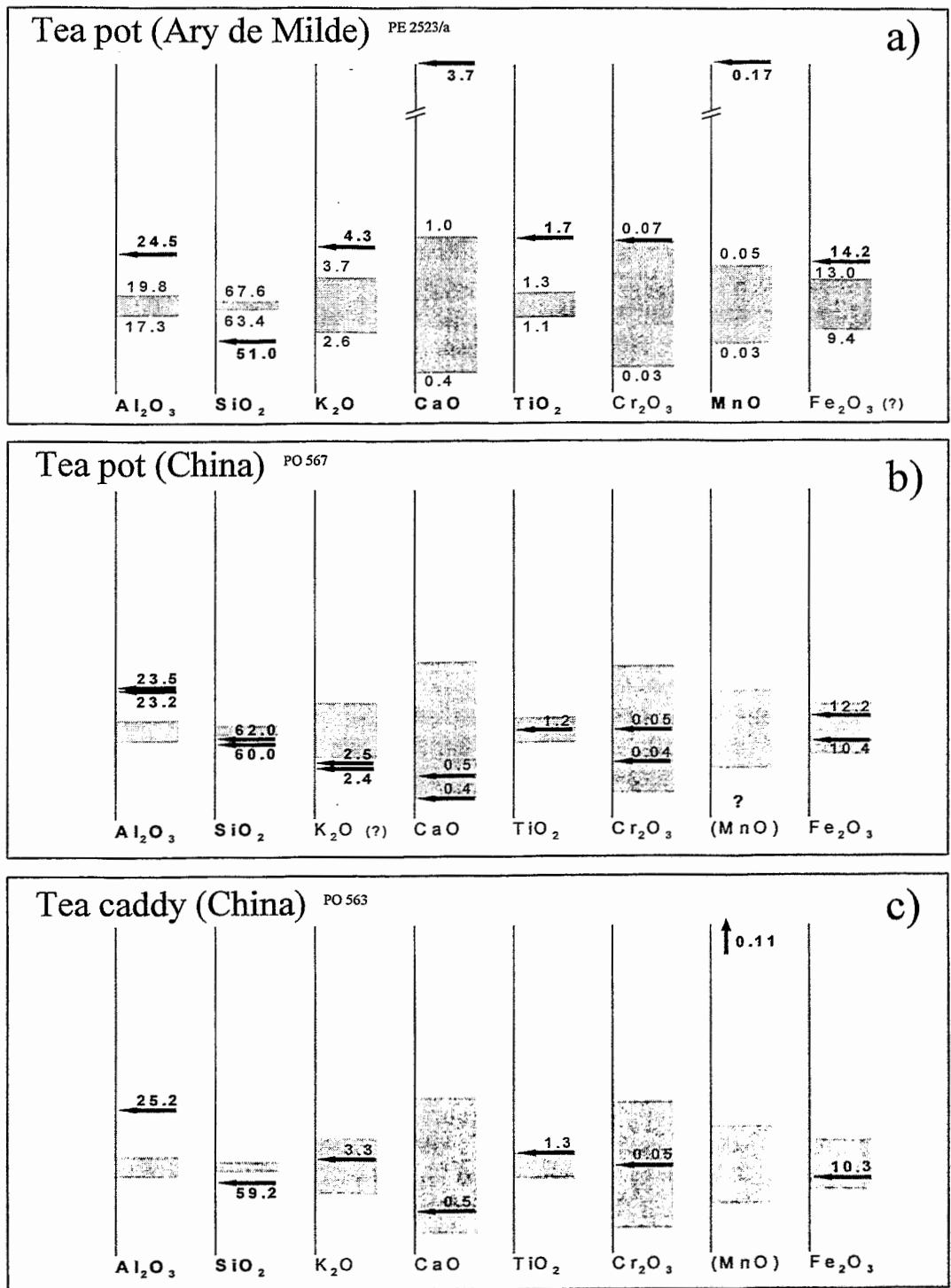
Fig. 2: Material compositions (main components, wt%), obtained for stoneware made in The Netherlands (a) and China (b, c), are graphed by black arrows. For comparison, the grey bars represent the results for 7 different authentic objects of Böttger stoneware (see text). Mean concentration values for Böttger stoneware can be deduced by averaging the upper and lower limits of fluctuations given at the bars in Fig. 2a as numbers. Note that the grey bars are identical in Figs. 2a-c.

knowledge is summarised in Fig. 2. For the main material components, the concentrations obtained from 7 objects of authentic Böttger stoneware (given by grey bars) are compared to those found in the case of single objects from China and The Netherlands (marked by black arrows). The lengths of the bars reflect different concentrations measured for the 7 objects of Böttger stoneware; the lowest and highest concentration values are given as numbers in Fig. 2a. Note that (i) the corresponding mean values are graphed in Fig. 2 at one and the same level of the ordinate, and (ii) the fluctuations are represented in percent of the mean values.

As can be deduced from Fig. 2, there are characteristic deviations of the contents for several oxide components. Compared to Böttger stoneware both the tea pot and the tea caddy (provenance: China) show a factor of 1.3 higher Al_2O_3 concentrations and a lower level of SiO_2. Most significant is the strongly enhanced MnO concentration (a factor of 5) in the case of the tea pot. This statement, however, must be reproduced by higher statistics in the Mn K-line (see Fig.1a) making use of a selective chromium X-ray filter. The tea pot of Ary de Milde (The Netherlands) indicates a broader spectrum of deviating components (Fig. 2). Again, the MnO concentrations exceed those of Böttger stoneware by more than a factor of 4. But also the CaO content is a factor of 5 higher. For Al_2O_3 and SiO_2 the tea pot of Ary de Milde shows the same trend as in the case of China stoneware; in comparison to Böttger stoneware the concentrations of K_2O and TiO_2 are enhanced.

In summary, regarding PIXE fingerprints for stoneware of different provenance, the preliminary results are promising. According to our present knowledge, for two private objects, a tankard and a tea pot of uncertain provenance, there was no contradiction between the PIXE analytical result and the attributed Böttger authenticity. Nevertheless, further efforts are necessary (i) to minimise concentration fluctuations due to low statistics in the PIXE peak areas and (ii) to improve the statistical accuracy for a given type of stoneware material by both examining a higher number of positions per object and including more authentic objects of given provenance.

References

[1] E. Zimmermann, Die Erfindung und Frühzeit des Meißner Porzellans, Verlag Georg Reimer, Berlin 1908
[2] O. Rücker-Embden, Chinesische Frühkeramik, Verlag Karl W. Hiersen, Leipzig 1922
[3] 1st International Workshop on the non-destructive characterisation of Böttger stoneware, J. Paul Getty Museum Los Angeles, Nov. 1998
[4] C. Neelmeijer, W. Wagner, H. P. Schramm, Nucl. Instr. Meth. B118 (1996) 338
[5] C. Neelmeijer, W. Wagner, Naturwissenschaften 81 (1994) 553

Modeling of Nanocluster Formation during Ion Implantation

M. Strobel and K.-H. Heinig

High-dose ion implantation is a powerful technique to synthesize nanoclusters (NCs) in the near surface region of a wide variety of host materials. In general, for sufficiently large ion fluences, NCs evolve by precipitation from a depth- and time-dependent supersaturated solid solution of impurity atoms. Depending mainly on the mobility and solubility of the impurity atoms, precipitation occurs either during the implantation stage or during a subsequent annealing step. Statistical equilibrium methods are not well suited to describe precipitation phenomena as encountered in ion beam synthesis (IBS), because in this process systems are usually driven to a state far from equilibrium. A more suitable description is a kinetic approach on an atomic level, where impurities are treated as effective particles in a homogeneous background (i.e. the substrate). Three-dimensional lattice Monte-Carlo (MC) simulations based on the nearest-neighbor kinetic Ising model allow for a detailed study of NC formation including consistently supersaturation, nucleation and growth.

In a first step towards a thorough understanding, homogeneous conditions throughout the simulation volume are assumed for simulations of NC formation during implantation. Any interaction of impurity atoms with collision cascades as well as possibly preferred heterogeneous nucleation of NCs in areas of high damage are neglected. In the course of the simulation, for each single atom implantation the new impurity atom is set into the simulation box (applying periodic boundary conditions) at a random lateral position and at a depth coordinate z chosen according to a Gaussian ion-range profile. The implantation parameters then determine the ratio of implantation steps to diffusion steps. For instance, for a fixed implantation current, the higher the implantation temperature the more diffusion jumps occur in the time interval between two deposition events.

The (depth-dependent) NC size distribution as well as the mean radius $\bar{R}$ depend on the implantation parameters, i.e. the temperature T_{imp} and ion current j. In a series of simulations, for a fixed ion fluence F the NC formation is studied qualitatively at three different implantation temperatures $\{T_<, T, T_>\}$ for a fixed ion flux j and at three different ion fluxes $\{j_<, j, j_>\}$ for a fixed T_{imp} [1]. The three ion currents $\{j_<, j, j_>\}$ differ one another by one order of magnitude, whereas the implantation temperatures are related by $T_>^{-1} : T^{-1} : T_<^{-1} = 2 : 3 : 4$.

A typical snapshot of a MC simulation would usually show some freely diffusing monomers and an ensemble of NCs (condensed impurities) of various sizes. However, in order to compare size distributions, a more suitable representation is to approximate every NC by a sphere whose size is determined by the number of its impurity atoms. Fig. 1 shows the NC distributions for the five parameter pairs $\{(T_<, j), (T, j_>), (T, j), (T, j_<), (T_>, j)\}$.

For constant parameters the process of NC formation can be divided into three stages: **Accumulation/Supersaturation:** Immediately after the start of ion implantation, the first impurity atoms can be found as (dissolved) monomers with a (basically) temperature-dependent mobility. Hence, the concentration of monomers c increases linearly with time. **Nucleation:** As c increases further and exceeds the solubility threshold, small agglomerations of impurity atoms (i.e. dimers, trimers, ...) start to
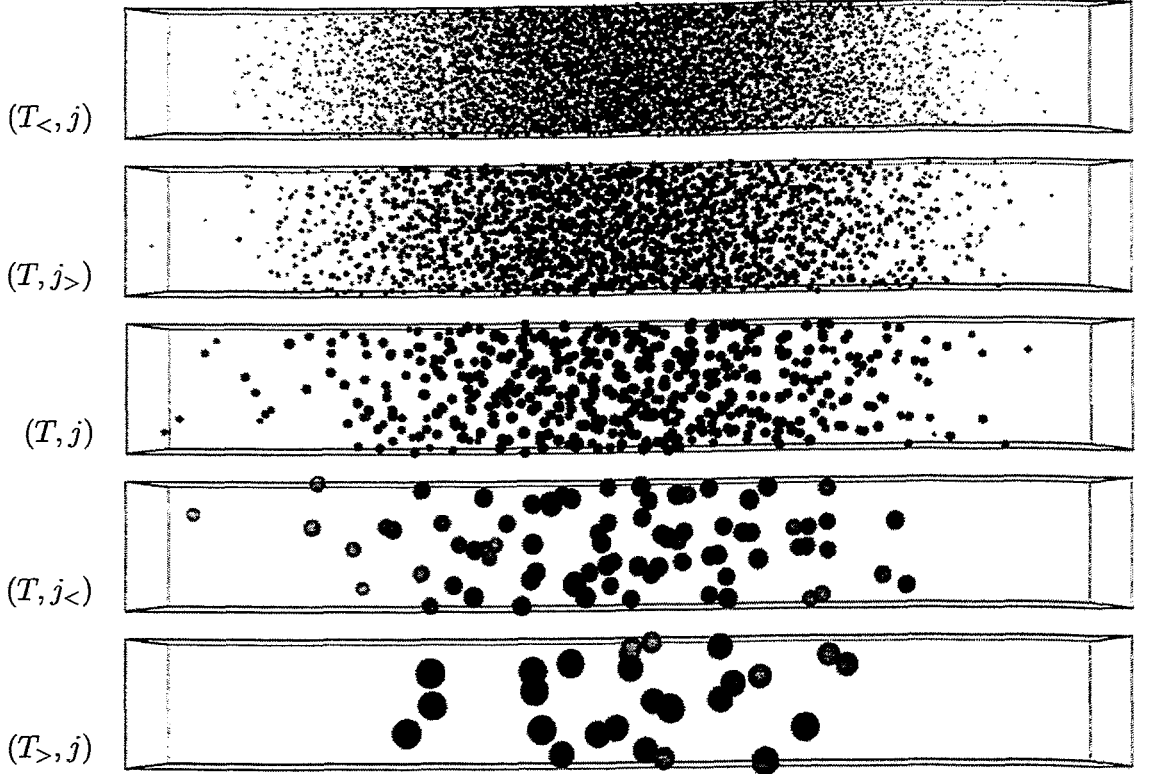
Fig. 1: MC simulation results of NC formation during ion implantation recorded immediately at the end of ion deposition. All NCs are represented as spheres and the grey scale is chosen according to their size.

form. From these tiny agglomerations, some grow by statistical fluctuations beyond the critical radius R_c forming stable precipitates and act later on as sinks for diffusing monomers. **Growth:** No additional NCs are formed and the existing ones grow by attachments of newly implanted impurity atoms rather than competitive ripening.

The observed NC distributions can be explained in terms of classical nucleation theory [2]. Bulk and surface atoms of a NC give different contributions to its free energy (capillary approximation), thus NC have to exceed a critical size R_c in order to become stable against dissolution. In general, R_c is given by the temperature-dependent degree of supersaturation (the nucleation probability is proportional to $\exp(-W(R_c)/kT)$, where W is the reversible work needed to form this NC). Furthermore, IBS of NCs is a time-dependent process. Thus, for different ion currents at a given T_{imp}, transient processes (depletion effects) influence precipitation.

From the viewpoint of homogeneous nucleation similar NC size distributions can be obtained either by increasing T_{imp} or by decreasing j (or vice versa) (see Fig. 1). This behavior suggests, that the mean NC size can be described according to a function $f(D(T)/G)$, where D is the (strongly temperature-dependent) diffusion coefficient and G the generation rate of impurity atoms per unit volume, which is proportional to j.

Additionally, MC simulations have been performed, where one parameter was changed for the second half of implantation. Fig. 2 shows the simulated NC distributions for
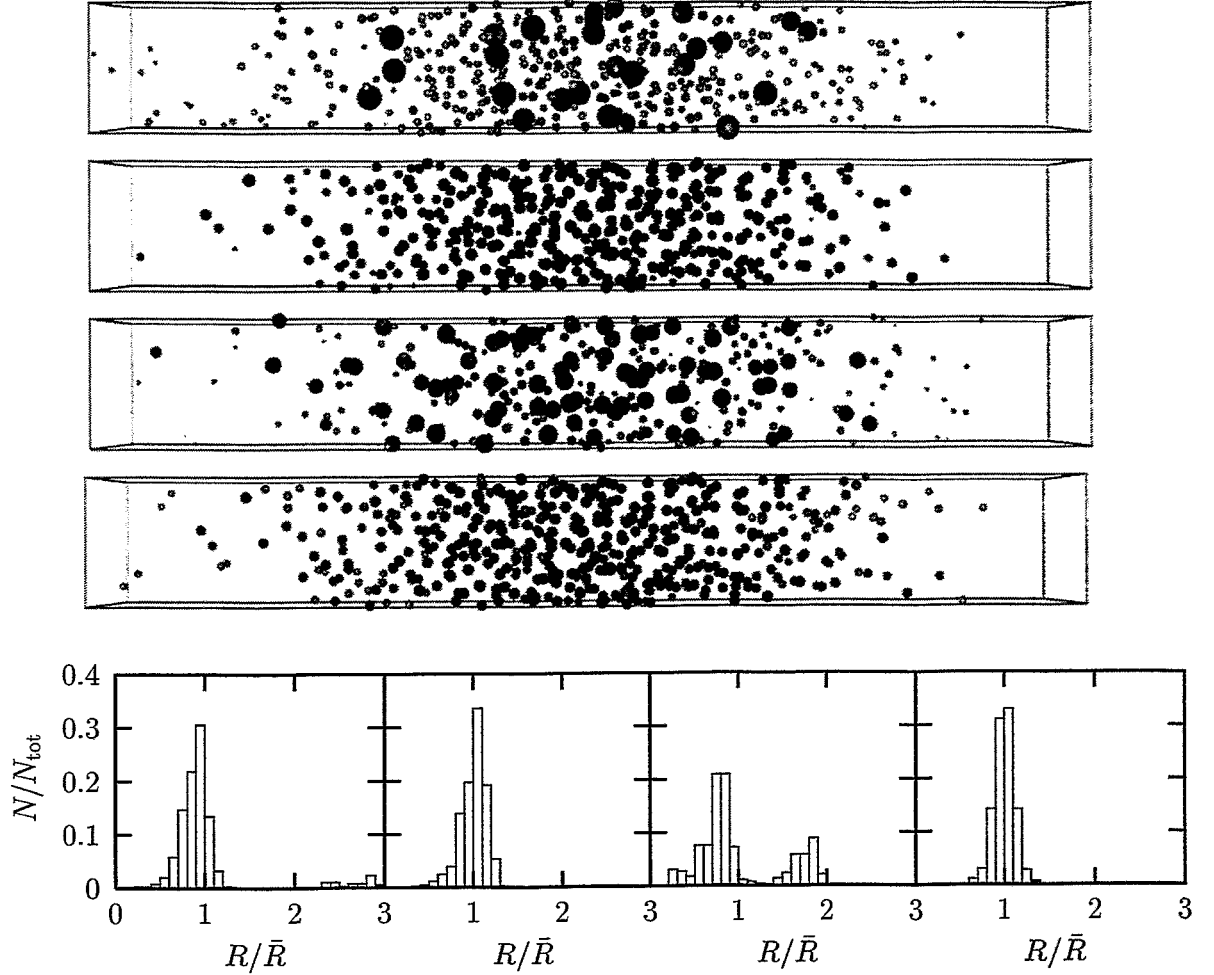
Fig. 2: Final NC distributions in the case of a change of the implantation parameters at half of the nominal fluence (from top to bottom: $(T_>, j) \to (T, j)$, $(T, j) \to (T_>, j)$, $(T, j_<) \to (T, j)$, and $(T, j) \to (T, j_<)$). The corresponding NC size distributions are shown in the bottom row.

the changes $(T_>, j) \leftrightarrow (T, j)$ and $(T, j_<) \leftrightarrow (T, j)$ together with the corresponding particle radius distributions (PRDs). For the implantation sequences $(T_>, j) \to (T, j)$ and $(T, j_<) \to (T, j)$, bimodal PRDs are predicted. This result can be explained by a corresponding change of R_c. By lowering T_{imp}, a second nucleation stage may be initiated, which results in a bimodal PRD. In the case of rising T_{imp} also R_c increases, which can become so large that previously formed NC may now be smaller than the critical size and consequently dissolve. This results in a very narrow PRD.

The IBS of Au nanoclusters in SiO_2 is well-suited for fundamental precipitation studies, because (i) Au does not tend to form an oxide or silicide (chemically inert), (ii) Au is observed to precipitate during the implantation stage, and (iii) no collective shift of the implanted Au atoms (e.g. due to charging effects) influences the nanocluster formation. The MC results in Fig. 1 reproduce experimentally observed temperature dependencies of NC distributions, e.g. for Au precipitates in SiO_2 [1] or $CoSi_2$ NCs in Si [3]. Systematic experiments with significant changes in j have not been performed so far. Fig. 3 shows Au implantation results for a controlled variation of T_{imp}. Clearly, the size distribution depends on the sequence of the temperature change. A rather broad PRD (possibly the
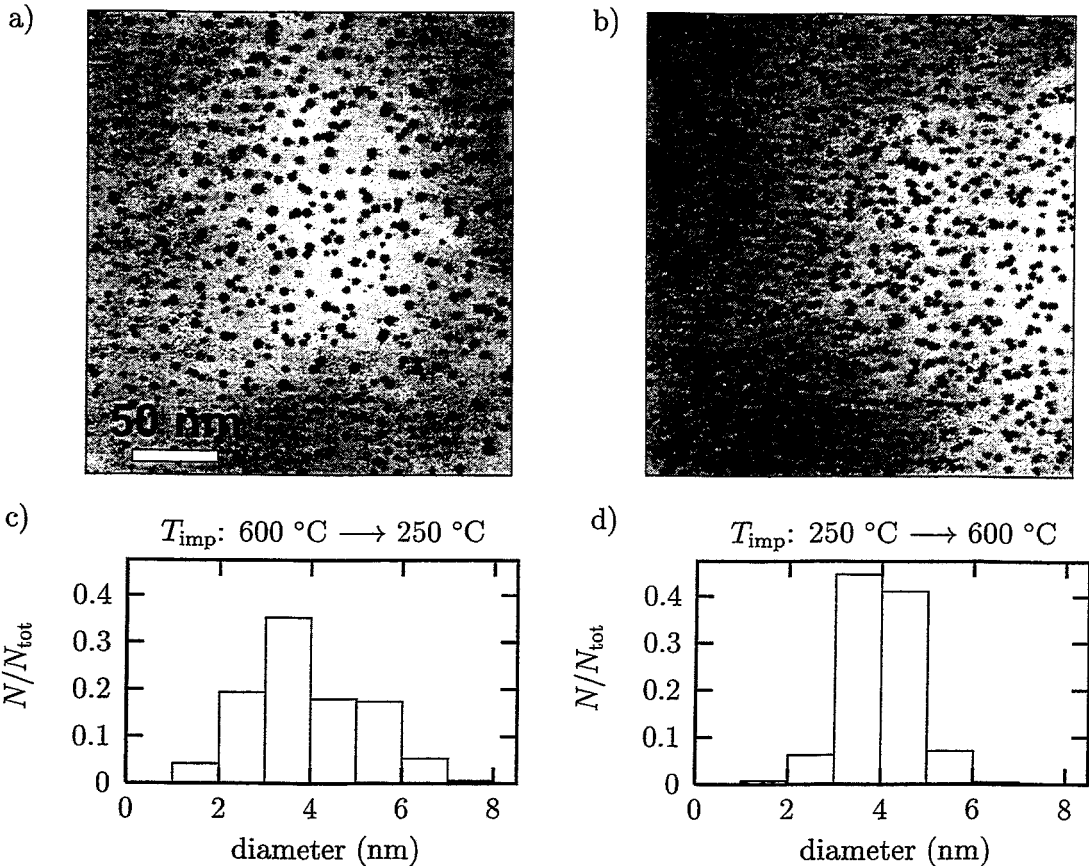
Fig. 3: TEM micrographs of the ORNL-group [1] for 2.75 MeV Au^+ implantation into SiO_2: a) 3×10^{16} cm^{-2} at 600 °C + 3×10^{16} cm^{-2} at 250 °C, b) 3×10^{16} cm^{-2} at 250 °C + 3×10^{16} cm^{-2} at 600 °C. The corresponding size distributions are shown in Figs. c) and d).

overlap of two individual distributions as suggested by the results of Fig. 2 is obtained by decreasing T_{imp} in the second implantation step.

A complete modeling should take into account collisional mixing, which causes damage not only to the substrate, but also to previously formed NCs [4]. For constant implantation conditions, a steady-state balance between collisional mixing and reattachment of impurities develops. In this case, the mixing can be described to some extent by an effectively higher T_{imp} and a corresponding NC distribution will evolve. This concept of an effective implantation temperature might explain the similarities between experiment and simulation results, even if collisional mixing has not been included in the MC method.

References

[1] M. Strobel, K.-H. Heinig, W. Möller, A. Meldrum, D.S. Zhou, C.W. White, R.A. Zuhr, Nucl. Instr. Meth. B 147 (1999) 343

[2] R. Becker, W. Döring, Ann. Phys. 24 (1935) 719

[3] E.H.A. Dekempeneer, J.J.M. Ottenheim, D.E.W. Vandenhoudt, C.W.T. Bulle-Lieuwma, E.G.C. Lathouwers, Nucl. Instr. Meth. B 55 (1991) 769

[4] G. Martin, P. Bellon, Solid State Physics 50 (1997) 189

Enhancement of the Intensity of the Short-Wavelength Visible Photoluminescence from Silicon-Implanted Silicon Dioxide Films Caused by Hydrostatic Pressure during Annealing

I.E. Tyschenko[*], L. Rebohle, R.A. Yankov, W. Skorupa and A. Misiuk[**]
[*]   Institute of Semiconductor Physics, 630090 Novosibirsk, Russia
[**] Institute of Electron Technology, al. Lotnikόw 32/46, 02-668 Warsaw, Poland

Recently, there has been an increasing interest in the formation of Si-based, low-dimensionality structures which exhibit visible-light emission at room temperature (RT). Various methods of creating luminescent nanocrystalline materials have been reported. Of these, perhaps the most promising has proven to be ion-beam synthesis of Si clusters and nanocrystals in thermally-grown SiO_2 films [1-3]. The technique of ion-beam synthesis involves two stages: high-dose ion implantation and subsequent annealing. The thermal processing conditions, that is annealing temperature and time [4] and ambient [5], play an important role. Our previous work [6] has shown that medium-dose Si^+ implants into thin SiO_2 layers followed by relatively low-temperature anneals (T_a=400 - 500 °C) produce structures which emit blue photoluminescence (PL) peaking at about 460 nm. The nature of this PL is believed to be associated with the $\equiv$Si-Si$\equiv$ center in SiO_2 (see discussion in Ref. [6]). Increasing the ion dose at constant T_a leads to a red shift of the PL peak and the appearance of a broad band centered around 600 - 650 nm whose origin is attributable to the formation of Si-rich regions in the oxide [1,4]. Increasing T_a to 1000 - 1200 °C has been found to quench both the blue and the red PL signals and gives rise to an intense peak in the near-infrared region at 800 - 850 nm. Most reports state that this PL is a consequence of the effects of quantum confinement (radiative recombination of quantum-confined electron/hole pairs) in Si nanocrystals [2-6]. There is evidence in the literature that besides the conventional anneal parameters, i.e. the temperature, time and ambient, pressure is an additional important factor which may influence strongly the solid-state atomic interactions. For example, the work described in Ref. [7] emphasizes the effect of even moderate low hydrostatic pressures (about 13 kbar) on the diffusion processes in Si. There have also been reports on the PL properties of porous Si under conditions of hydrostatic pressure [8]. It has been shown that at pressures up to 20 kbar, which are by an order of magnitude lower than those causing the first structural transition in bulk Si, one observes a blue shift in the PL spectrum with an attendant reduction in the PL intensity. Here we report on first experiments to explore the effects of hydrostatic pressure as a parameter of the ion beam synthesis process which acts on the intensity of the visible PL from a Si^+-implanted SiO_2 layer.

An n-type, 5-10 Ω cm, (100)-oriented Si wafer was wet-oxidized at 1000 °C to grow a 500 nm SiO_2 layer. The oxide layer was implanted with Si^+ ions first at an energy of 100 keV and then at 200 keV using respective doses of 1.2×10^{16} and 2.0×10^{16} cm^{-2} (low doses - LD), 1.8×10^{16} and 3.0×10^{16} cm^{-2} (medium doses - MD), 2.3×10^{16} and 4.4×10^{16} cm^{-2} (high doses - HD) and 3.9×10^{16} and 6.3×10^{16} cm^{-2} (very high doses - VHD). During implantation the ion beam current density and the substrate temperature were kept at 0.5 - 1 μA cm^{-2} and at 120 - 130 K, respectively. Post-implantation annealing was performed at T_a=400 °C or 450 °C for 10 h in an Ar ambient under conditions of either atmospheric pressure or hydrostatic compression in the range of 0.1 to 15 kbar using an Al_2O_3-coated containment. PL spectra from the samples were recorded at RT employing a Spex Fluoromax spectrometer and R 928 Hamamatsu photomultiplier.
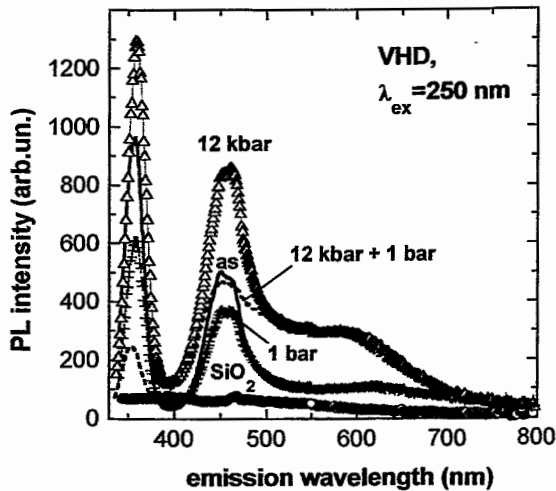
Fig. 1: PL spectra from unimplanted, thermally grown, 500-nm SiO_2 films as well as from VHD Si^+-implanted SiO_2 films before (as) and after 400 °C, 10 h annealing in Ar at 12 kbar. The dashed line shows the PL spectrum after annealing first at 12 kbar and then at atmospheric pressure for 30 min.
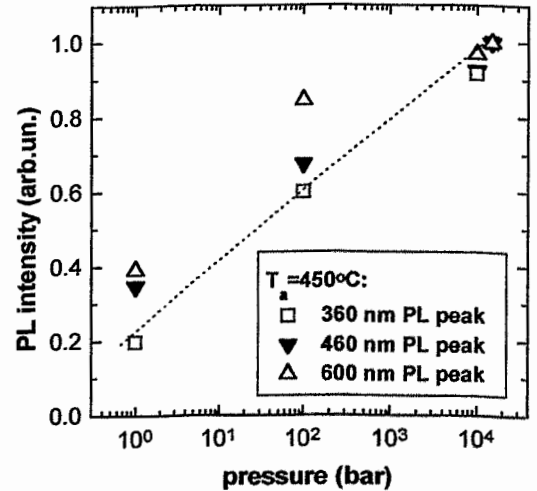
Fig. 2: Dependence of the PL intensity peaks at 360, 460 and 600 nm on hydrostatic pressure during annealing at 450 °C for 10 h in Ar atmosphere obtained from VHD Si^+-implanted SiO_2 films.

Fig. 1 shows PL spectra (excitation wavelength λ_{ex}=250 nm) recorded from both the as-implanted (VHD) samples and those that were annealed at 400°C at atmospheric pressure or hydrostatic pressure of p=12 kbar. The as-implanted samples exhibit two PL peaks in the short-wavelength range at about 360 nm (ultraviolet) and 460 nm (blue). A much less intense peak is also seen in the red region at about 600 nm. It should be noted that the 360 nm PL peak has never been observed in our previous studies, neither has it been reported by other authors dealing with PL from ion-implanted SiO_2 since the longer-wavelength range (> 400 nm) has been traditionally studied. The 400 °C, 10 h anneal at atmospheric pressure leads to a reduction in the intensity of the two short-wavelength peaks while no significant changes are registered in the red region. As the pressure is raised to 12 kbar the PL intensity of all the PL peaks is found to increase by a factor of 1.5 to 2 with the wavelength positions of the peaks showing no variation. Combining the anneal at 12 kbar with a subsequent 400 °C, 30 min heat treatment at atmospheric pressure leads again to a reduction in the intensity of the short-wavelength PL. The intensity of the blue peak (460 nm) drops to values comparable to those of the blue signal from the as-implanted sample while the decrease in the intensity of the near-ultraviolet peak (360 nm) is more pronounced. Interestingly, the intensity of the red PL band does not show any appreciable changes, with the exception of a small blue shift observed after additional 30 min annealing at atmospheric pressure. For comparison, Fig. 1 shows also the PL spectrum from the as-grown (unimplanted) thermal oxide after 400 °C, 10 h annealing at p=12 kbar exhibiting no significant effect of the pressure on the PL intensity. The dependence of the PL peaks described above on hydrostatic compression has been studied in more detail after annealing at 450 °C for 10 h as shown in Fig. 2. As the pressure is raised, the intensity of all the three PL peaks increases following a near-logarithmic relationship over the pressure range of 1 bar to 15 kbar. Fig. 3 shows PL spectra obtained after Si^+ implantation using LD, MD and HD after 450 °C, and 10 h annealing at 12 kbar. Surprisingly, the use of hydrostatic compression during annealing increases the blue PL intensity with increasing ion dose while in our earlier work [3,4] the PL intensity during heat treatment at atmospheric pressure has been found to decrease for growing doses over the same dose range. The investigation of the PL excitation (PLE) spectra of the observed PL peaks reveals that the use of hydrostatic com-
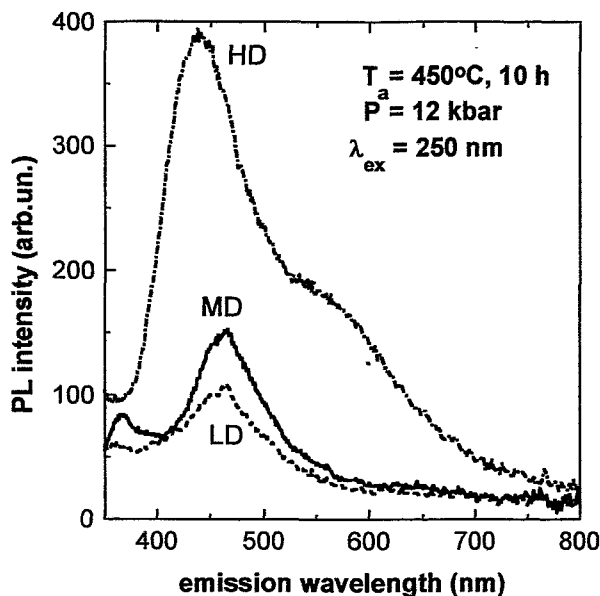
Fig. 3: PL spectra from SiO_2 films implanted with low (LD), medium (MD) and high (HD) Si^+-ions doses after 450 °C, 10 h annealing in Ar at 12 kbar. The excitation wavelength is 250 nm.

pression results in an enhanced excitation of the blue PL peak. The main excitation peak occurs at the same wavelength (about 250 nm) as in the case of annealing at atmospheric pressure.

It is apparent from these experiments that even relatively low hydrostatic pressures during heat treatment of Si^+-implanted SiO_2 films have an appreciable influence on the short-wavelength visible PL. There are two possible ways of interpretation: First, PL might be increased through enhanced formation of light-emitting centers under the action of hydrostatic pressure during thermal processing, and second, via decreasing the number of non-radiative recombination centers. These two processes may also be interrelated to a certain extent. However, the fact that the intensity of the short-wavelength PL increases with increasing concentration of the excess Si atoms during annealing under elevated pressure and, conversely, decreases for annealing at atmospheric pressure suggests that the hydrostatic pressure favours the formation of short-wavelength light-emitting centers within those regions of the oxide layer containing an excess of Si. Otherwise the dose dependence would follow one and the same trend, irrespective of the pressure, and would be accompanied solely by an increase in the PL intensity after annealing under elevated pressure. Furthermore, these results together with the invariability in the wavelength positions of the PL peaks imply that the hydrostatic pressure itself does not create any new type of emitting centers in comparison to those formed at atmospheric pressure, but rather stimulates their formation. In our previous studies [3,6] the nature of the PL peak at 460 nm has been associated with the neutral oxygen vacancy in the oxide network (i.e. the $\equiv$Si-Si$\equiv$ center) whose excitation maximum occurs at λ_{ex}=250 nm. Thus, in discussing the mechanism by which the hydrostatic pressure influences the intensity of the short-wavelength PL we shall consider, first of all, the enhanced formation of $\equiv$Si-Si$\equiv$ centers. The values of the hydrostatic pressure used in our experiments have been by an order of magnitude lower than those causing structural phase transitions in bulk Si and SiO_2 [9]. Therefore, volume changes reducing the interatomic distances in the whole amorphous network are unlikely to cause the enhanced coalescence of Si atoms. An explanation of the observed effects can be made in terms of the concept of enhanced structural transitions within specific metastable regions [10] such as the Si-rich regions of the oxide. This means that the activation energy corresponding to the change in the short-range order may be significantly reduced in the case when the atomic matrix is not in equilibrium. The reason for such a reduction in the local activation energy may be the disappearance of one or several lattice vibrational frequencies near the threshold of equilibrium loss. In effect, the formation of a larger number of small Si clusters might become energetically more favourable which may be the reason for the increased short-wavelength PL intensity with increasing ion dose under the action of hydrostatic pressure (Fig. 3). In the case of ion-implanted SiO_2 the composition and structure of which are rendered after implantation highly inhomogeneous on a nanometer scale, one may expect the existence of a range of local elastic

constants and vibrational frequencies corresponding to a particular nano-scale volume. In such a system under non-equilibrium conditions the attenuation of individual frequencies may occur within nano-sized regions of the amorphous matrix. In the case of Si^+-implanted SiO_2 such regions are those containing an excess of Si atoms. Specifically, the overstoichiometric excess Si atoms after implantation are mainly in the form of E' centers. The use of moderate hydrostatic pressure may alter the vibrational spectrum of the E' center, e.g. might attenuate some of the vibrational modes of the Si dangling bond. This may in turn lead to a release of other vibrational modes in the direction of the dangling bond of a neighbouring E' center with subsequent linking to produce a $\equiv$Si-Si$\equiv$ center. In this case $\equiv$Si-Si$\equiv$ centers are created without displacement of the host atoms.

In summary, we have demonstrated for the first time that the use of hydrostatic pressure during annealing leads to appreciable enhancement in the intensity of the short-wavelength photoluminescence from Si^+-implanted SiO_2 films. When applied at relatively low anneal temperatures (400 - 450 °C), the hydrostatic pressure does not result in the formation of a new type of light-emitting centers as compared to those formed after annealing at atmospheric pressure, but rather favours the increase in the number of the pre-existing luminescent centers. It is suggested that the nature of these PL centers is associated with the neutral oxygen vacancy and larger clusters of excess Si atoms in the oxide network. The results obtained have been interpreted in terms of a non-activated formation of $\equiv$Si-Si$\equiv$ centers and Si nanoclusters within metastable regions of the ion-implanted oxide matrix.

Acknowledgements

References

[1] T. Shimizu-Iwayama, K. Fujita, S. Nakao, K. Saitoh, T. Fujita, N. Itoh, J. Appl. Phys. 75 (1994) 7779

[2] H.A. Atwater, K.V. Shcheglow, S.S. Wong, K.J. Vahala, R.C. Flagan, M.L. Brongersma, A. Polman, Mater. Res. Soc. Symp. Proc. 321 (1994) 363

[3] W. Skorupa, R.A. Yankov, I.E. Tyschenko, H. Fröb, T. Böhme, K. Leo, Appl. Phys. Lett. 68 (1996) 2410

[4] I.E. Tyschenko, G.A. Kachurin, K.S. Zhuravlev, N.A. Pazdnikov, V.A. Volodin, A.K. Gutakovsky, A.F. Leier, H. Fröb, K. Leo, T. Böhme, L. Rebohle, R.A. Yankov, W. Skorupa, Mater. Res. Soc. Symp. Proc. 438 (1997) 453

[5] T. Komoda, J.P. Kelly, R.M. Gwilliam, P.L.F. Hemment, B.J. Sealy, Nucl. Intrum. Meth. B112 (1996) 219

[6] L. Rebohle, I.E. Tyschenko, H. Fröb, K. Leo, J. von Borany, G.A. Kachurin, W. Skorupa, Microelectr. Engin. 36 (1997) 107

[7] I.V. Antonova, A. Misiuk, V.P. Popov, L.I. Fedina, S.S. Shaimeev, Phys. B.: Cond. Matter 225 (1996) 251

[8] W. Zhou, H. Shen, J.F. Harvey, R.A. Lux, M. Dutta, F. Lu, C.H. Perry, N.M. Kalkhoran, F.Namavar, Appl. Phys. Lett. 61 (1992) 1435

[9] O.B. Tsiok, V.V. Brazhkin, A.G. Lyapin, L.G. Khvostantsev, Phys. Rev. Lett. 80 (1998) 999

[10] V.V. Brazhkin, J. Non-Cryst. Sol. 124 (1990) 34

Efficient p-Type Doping of 6H-SiC: Flash-Lamp Annealing after Aluminum Implantation

H. Wirth, D. Panknin, W. Skorupa and E. Niemann[*]
[*]Daimler Benz AG, Goldsteinstraße 235, D-60528 Frankfurt, Germany

Because of the outstanding properties of the wide band gap semiconductor SiC like high thermal conductivity and high breakdown field, SiC is becoming a material of increasing importance for special applications [1]. SiC single crystalline material of high quality can now be produced satisfying the requirements for device fabrication [2]. The implantation of group III ions into single crystalline SiC is the only method to produce laterally structured p-doped layers. However, ion implantation is always accompanied by radiation damage creating deep level carrier traps. The post-implantation annealing is very important for the crystal recovery and the electrical activation of implanted dopants. Especially investigations of highly implantation-doped p-type layers exhibiting high electrical conductivity are rare up to now [3].

Short-time annealing of aluminum-implanted 6H-SiC in argon using a pulsed 308 nm XeCl excimer laser with a pulse duration of 27 ns was carried out by Ahmed et al. [4]. Using spreading resistance measurements they deduced a complete electrical activation, but also observed a strong redistribution of the implanted aluminum towards the surface. In addition, by laser irradiation only small areas can be annealed with a single shot requiring a step-by-step processing for larger areas. Therefore, it is not useful for wafer processing. For annealing of SiC with halogen lamps, no equipment with the required high power density is available on the market up to now. We report on flash-lamp annealing of Al-implanted 6H-SiC for electrical activation with the advantage of large-area processing in comparison with laser annealing.

Aluminum was implanted into n-type 6H-SiC epitaxial layers ($c_n = 10^{16}$ cm^{-3}) at 400 °C with four different energies and doses in order to obtain a box-shaped, 500 nm thick buried (100 nm) profile with plateau concentrations between 5×10^{19} and 1.5×10^{21} cm^{-3}. The samples were annealed in argon ambient using a flash from an array of xenon lamps with a flash duration of 20 ms [5]. In order to avoid possible thermal degradation of the implanted layers the rearside of the samples was irradiated. To improve light absorption, especially at lower aluminium concentration, the rough rear surface was amorphized by high-dose argon-implantation (3×10^{16} cm^{-2}, 200 keV) at room temperature. The maximum sample temperature during the flash was about 2000 °C as evaluated by metal layer melting tests. For comparison, annealing was performed using an inductively heated furnace in argon ambient.

Although, after flash lamp annealing, an etching and/or sublimation of an about 100 nm thick surface layer was found, the surface exhibits a relatively low roughness of about 10 nm. It was investigated by SIMS, that even after the high temperature annealing at 2000 °C during the flash no significant diffusion of aluminum is observed.

Combined Hall effect and conductivity measurements were carried out with a BIORAD HL

5500 apparatus, additionally equipped with a sample chamber for high temperature measurements up to 500 °C.

The results of Hall effect measurements vs. temperature are shown in Fig. 1 for representative samples with Al concentrations of 5×10^{19} and 5×10^{20} cm^{-3} for both flash-lamp (2000 °C, 20 ms in argon) and furnace annealing (10 min at 1650 °C in argon). Al-concentrations of 5×10^{19} cm^{-3} result in a typical thermally activated conduction with increasing free hole concentration vs. temperature, independent of the annealing techniques.
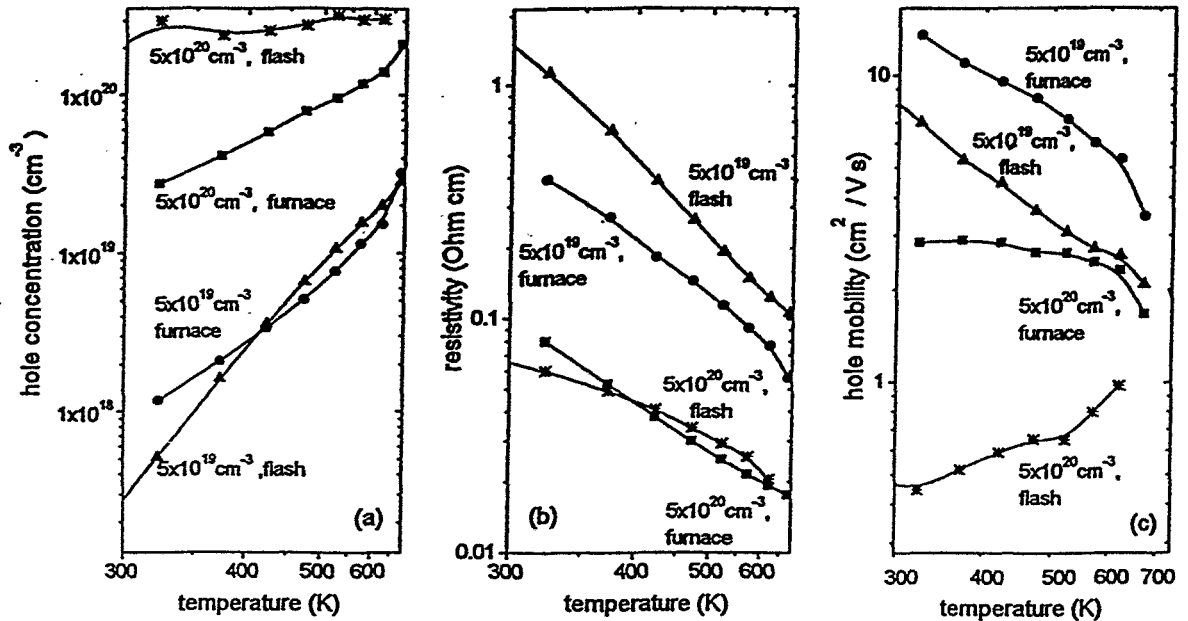
Fig. 1:
Hole concentration (a), resistivity (b) and hole mobility (c) as a function of the temperature for Al-implanted 6H-SiC after flash lamp resp. furnace annealing for two different Al concentrations of 5×10^{19} and 5×10^{20} cm^{-3}.

For the highly doped samples with Al concentrations of $\geq 5 \times 10^{20}$ cm^{-3}, a different dependence on the measuring temperature is found only after flash-lamp annealing. High, approximately constant values of the hole concentration vs. temperature are observed. This behaviour can be explained only by metallic like conduction within an impurity band, being formed above the valence band because of the high density of acceptor states being no more spatially insulated. Here metallic conduction refers to the constant number of carriers, while the carrier scattering mechanism is different from that in real metals. Compared to conventional furnace annealing the hole concentrations after flash lamp annealing are much higher. In contrast to the metallic conduction of flash-lamp annealed samples, furnace annealing leads to thermally activated conduction even at high Al concentrations. A resonable explanation is, that the solubility of aluminum in SiC limits the concentration of electrically active acceptor atoms on lattice sites. Because the solubility increases with temperature, the higher sample temperature during the flash leads to a higher substitutional Al concentration

and thus to metallic like conduction at a high level of hole concentrations. The low diffusion coefficient of Al in SiC permits a 'freezing-in' of this high Al concentration after the end of the flash as a result of rapid radiation cooling. We want to emphasize, that in the case of boron with its higher diffusion coefficient the described effect can not be observed. Instead, a saturation at $\approx 2 \times 10^{19}$ cm^{-3} occurs [6].

The hole mobility (Fig. 1c) depends on Al concentration and annealing technique in a different way. Theoretically, in addition to the invariant contribution of phonon carrier scattering at the SiC lattice, the hole mobility μ due to scattering at ionized dopant atoms follows the relation

$$\mu \sim T^{1.5} \, [(N_{ion} ln(1 + AT/N_{ion}^{-1/3}))]^{-1},$$

where T - temperature, N_{ion} - concentration of ionized dopant atoms and A - constant [7]. Thus, in the case of thermally activated conduction the hole mobility decreases with increasing temperature because of the exponentionally increasing concentration of thermally ionized dopants over-compensating the factor $T^{1.5}$, while the logarithmic dependence is very weak. The lower mobility after flash-lamp annealing compared to furnace annealing at an Al concentration of 5×10^{19} cm^{-3} is probably caused by additional, quench-induced defects. However, in the case of metallic conduction N_{ion} is constant and thus the hole mobility raises with temperature at a low level. Both dependences are observed experimentally as shown in Fig. 1.

Estimating the critical acceptor concentration for metallic conduction theoretically [7], the criterion is the beginning overlap of the acceptor state wave functions: $Na^3 \approx 1$ (N acceptor concentration, a - Bohr-radius of the acceptor state wave function). Assuming a simple hydrogen model for the ground state, one obtains a critical concentration for metallic conduction of 8×10^{21} cm^{-3}. The Mott transition from thermal to metallic conduction is predicted to begin already for $Na^3 > 0.02$ corresponding to a volume concentration of 1.6×10^{20} cm^{-3}. This agrees with the present experimental result showing metallic conduction for 5×10^{20} cm^{-3}.

In Fig. 2 the hole concentrations, measured at room temperature after annealing using the different techniques, are shown in dependence on the Al plateau concentration. The hole concentration increases with increasing Al concentration as well as with increasing annealing temperature. Flash lamp annealing results in a hole concentration of 1.5×10^{21} cm^{-3}, which is the highest value reported for SiC so far.

Tone et al. [3] and Rao et al. [9] reported on high-dose co-implantation of Al and C into 6H-SiC. Their idea is to maintain the Si-C parity as the implanted aluminum prefers the Si sublattice sites of SiC. Their results are contrary. Tone at al. observed after annealing at 1550 °C an enhanced conductivity compared to pure aluminium implantation in the Al concentration range $8 \times 10^{19} \dots 1 \times 10^{20}$ cm^{-3}. However, Fig. 2 clarifies, that after Al/C co-implantation the hole concentrations are at best similar to our results for pure Al implantation. Against it, Rao et al. observed a decrease of the conductivity after co-implantation and annealing at 1600 °C.

In conclusion, flash-lamp annealing is an economic large area processing technique for the formation of p^+(Al) regions in 6H-SiC electronic devices. Compared to conventional furnace annealing it results in higher hole concentrations and lower resistivity as well as a weaker temperature dependence of the electrical material parameters for Al-concentrations exceeding 5×10^{20} cm^{-3}.
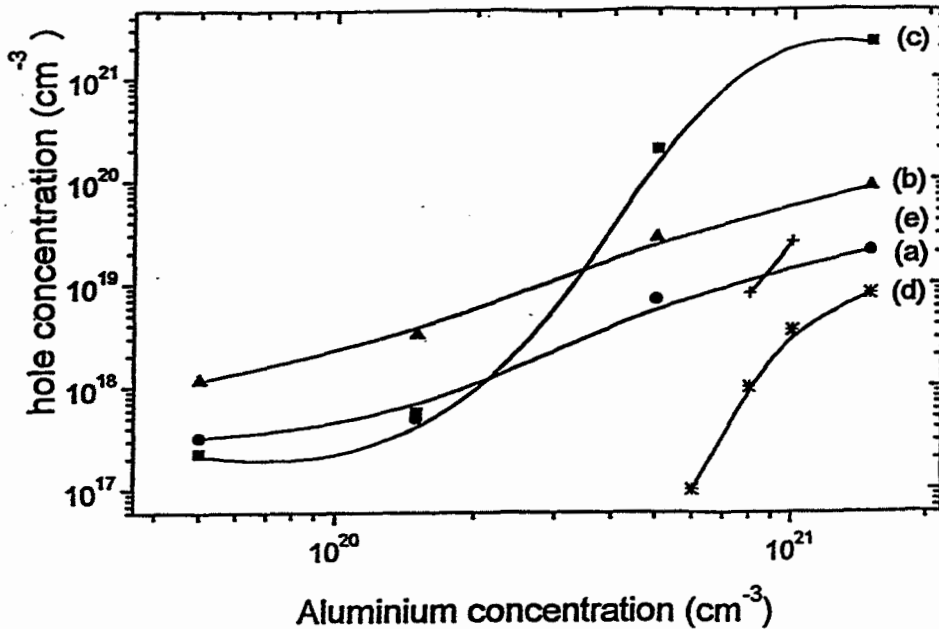
Fig. 2:
Comparison of the hole concentrations in 6H-SiC measured at room temperature after annealing using different techniques for pure Al implantation and Al + C co-implantation [3].
Al implantation and furnace annealing: (a) 1550 °C; (b) 1650 °C; (c) flash annealing (2000 °C).
Furnace annealing at 1550 °C by Tone et al. [3]: Al implantation (d); Al + C coimplantation (e).

References

[1] W.J. Choyke, G. Pensl, MRS Bulletin 3 (1997) 25
[2] O. Kordina, A. Henry, E. Janzen, C.H. Carter, Mat. Sci. Forum 264-268 (1998) 97
[3] K. Tone, S.R. Weiner, J.H. Zhao, Mat. Sci. Forum 264-268 (1998) 689
[4] S. Ahmed, C.J. Barbero, T.W. Sigmon, Appl. Phys. Lett. 66 (1995) 712
[5] H. Wirth, E. Niemann, D. Panknin, W. Skorupa, Patent Nr. 198 08 246.0
[6] D.Panknin, H. Wirth, A. Mücklich, W. Skorupa, submitted to J. Appl. Phys.
[7] S.M. Sze, Physics of Semiconductor devices, J. Wiley, New York 1981
[8] B.I. Shklovski, A.L. Efros, Electronic Properties of Doped Semiconductors, Springer, Berlin 1984
[9] M.V. Rao, P. Griffiths, J. Gardner, O.W. Holland, M. Ghezzo, J. Kretchmer, G. Kelner, J.A. Freitas, J. Elec. Mat. 25 (1996) 75

Annealing and Recrystallization of Amorphous Silicon Carbide Produced by Ion Implantation

A. Höfgen, V. Heera, F. Eichhorn and W. Skorupa

Being one of the most promising semiconductor materials for high-temperature, high-frequency, and high-power electronic devices, silicon carbide (SiC) has attracted considerable interest during the last few years. In search of a processing technology which would be practicable for industrial scale SiC-device production, it turned out that conventional diffusion-based techniques fail due to the low atomic mobilities in SiC below 1700 °C [1]. Ion implantation doping also suffers from this problem. For instance, radiation damage in SiC is extremely stable, and the material is easy to amorphize [2]. This amorphization is accompanied by strong volume swelling. Unfortunately, there was only limited success in thermal annealing of amorphized SiC, which led to contradictory results in the literature. A temperature of about 1450 °C [3] was commonly accepted as the threshold temperature for the epitaxial recrystallization of implantation-amorphized SiC, whereas more recent investigations [4,5] have shown, that recrystallization can be achieved already at about 1000 °C. On the other hand, densification of a-SiC after thermal annealing at 500 °C was reported recently [6]. The authors infered the existence of a relaxed amorphous state from this behavior. In order to reveal the reason of this low temperature densification and to elucidate the thermal recrystallization behavior of amorphized SiC, a systematic investigation was performed on the densification of a-SiC by step height measurements after thermal annealing. X-ray diffraction (XRD) under grazing incidence was used to prove possible structural changes and the recrystallization of the amorphous layer.

Thick amorphous surface layers (1.75 µm) were produced by 2 MeV, 2×10^{16} Si$^+$/cm^2 implantation into single crystalline 6H-SiC wafers at room temperature (RT). Small areas of the wafers were covered by pieces of Si to obtain unirradiated regions for step height measurements. After implantation all wafers were cut into suitable pieces. The samples were annealed in argon atmosphere at definite temperatures. After each anneal, the samples were cooled to room temperature and their step height was recorded by using a DEKTAK 8000 mechanical surface profiler. X-ray diffraction analysis was performed on a Siemens D5000 diffractometer with a Cu radiation source. To get information mainly from the amorphous surface layer, it was important to minimize X-ray reflections of the crystalline 6H-SiC substrate which could overlap the amorphous signal. Therefore, X-ray 2θ-diffraction patterns were measured under grazing incidence, i.e., under a small (6 °) but fixed angle of incidence. In this case most of the substrate reflexes do not meet the Bragg condition and thus they do not appear in the spectra.

After amorphization a step height of (196±5) nm is observed, which clearly indicates strong volume swelling. In Fig.1 the step height of the Si implanted samples is shown as a function of the annealing time. Each curve corresponds to a sequence of isothermal annealing steps of one sample. Annealing at temperatures below 800 °C already results in a substantial reduction of the step height after 5 min. Further annealing up to 10 h changes the step height only negligibly. This means that the annealed layer arrived at a metastable state which is characterized by a higher density than that of the initial as-amorphized layer. Interestingly, the remaining step height decreases with increasing annealing temperature. Therefore, it can be assumed that a continuum of metastable states characterized by different densities can be produced by low temperature annealing. This is in agreement with recent results of Musumeci et al. [7], who found a continuum of metastable states with distinct optical properties after low temperature annealing of SiC amorphized with 200 keV Kr. At higher temperatures a second drop of the step height is found after continued annealing which ends up in a residual step height of only 40 nm. The
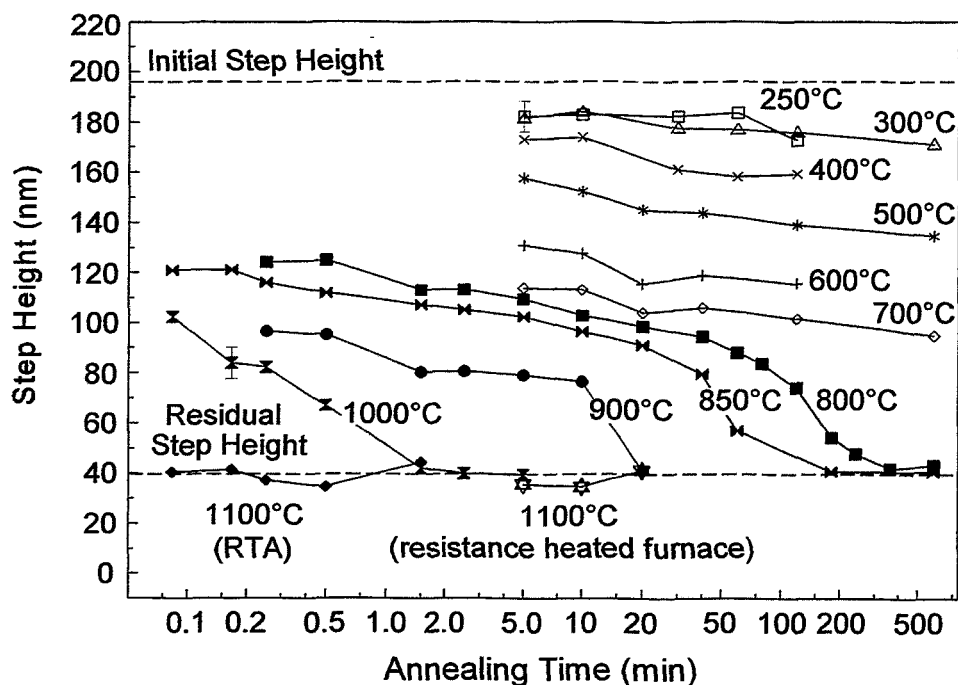
Fig. 1: Step height of the annealed samples as a function of the annealing time. The initial and residual step height are marked by dashed lines.

annealing time at which this second shrinking occurs decreases exponentially with increasing temperature. It is clear that the final state must be crystalline. Therefore, the second stage of step height shrinkage can be considered as a consequence of crystallization. A complete disappearance of the residual step height by crystallization cannot be expected since the structure is now polycrystalline [4,8] and the grain boundaries occupy additional volume.

To elucidate the nature of the two stages of annealing, we performed XRD measurements under grazing incidence. Fig. 2 shows the X-ray diffraction results. A diffraction curve (Fig. 2a) taken from the single crystalline 6H-SiC substrate (virgin) demonstrates the possibility of avoiding crystalline reflections from the substrate. As it is evident from Fig. 2, there is a clear difference between the results obtained after the first and second stage of annealing. The first group (Figs. 2c-2e) consists of low intensity, symmetric, broad, and featureless peaks, which are almost identical to the diffraction curve of the as-amorphized layer (Fig. 2b). Thus, it can be infered that no recrystallization did take place during the low temperature annealing. A quite different shape of the diffraction curve is observed after high-temperature, long-time annealing (Figs. 2f and 2g). In this case the step height is decreased to the final value of 40 nm. The intensities are markedly higher than that of the "amorphous signal ". Moreover, the peaks are asymmetric and have a substructure typical for polycrystalline SiC. By comparing the step height measurements (Fig. 1) and the X-ray diffraction curves (Figs. 2e and 2f) obtained after annealing for 1 and 10 h at 800 °C, a clear correlation between the second stage densification and the appearance of the polycrystalline diffraction pattern can be recognized. This means that the second stage densification is an unambiguous indication for crystallization.

On the other hand, the reason for the gradual increase of the density with temperature in the first stage of annealing is not quite clear. It cannot be understood in terms of partial recrystallization. The step height decrease obeys an Arrhenius law with an activation energy of $E_a=184\pm15$ meV.
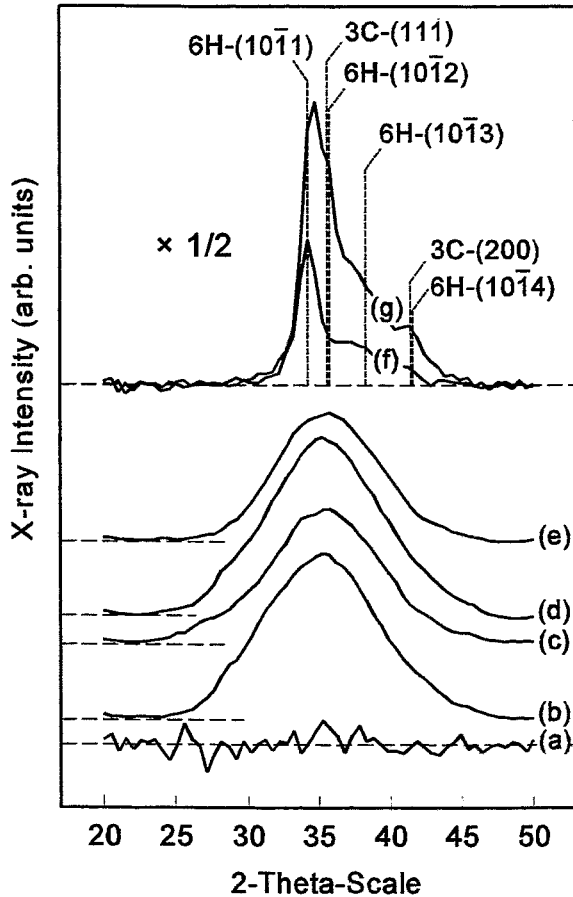
Fig. 2: X-ray diffraction curves under grazing incidence (6 °) of (a) virgin 6H-SiC, (b) an as-amorphized sample, and of samples annealed at (c) 300 °C for 10 h, (d) 500 °C for 10 h, (e) 800 °C for 1 h, (f) 800 °C for 10 h, and (g) 1000 °C for 5 min. Curves (b)-(e) are smoothed to suppress statistical noise.

This activation energy is much too low for crystallization processes in covalent materials. Typical values found in covalent semiconductors amount to some eV, e.g. 2.7 and 3.0-4.0 eV for solid phase epitaxial crystallization and randomly nucleated crystallization, respectively, of Si [9]. It has been discussed recently [6] that point defects cause the strong swelling of SiC during amorphization. In particular, interstitial atoms cannot be accommodated in the very dense SiC lattice. Consequently, the annihilation of point defects could lead to a remarkable densification. This possibility of defect annealing at temperatures below 1000 °C has been demonstrated by electron paramagnetic resonance (EPR) [10] and positron annihilation spectroscopy (PAS) [11] measurements. Therefore, we suggest that the activation energy for the low temperature annealing is attributed to defect annealing. Pino et al. [12] found a binding energy between a silicon vacancy and a carbon atom of 190 meV which is consistent with the activation energy found in the present experiments. The picture of point defect annealing is in agreement with the unchanged shape of the amorphous X-ray diffraction pattern recorded at different temperatures (Figs. 2b-2e), because short-range point defect annealing will not alter the basic structure of the amorphous network. In contrast to the low temperature annealing stage, the density increase at higher temperatures is determined by the crystalline fraction in the layer. Therefore, the crystallization kinetics can be determined from the observed step height changes. To describe the kinetics, we analyzed the step height decrease in the second stage of annealing in terms of the Johnson-Mehl-Avrami equation [13]. As shown in detail in Ref. [14] nucleated growth is the dominating crystallization mode during annealing between 800 and 850 °C. However, the recrystallization behavior changes at higher temperatures and epitaxial and columnar regrowth dominates at 1000 °C, which corresponds well to the result of previous TEM investigations [4,5,8].

It is known that strong compressive stress is generated in the initial phase of amorphization that is gradually released by volume swelling [15]. On the other hand, one can expect that tensile stress appears during the crystallization of the amorphous layer. In Fig. 3 a set of optical micrographs of the sample surface after annealing at different temperatures is shown. Already at 800 °C (Fig. 3a) a surface structuring starts and cracks along the cleavage plane parallel to the [11$\bar{2}$0] direction appear. Annealing at higher temperatures generates additional cracks along the

Fig. 3: Optical micrographs of the sample surfaces after annealing at (a) 800 °C for 2 min 30 s, (b) 900 °C for 2 min 30 s and (c), (d) at 1100 °C for 5 s. Images (a)-(c) were taken under dark field and image (d) under transmitted light illumination.

other cleavage planes (Fig. 3b) and results in the formation of triangular tiles (Fig. 3c and 3d). As evident from the trans-mission light micrograph (Fig. 3d) the bigger tiles are cracked off from the substrate as indicated from the curved interference pattern. Some tiles are removed and leave a crater (not shown in Fig. 3). Surprisingly, the crater is much deeper (about 4 μm) than the thickness of the amorphized layer. This implies that the stress which is generated during crystallization reaches far into the substrate and leads to substrate modification. The crackup of the surface is not observed after annealing of thin amorphous layers (70 and 165 nm) produced by 90 keV 5×10^{14} Ge$^+$/cm^2 and 200 keV 1×10^{15} Ge$^+$/cm^2 ion implantation into 6H-SiC wafers at RT. Therefore, it can be concluded that there exists a layer thickness in the range between 165 nm and 1.75 μm at which the accumulated stress exceeds a critical value. Further investigations are necessary in order to determine this critical thickness.

In summary, two stages of annealing were found for amorphous SiC. Each of them causes a specific densification of the amorphous layer. At temperatures below 700 °C point defect annealing processes are responsible for densification. Amorphous states with continuously varying densities can be produced in this first stage of annealing. Annealing at temperatures above 700 °C is characterized by a combination of defect annealing and recrystallization. The recrystallization produces stress in the layer which leads to surface cracking if the layer exceeds a critical thickness. Therefore, the formation of thick amorphous layers must be absolutely avoided in technological processes for electronic device production.

Acknowledgments

References

[1] R.F. Davies, G. Kelner, M. Shur, J.W. Palmour, J.A. Edmond, Proc. IEEE 79 (1991) 677
[2] V. Heera, W. Skorupa, Mater. Res. Soc. Symp. Proc. 438 (1997) 241
[3] H.G. Bohn, J. M. Williams, C.J. Mac Hargue, G.M. Begun, J. Mater. Res. 2 (1987) 107
[4] V. Heera, R. Kögler, W. Skorupa, J. Stoemenos, Appl. Phys. Lett. 67 (1995) 1999
[5] M. Ishimaru, S. Harada, T. Motooka, T. Nakata, T. Yoneda, M. Inoue, Nucl. Instrum. Methods Phys. Res. B 127/128 (1997) 195
[6] V. Heera, F. Prokert, N. Schell, H. Seifarth, W. Fukarek, M. Voelskow, W. Skorupa, Appl. Phys. Lett. 70 (1997) 3531
[7] P. Musumeci, R. Reitano, L. Calcagno, F. Roccaforte, A. Makhtari. M. G. Grimaldi, Philos. Mag. B 76 (1997) 323
[8] Y. Pacaud, W. Skorupa, J. Stoemenos, Nucl. Instrum. Methods Phys. Res. B 120 (1996) 181
[9] G.L. Olson, J.A. Roth, Mater. Sci. Rep. 3 (1988) 1
[10] R. C. Barklie, M. Collins, B. Holm, Y. Pacaud, W. Skorupa, J. Electron. Mater. 26 (1997) 137
[11] A. Kawasuso, H. Itoh, S. Okada, H. Okumura, J. Appl. Phys. 80 (1996) 5639
[12] A. D. Pino, A. M. Rappe, J. D. Joannopoulos, Phys. Rev. B 47 (1993) 12554
[13] J. W. Christian, The Theory of Transformations in Metals and Alloys (2nd ed.), Pergamon, Oxford 1975
[14] A. Höfgen, V. Heera, F. Eichhorn, W. Skorupa, J. Appl. Phys. 84 (1998) 4769
[15] R. Nipoti, E. Albertazzi, M. Bianconi, R. Lotti, G. Lulli, M. Cervera, A. Carnera, Appl. Phys. Lett. 70 (1997) 3425

Oxidation Protection of Intermetallic Ti50Al Using Ion Implantation of Chlorine

U. Hornauer, E. Richter, E. Wieser, H. Reuther, G. Schumacher[*], F. Dettenwanger[*] and M. Schütze[*]

[*]Karl-Winnacker-Institut der DECHEMA e.V. (Frankfurt a.M.)

γ-TiAl based intermetallic compounds are very promising for structural materials in high temperature application, because of the low density of 3.6 g/cm^3. The problems, which hinder the use of this material, are the low ductility at room temperature and the oxidation above 700 °C. Many efforts have been made to investigate the effects of ternary additives to improve the long term oxidation resistance, but the basic effects of oxidation and alloying ternary elements are still not understood completely. Because the equilibrium oxygen partial pressure of Ti/TiO and Al/Al$_2$O$_3$ is very similar [1], a mixed oxide layer is formed during oxidation. Whether a dense protective layer of Al$_2$O$_3$ is formed or a fast growing scale, depends on the local activity of the metals and the oxides formed, which is influenced by the oxygen partial pressure, but also by the alloying elements [2, 3]. In reference [4] it is found, that very small amounts of chlorine improve the oxidation behaviour dramatically. The 'Cl effect' protects TiAl even at very low Cl concentration below 500 ppm. As a first suggestion of the mechanism it is assumed that the fast growing TiO$_2$ is doped with Cl at oxygen sites. Charge neutrality leads to a suppression of oxygen vacancies, which reduces the oxygen diffusivity in TiO$_2$. Thus oxidation of Al is favoured. Schütze and Hald [5] propose a more sophisticated model based on thermodynamic calculations, in which the oxidation behaviour is determined by a catalytic process of volatile chlorides. At certain conditions the vapour pressure of aluminium chloride is higher than that for titanium chloride. This leads to a significant selective Al transport via pores and fissures. Therefore formation of Al$_2$O$_3$ is favoured in a specific depth in the scale. When the Cl concentration is too high both metals are transported, the positive Cl effect is expected to turn into a negative effect.

In the present work, a first systematic variation of Cl concentration is accomplished via ion implantation. In order to investigate the mechanism of the Cl effect, the dopant concentration and depth can be reproduced and controlled with high precision. This gives a possibility to make a fast screening of the implantation parameters to find optimum oxidation protection [6]. For application ion implantation can be used to make the Cl effect applicable also for cast material, since this effect is found only in powder metallurgically fabricated TiAl, where the Cl impurity of the titanium sponge stays in the alloy. Alloys, which are produced by casting will degas and the Cl content is negligible. Therefore a cast Ti50Al alloy is used in the present study. Specimens of the dimension 10 x 10 x 1 mm^3 were prepared from the ingot. After grinding they were polished with 4000 grit SiC paper. Before implantation organic substances were removed in an ultrasonic acetone bath. The samples were mounted on a water cooled sample holder using a special carbon foil to improve the heat contact. The implantations were performed using a 500 kV implanter (HVEE) and a high current tandetron (HVEE) for energies up to 3 MeV. In order to find the optimum parameters for the Cl concentration an extensive screening has been performed (200 keV - 2 MeV with constant fluence of 10^{16} cm^{-2} and 10^{15} - 10^{17} cm^{-2} at 1 MeV). In all cases the implantation temperature was below 70 °C. Both 100 mm^2 sides of the samples were implanted in order to optimise the thermogravimetric tests. The outer edges remained unimplanted (relative area < 20 %).

The element distribution was measured by depth profiling with Auger electron spectroscopy (AES). An approximated depth scale is achieved by determination of the final sputter crater depth and the assumption of a constant sputter rate. The implanted profiles closely follow the profiles predicted by the TRIM95 code [7]. The thermal treatment was done in a conventional furnace and in a rapid thermal annealing unit (RTA). Thermogravimetric oxidation tests (TGA) were performed at 900 °C in air (rel. humidity of 25% at 295 K) for 100 h using a thermobalance to continuously record the mass gain during oxidation.
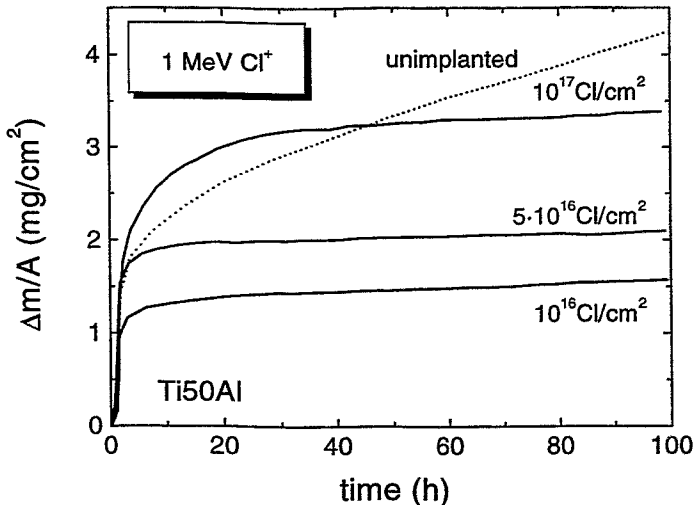
Fig. 1: Thermogravimetric oxidation tests (TGA) at 900 °C in air for 100 h [10]. Compared to an unimplanted sample (dotted line) the oxidation kinetics for $1 \cdot 10^{15} cm^{-2}$ and $5 \cdot 10^{15} cm^{-2}$ are unchanged (not shown). The Cl implanted samples (1 MeV, $1 \cdot 10^{16} cm^{-2}$-$1 \cdot 10^{17} cm^{-2}$) show a protective behaviour.
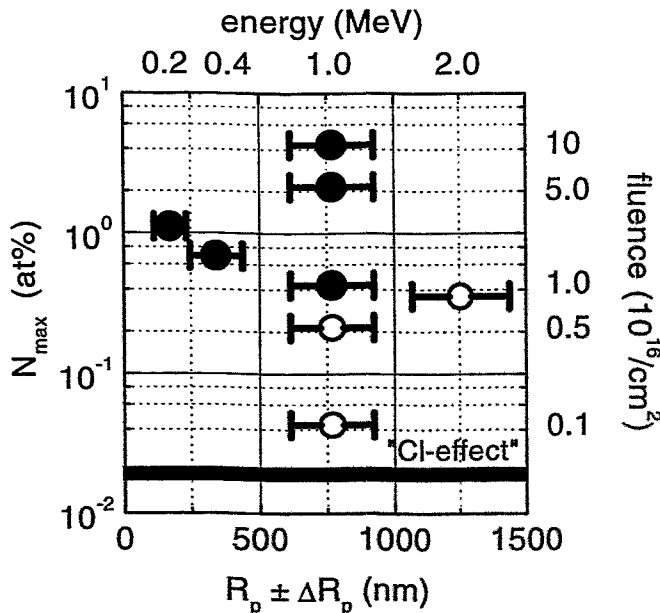
Fig. 2: Compilation of the Cl implantation parameters described in this study [10]. N_{max} represents the local concentration in the maximum of the profile at the depth R_p. The error bars mark the straggling ΔR_p. Closed symbols stand for TGA measurements showing a protective effect, for open symbols the oxidation is not improved. The line at 0.05at% represents the order of magnitude needed for the „Cl-effect" in bulk samples.

Fig. 1 shows the TGA results obtained with different fluences at 1 MeV [8, 10]. The specimens implanted with $10^{15} cm^{-2}$ and $5 \cdot 10^{15} cm^{-2}$ did not show a change in oxidation compared with the unimplanted sample Ti50Al (shown in Fig. 1). For a sufficiently high fluence (10^{16} - $10^{17} cm^{-2}$), the mass gain almost stops after an incubation period in the first hours. The oxidation kinetic is similar to that of Al_2O_3 forming materials. The oxidation rate after the incubation time is reduced by about 2 orders of magnitude and is nearly independent of the fluence. For the optimum dose ($10^{16} cm^{-2}$) it has been proven that this protection holds also up to 1000 h.

The duration of the incubation period increases with increasing concentration of Cl. This leads to an increase of the total mass gain after 100 h. For the highest fluence the mass gain in the beginning becomes even higher compared to the unimplanted material. That is an indication for a negative Cl effect as proposed in [5]. Following that model, based on a catalytic process of metal transport via volatile chlorides, at high Cl concentration both metals are transported significantly. If the Cl concentration decreases during oxidation, first the transport via $TiCl_3$ is reduced. An enrichment of Al leads to the formation of an protective Al_2O_3 layer within the scale.

The results of all implantations

33

are compiled in Fig. 2. A region of the protective effect is visible towards low energy and above a threshold of 10^{16} cm^{-2}. By varying the energy from 200 keV to 2 MeV, a comparable reduction of oxidation occurs for energies up to 1 MeV. No protection is found after 2 MeV implantation. As long as there is a local concentration in the order of 1 at% close enough to the surface, the protection appears to be independent of the implantation energy. If the Cl profile is too deep, the Cl concentration near the surface drops below this threshold. Compared to homogeneously doped material the concentration N_{max} needed for oxidation protection is about ten times higher. This can be explained by the limited Cl reservoir delivered by ion implantation in a shallow depth, whereas additional Cl is provided in the homogeneously doped material due to its fast diffusion in TiAl at 900 °C.

In order to monitor the redistribution of Cl and to get a deeper insight into details of the protection mechanism in the first stage of oxidation, a high dose implantation has been carried out (200 keV, $2 \cdot 10^{17}$ cm^{-2}). Changes in the near surface layer were studied by measuring AES depth profiles of Ti, Al, Cl and O after annealing at 900 °C for 1 min and 10 min. Because in the beginning a very fast oxidation takes place [9] and the maximum sputter depth of AES is limited, the annealing was done in pure Ar (O$_2$, H$_2$O, N$_2$ <5 ppm) to avoid a too fast oxidation. The as-implanted depth profile is shown in Fig. 3a. Already after 1 min at 900 °C (Fig. 3b) almost 70% of the incorporated Cl is lost out of the sample. An enrichment of Al in front of the Cl profile indicates an early stage of the formation of Al$_2$O$_3$. After 10 min at 900 °C (Fig. 3c) no titanium is detectable at the depth of about 400 nm and a

Fig. 3: AES depth profiles of the very first stage of oxidation [10]. (a) as-implanted (200 keV Cl$^+$, $2 \cdot 10^{17}$ cm^{-2}): Profile at a depth of 200 nm with a peak concentration of 30 at%. (b) 1 min at 900 °C: Almost 70% of the incorporated Cl is lost out of the sample. (c) 10 min at 900°C: At the approx. depth of 400 nm no titanium is detectable, a dense layer of Al$_2$O$_3$ has formed. (d) unimplanted sample at 900 °C for 10 min: No Al$_2$O$_3$ is formed.

dense layer of Al_2O_3 has formed. The Cl concentration decreases further. A local concentration of 1 at% Cl remains underneath to the Al_2O_3-layer. The pronounced structure of the oxide scale and the shallow penetration depth of oxygen compared to the unimplanted sample (Fig. 3d) show that already after 10 min the Cl effect is detectable. Hence this formation of the Al_2O_3-layer and its depth correlation with the remaining Cl confirm the model of Schütze and Hald [5]. The very low concentration of Cl in the outer TiO_2 contradicts the model of TiO_2 doping.

For an economically feasible application it is very interesting to reduce the implantation energy. This being successful, plasma immersion implantation (PI^3) could be used for a three-dimensional protection of e.g. components of turbines against oxidation. Beam line implantations at 15 keV for fluences from $5 \cdot 10^{15}$ cm^{-2} to $2.5 \cdot 10^{16}$ cm^{-2} were performed to prove that the Cl effect is also effective at low energy. The resulting AES depth profiles after an oxidation for 10 min at 800 °C in air show that a protective effect of Cl is obtained in the same range of fluence as for the high energy implantations. For the fluence of 10^{16} cm^{-2} an Al enrichment in the scale is found at the depth of the remaining Cl, which is not observed for the lower fluence. Long term TGA oxidation tests at 800 °C show a positive effect of this treatment for 10^{16} cm^{-2}.

It has been shown that it is possible to improve the oxidation resistance of Ti50Al using the microalloying effect. Cl implanted cast Ti50Al can be protected at 900 °C in air up to 1000 h. Therefore the oxidation and the mechanical properties of relatively cheap cast material could be optimised separately. A systematic screening of the implantation parameters shows that there is a narrow regime for the optimum fluence of Cl ion implantation. The implantation energy is not a sensitive parameter, because the implanted profile changes very quickly during high temperature oxidation. The results of the variation of the implantation parameters supports the catalytic model of Schütze and Hald [5].

Acknowledgements

References

[1] A. Rahmel, W.J. Quadakkers, M. Schütze, Materials and Corrosion 46 (1995) 217
[2] K. Maki, M. Shioda, M. Sayashi, T. Shimizu, S. Isobe, Mat. Sci. Eng. A 153 (1992) 591
[3] Y. Shida, H. Anada, Materials Transactions 35 (1994) 623
[4] M. Kumagai, K. Shibue, K. Mok-Soon, Y. Makoto, Intermetallics 4 (1996) 557
[5] M. Schütze, M. Hald, Mat. Sci. Eng. A 239-240 (1997) 847
[6] M.F. Stroosnijder, N. Zheng, W.J. Quadakkers, R. Hofman, A. Gil, F. Lanza, Oxidation of Metals 46 (1996) 19
[7] J. Ziegler, J. Biersack, U. Littmark, The stopping of ions in solids, program version 1995, Pergammon Press, New York 1995
[8] G. Schumacher, C. Lang, M. Schütze, U. Hornauer, E. Richter, E. Wieser, W. Möller, Materials and Corrosion, accepted for publication
[9] C. Lang, M. Schütze, Materials and Corrosion 48 (1997) 13
[10] U. Hornauer, E. Richter, E. Wieser, W. Möller, G. Schumacher, C. Lang, M. Schütze Nucl. Instr. Meth. B 148 (1999) 858

Structure of Laser Deposited Fe/Al Multilayers and their Modification by Ion Beam Mixing and Thermal Annealing

J. Noetzel, K. Brand[*], M. Dobler, H. Geisler[**], A. Gorbunov[**], A. Mücklich, F. Prokert, A. Tselev[**] and E. Wieser
[*] Institut fürAngewandte Physik, TU Dresden
[**] Institut für Werkstoffwissenschaft, TU Dresden

Metallic multilayers with a period length in the nanometer range are interesting both from the scientific point of view and for the development of nanoscale technology and nanostructures. Depending mainly on the mean kinetic energy of the deposited particles a transition region of a few monolayers to several nm between adjacent layers will develop. The structure - the phases and their morphology - of these transition layers often differs from the equilibrium behaviour of the binary alloy and may be very important for the properties of the system.

In this contribution the structure of the transition regions of laser deposited Fe/Al multilayers is investigated and further modified by ion beam mixing and thermal annealing. The multilayers were prepared by crossed beam pulsed laser deposition (CBPLD). This deposition technique is characterised by high kinetic energies (about 100 eV) of the deposited particles, very high cooling rates (up to 10^{11} K/s) and dense pulsed particle fluxes [1]. The intermixing of the incoming plasma particles with the previously deposited material can be divided into ballistic and chemical mixing as it is known from ion beam mixing. Ballistic mixing occurs first, when the kinetic energies of the particles are too high to be influenced by chemical forces. The particle movement is then controlled by collisional kinetics. When the particles slow down to an average kinetic energy of about 1 eV their movement is influenced by chemical forces [2]. During the chemical phase the mixing may increase if the system has a negative heat of mixing or become partly reversed if the heat of mixing is positive. Also the respective solubilities have an influence. It is possible to simulate the ballistic mixing and to compare the simulation with the experimentally observed mixing which is always the result of ballistic and chemical mixing. By this one can study the influence of chemical forces on the mixing process.

The system Fe/Al has a negative heat of mixing and is further characterised by a large difference in the atomic sizes and the equilibrium structure of both components. Fe exists in the loosely packed bcc structure, while Al exists in the dense fcc lattice. For this reasons the solubility of Al in Fe is much larger than vice versa. In thermodynamic equilibrium up to 20 at.% of Al may be solved in Fe, but only 0.04 at.% Fe in Al. Another consequence is that the intermetallic phases on the Fe rich side of the phase diagram have a simple structure and a wide range of existence. On the Al rich side complicated phases exist that occupy only very narrow composition regions. If Fe and Al are mixed by non-equilibrium processes like CBPLD, ion beam mixing, mechanical alloying, melt spinning, etc. the system has not enough time to form complicated structures, so rather simple non-equilibrium phases will be built. As the bcc structure of Fe is less dense than the fcc lattice of Al, up to 70 at.% of Al can be solved in Fe by non-equilibrium processes, but only 10 at.% of Fe in Al. For Fe with an Al content between 70 at.% and 90 at.%, an amorphous phase is formed according to the literature [3]. Considering this very different behaviour of Fe-rich and Al-rich alloys the transition regions in the multilayers are divided in an Fe-rich and an Al-rich side and discussed separately.

The multilayers were investigated using Rutherford backscattering (RBS) for composition and layer thicknesses, conversion electron Mössbauer spectroscopy (CEMS) for phases containing Fe and transmission electron microscopy (TEM) as an additional tool for phase identification. The multilayers have an overall thickness of about 100 nm and consist of four Fe and three Al

layers. Two additional Al layers separate the multilayer from the SiO_2 substrate and cover the surface to protect the multilayers from oxidation (see Tab. 1 and also Fig. 2).

Sample	Design
(a/b)	$SiO2$ - Al(25 nm) - 6x[Fe(7.2 nm)- Al(6.5 nm)] - Fe(7.2 nm) - Al(4 nm)
(c)	$SiO2$ - Al(5 nm) - 3x[Fe(18 nm)- Al(8 nm)] - Fe(18 nm) - Al(5 nm)
(d)	$SiO2$ - Al(5 nm) - 3x[Fe(17 nm)- Al(10 nm)] - Fe(17 nm) - Al(5 nm)

Tab. 1: The design of the discussed samples. The respective CEM spectra are shown in Fig. 1. The thicknesses were measured by RBS under the assumption of bulk density.

By CEMS one can determine the probability $p_{exp}(n)$ for an Fe atom of the sample to have $n=0,...,4$ nearest Al neighbours. The hyperfine magnetic field at the Fe nuclei depends on n. This is reflected in CEMS by different distances of the six lines of the spectrum of magnetically ordered Fe for different n (see Fig.1a). Fe with $n \leq 4$ is mainly found in the Fe-rich transition zone. Fe atoms in an Al-rich evironment have mainly $n \geq 5$ and are non-magnetic. They exhibit a single line if the neighbourhood of the Fe nucleus is of cubic symmetry. If the local environment is non-cubic, a doublet is emitted. It is possible to calculate expected probabilities $P_{theo}(n)$ from the simulated concentration profiles. As stated above, the simulation considers only ballistic effects while the measured probabilities show the result of ballistic and chemical mixing. Differences between the calculated $P_{theo}(n)$ distribution and the measured one show the influence of chemical forces in the deposition process (see Ref. [4], for details).

For the Fe-rich side of the as-deposited state it is found by CEMS that the experimental $p_{exp}(n)$ are twice as high as it could be expected from ballistic simulations. As this factor of two is nearly independent of n it can be concluded that amount and mixing depth of Al into Fe is increased by chemical forces. No ordered equilibrium phases like Fe_3Al and FeAl were found, but an Fe-rich solid solution. This is proven by the fact that none of the characteristic "fingerprints" of these ordered phases were found by CEMS. In addition, X-ray diffraction (XRD) shows no superlattice lines of the ordered phases. The Al-rich side of the transition layer is characterised by a doublet in the CEM spectrum (Fig. 1a), that could correspond to several non-cubic Al-rich phases, including Fe_2Al_5, quasicrystalline and amorphous phases. Here TEM investigations are necessary. Fig. 2a shows a cross sectional view of a multilayer. Due to the higher atomic number, the "Fe layers" (Fe and Fe-rich transition region) appear darker then the "Al layers" (Al and Al-rich transition region). In the Al layers diffraction contrast is only occasionally found as islands in the middle of the layer. Fig. 2b shows a high resolution image of such an area. The island is separated from the Fe layers by disordered, amorphous zones. The thickness and the morphology of the disordered zone depends on the sequence of deposition. In the case of Al deposited on Fe ("Al on Fe", see Fig. 3a) the amorphous zone is quite smooth , so an average thickness of about 3-4 nm can be derived from the high resolution image (Fig. 3b). In the "Fe on Al" case the amorphous band appears thinner but is very rough, so it is not reasonable to measure a thickness in this case (Fig. 3b). It can be concluded that in Al layers with an areal density below $5x10^{16}$ at/cm^2 ($\cong 8$ nm pure Al of bulk density) the amorphous Al(Fe) regions already overlap.

The transition layers were modified by ion beam mixing using 150 keV Fe^+ ions and a fluence of 10^{15} at/cm^2 and by thermal annealing in vacuum at 573 K for up to 1h. The former is another non-equilibrium process, the later will drive the system towards thermodynamic equilibrium.
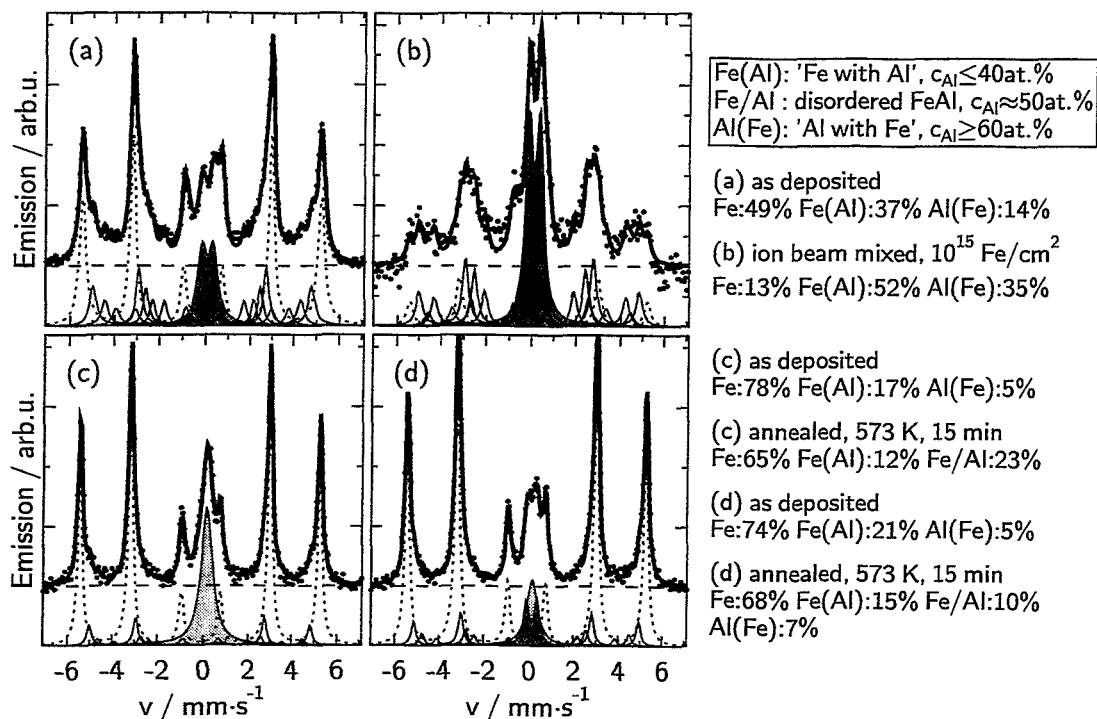
Fig. 1: Typical CEM spectra for the discussed states. Markers are the measured values and thick solid lines are the fitted spectra that consist of several subspectra (drawn with offset). The relative area of the respective subspectrum is listed on the right of the figure. For the samples (c) and (d) the values are also given for the as-deposited state that is not shown. Dotted lines are Fe with $n=0$ and thin solid lines are Fe with $n=1,...,4$ (called Fe(Al)). Phases with $n\geq5$ are the cubic, disordered FeAl ('Fe/Al', drawn with light grey filling) and the non-cubic phases ('Al(Fe)') that are coloured in dark grey.

(a) The as-deposited state (see also Fig. 2a). (b) The same sample, ion beam mixed. (c) A sample with 8 nm thick Al layers annealed at 573 K for 15 minutes. (d) A sample with 10 nm thick Al layers, also annealed at 573K for 15 minutes. The design of the samples is listed in Tab. 1.
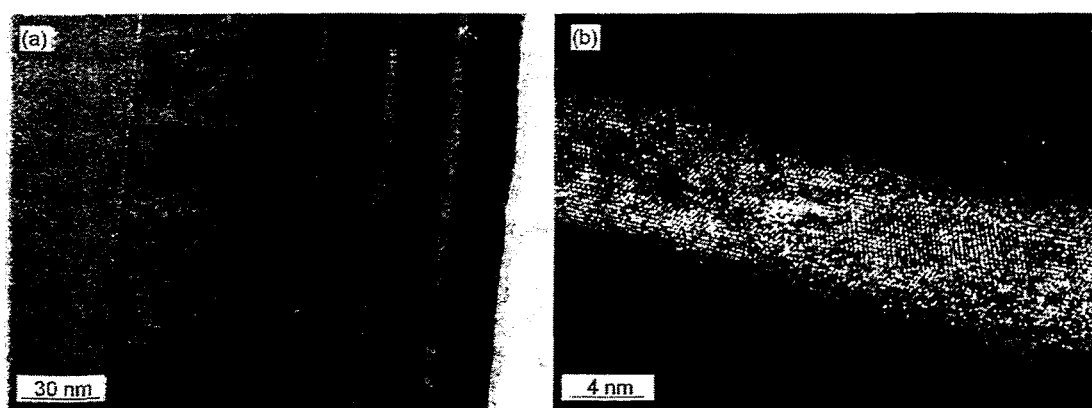
Fig. 2: (a) TEM image of a multilayer. Due to the higher atomic number, Fe appears darker than Al. The "Al layers" show diffraction contrasts only as islands in the centre of the layers. (b) HR-TEM image of an Al layer with islands. The island is separated from the Fe layers by disordered, amorphous zones.

Fig. 1b shows the CEM spectrum of a mixed sample (the as-deposited state is shown in Figs. 1a and 2). As expected, the amount of Fe with $n=1,...,4$ increases from 38% to 52%. Again no ordered phase can be detected, the Fe-rich side is still a random solid solution of Al in bcc-Fe.

The amount of Fe with $n \geq 5$ increases from 14% to 35%. This cannot be explained by an increase of the width of the amorphous layer, because in this sample the Al is completely amorphized by incorporated Fe. So the ion beam mixing increased the Fe concentration in the Al-rich region. TEM investigations suggest a phase transformation from the amorphous state to a non-cubic nanocrystalline phase.
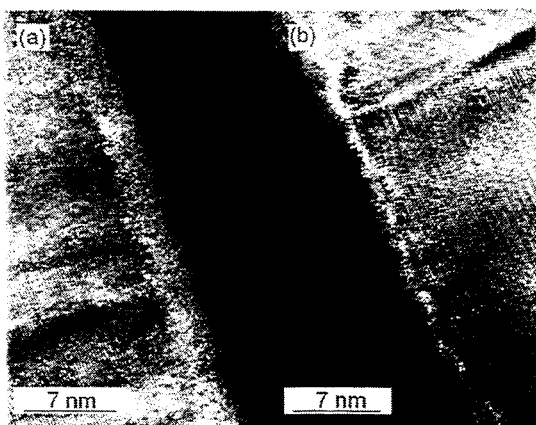
Fig. 3: TEM images of the transition layer formed by different deposition sequences.
(a) TEM image of the „Al on Fe" case. The Al-rich side of the transition layer is a smooth band interrupting the columnar structure of the Al layer. The width of the disordered, amorphous zone is about 3-4 nm.
(b) TEM image of the „Fe on Al" case. The transition region is thinner and rougher than in the former case.

The results of thermal annealing depend on the thickness of the deposited Al layers. For the as-deposited state it was found that thin Al layers (d_{crit}=5x10^{16} at/cm^2) will be completely mixed with Fe, while the deposition of thick Al layers leads to crystalline Al layers with an amorphous transition region. Fig. 1c shows the CEMS result for a sample with 8 nm Al layers, annealed at 573 K for 15 minutes. The doublet is replaced by a broad single line indicating the formation of a disordered bcc solid solution with an FeAl-like composition. This observation is also confirmed by TEM. A sample with 10 nm Al (Fig. 1d) shows a singlet and a doublet, so in this case also a non-cubic Al-rich phase exists beside the FeAl-like phase. TEM confirms that the metastable amorphous phase was transformed into a non-cubic crystalline phase.

The investigations show that the structure of laser deposited Fe/Al multilayers is determined not only by the non-equilibrium character of the CBPLD process, but also by the structural differences between Fe and Al. Amorphous and non-cubic phases are obviously needed as a bridge between the bcc structure of Fe and the fcc structure of Al.

Acknowledgements

References

[1] A. Gorbunov, W. Pompe, A. Sewing, S. Gaponov, A. Akhsakhalyn, I. Zabrodin, I. Kaskov, E. Klyenkov, A. Morozov, N. Salaschenko, R. Dietsch, H. Mai, S. Völlmar, App. Surf. Sci. 96-98 (1996) 649
[2] F. Saris, in: Structure-Property in Surface-Modified Ceramics, ed. C. McHargue, pages 103-116, Kluwer Academic Publishers, 3rd edition, Dordrecht 1989
[3] H. Sheng, Y. Zhao, Z. Hu, K. Lu, Phys. Rev. B 56 (1997) 2302
[4] J. Noetzel, K. Brand, H. Geisler, A. Gorbunov, A. Tselev, E. Wieser, W. Möller, to be published in Applied Physics A

Short
Contributions

Hard Coatings

W. Fukarek
C. Fitz
A. Kolitsch
B. Schmidt

In situ measurement of stress in thin films

A laser based system has been set up that allows the mechanical stress in thin films to be measured dynamically during processing. The system combines the measurement of bending of a cantilever (laser deflection) with reflectometry and thus, besides the stress also the actual film thickness during growth can be determined. The system has been applied to the measurement of dynamic stress induced in Si <100> during amorphization by Ar ion implantation.

The stress in thin BN films during deposition by IBAD has been analyzed. The formation of the cubic phase (c-BN) has been found to result in an abrupt increase in the compressive stress in the growing film. Growth rate variations that have been identified by SE measurements previously are also reflected in the dynamic stress data.

X. Wang
A. Kolitsch
W. Fukarek
S. Oswald[*]

Effects of Ti and Al incorporations on the structure of BN thin films

Boron nitride (BN) based composite thin films have been prepared by IBAD employing two electron beam evaporators. 3~5 at.% either Ti or Al was incorporated into the BN films. FTIR spectroscopy was used for phase identification. It has been found that no cubic BN (c-BN) can be formed for Al containing BN films for the used ion-bombardment parameters. However, the disturbance of 3~5 at.% Ti addition depending on the preparation conditions for the BN thin films, only shifts the N/B-ration threshold of the IBAD process which is required for c-BN formation to a higher value. In order to understand the different behaviours of the Ti and Al incorporations, the chemical states of the Ti and Al additions in the BN composite films were examined by XPS, indicating preferential formation of TiB_2 and AlN, respectively. The formation of AlN takes nitrogen from the system resulting in a boron overstoichiometry and prevents the c-BN nucleation.

Collaboration: *Institut für Festkörper- und Werkstoffforschung, Dresden

X. Wang
A. Kolitsch
A. Mücklich
D. Manova
W. Fukarek

A multilayer configuration of TiN/BN deposited by IBAD

The microstructure of BN/TiN multilayers prepared by IBAD was investigated by HRTEM. Special attention has been paid to the two types of interfaces, BN on TiN and TiN on BN, which are associated with two different growth sequences. The layer structure in the BN part of the film shows no interfacial amorphous layer on the TiN, which is commonly observed in BN monolithic thin films on Si substrates. In certain case, a fixed crystallographic orientation relation, rather than a disordered connection, has been found between TiN/BN interfaces but also between TiN and the underlying BN. The adhesion and therefore the correlating lifetime of the c-BN films on TiN was drastically higher than on other substrates. The deposition of nanoscaled TiN/BN multilayer films up to 20 nm single film thickness leads only to h-BN films caused by the to low BN film thickness for the c-BN nucleation. With increasing BN film thickness the typical c-BN nucleation and growth was obtained. The practical application of the TiN/BN multilayer structure as superhard coatings needs an optimization of the film thickness of both film types in the system.

A. Kolitsch

Synthesis and characterization of nitrogen containing carbon films

CN_x films were prepared by IBAD for sample circulation in the TMR network in order to characterize the mechanical properties, the film structure, the stoichiometry and the chemical state. Substrate temperature (ranging from RT to 1000°C), assisting ion energy (200 to 1200 eV), and ion-to-atom transport ratio were varied to maximize the nitrogen content in the films. The highest nitrogen content of the IBAD films is about 33 at.% at nitrogen to carbon transport ratios from 1.2 to 1.3 and substrate temperatures between 200 and 300°C. The influence of the ion energy on the nitrogen content of the films is low. TEM investigations with selected area diffraction show graphitization with increasing crystal size at increasing deposition temperature from 600 to 1000°C, and a decreasing nitrogen content of the CN_x films.

Collaboration: University of Stockholm, University of Linköping, University of Newcastle, Universite Paris-Sud, CNRS

W. Fukarek
U. Kreißig
R. Grötzschel
V. Stundžia*
D. Slavínská*
J. Žalman*
H. Biederman*

Composite Ge/C:H films prepared in an unbalanced magnetron

Composite films Ge/C:H (Ge doped hard plasma polymer (C:H)) have been deposited using an unbalanced planar magnetron equipped with a germanium/graphite target and operated in an Ar/n-hexane gas mixture. The composition of the films has been determined by RBS, ERDA and XPS. Ge concentrations up to 30 at.% have been confirmed. Ge depth-distributions have been found to be rather homogenous or decrease towards the surface due to target poisoning effects. TEM investigations revealed that Ge forms clusters with a maximum diameter of 2 nm embedded in a C:H and GeC alloy matrix. DC electrical properties have been measured in the planar electrodes-composite film-configuration. The electrical conductivity has been found to be strongly dependent on germanium concentration and on substrate temperature during deposition. Current-voltage characteristics are linear at low and super-linear at higher electrical fields, respectively.

Collaboration: * Faculty of Mathematics and Physics, Charles University, Prague

H.-U. Jäger

Molecular-dynamics simulations for a steady-state growth of carbon ion deposited tetrahedral amorphous carbon films

Molecular dynamics calculations were performed to simulate ion beam deposition of diamondlike carbon films. The number of carbon atom impacts was large enough that steady-state film properties could be computed and analyzed. Empirical many-body potentials based on Tersoff's covalent-bonding formalism were used. The calculations with Brenner's hydrocarbon potentials, which include overbinding corrections and nonlocal effects, predict films of high density, but with a fraction of fourfold coordinated carbon atoms of only a few percent. Such an unreal "compressed graphite"-like structure is favoured by the small cutoffs for the near-neighbour pair interactions in the Brenner potentials. If a larger C-C interaction cutoff value is chosen, which is still consistent with the bond-order concept, a distinct improvement can be achieved in modeling the sp^3 content of 20-90 eV C^+ ion deposited films.

Plasma-Immersion-Ion-Implantation/Low-Energy Ion Implantation

S. Parascandola
O. Kruse
M. Betzl
E. Richter

Nitrogen retention and loss during ion nitriding of austenitic stainless steel

Nitrogen transport mechanisms relevant for the understanding of ion nitriding of austenitic stainless steel were investigated. During low-energy nitrogen implantation time- and depth-resolved quantitative compositional analysis was performed by ERDA. Molecular nitrogen from the residual gas does not contribute to the nitriding even if no oxide layer is present on the surface of the samples. At a temperature of 320°C no significant nitrogen loss due to out-diffusion could be detected. The influence of the surface oxide layer on the amount of retained nitrogen was systematically examined at a temperature of 320°C, an ion energy of 2 keV and an ion flux of 0.2 mA/cm^2 by varying the oxygen partial pressure of the residual gas. Glancing angle XRD revealed the formation of expanded austenite. The amount of nitrogen retained was measured by NRA and shows a maximum at an oxygen partial pressure of 3×10^{-4} Pa. At this oxygen partial pressure during the nitriding process a stationary oxygen areal density is observed corresponding to a few monolayers assuming a stoichiometric Fe_2O_3 layer. This result sustains the assumption that the nitrogen retention can be optimized by implanting nitrogen behind a surface oxide layer.

T. Telbizova
S. Parascandola
O. Kruse
A. Mücklich

Ion nitriding of aluminium

Polycrystalline aluminium has been ion nitrided from a Kaufman ion source. The role of temperature was examined over a range from 100°C to 500°C at fixed process conditions of 1 keV ion energy, 0.2 mA/cm^2 ion flux and 15 minutes processing time. Additionally the role of the ion flux was investigated over a range from 0.05 mA/cm^2 to 1 mA/cm^2 for 15 min at a fixed temperature of 400°C. During processing *in-situ* time- and depth-resolved compositional analysis was performed by ERDA. It was observed that for all process parameters the native surface oxide layer is completely removed within 2 min and subsequently nitriding takes place. The N depth profiles were analyzed using RBS. The N/Al-ratio is about 1 for all samples treated at temperatures above 300°C. For the highest ion flux TEM shows a dense and continuous layer of 3 μm thickness. Diffraction analysis of the sample treated at the highest temperature shows aluminium nitride nanocrystals of hexagonal structure.

supported by
SMWA

R. Günzel
E. Richter
V.V. Uglov*
V.V. Khodasevich*
A.K. Kuleshov*
J.A. Fedotova*
D.P. Rusalsky*

Improvement of the mechanical properties of AISI M2 steel after nitrogen PIII treatment

The influence of nitrogen PIII on the mechanical properties of AISI M2 steel was investigated. An implantation voltage of 40 kV was applied in the fluence range of $2\text{-}8 \times 10^{18}$ ions/cm^2, at a sample temperature of 380°C. The maximum hardness of M2 steel after PIII treatment is observed for implan-tation fluences of 4 and 8×10^{18} ions/cm^2. The hardness reaches the value of ~25 GPa which is more than 2 times larger than the hardness of untreated steel, while the friction coefficient is reduced by 50 %. CEMS analysis indicate that nitrogen implantation significantly changes the local iron environment, with an implantation-induced paramagnetic phase being dominant. This phase is most probably attributed to a γ-Fe(C, N) fcc structure with

nitrogen at interstitial sites. CEMS and AES investigations reveal that the phase transition into highly doped (up to 40 at.% N+C) austenite occurs in a shallow surface layer of about 0.1 μm thickness.
Collaboration: *Minsk State University, Belarus

S. Mändl
E. Richter
R. Günzel

Nitrogen PIII into high speed steel

High speed steel (HSS) is a standard material for cutting tools with operation temperatures up to 500°C. PIII is a technique suitable for surface modifications at moderate temperatures around 300-400°C. The diffusion behaviour of nitrogen during PIII and subsequent annealing was investigated to see whether low temperature implantation's are suitable for HSS tools. Nitrogen implantation using PIII into M3 HSS at 400°C at fluences between 1 and $6x10^{18}$ atoms/cm^2 was performed. The depth profiles were determined using GDOS-technique. Additionally depth-resolved micro-hardness measurements were performed. The hardness increased from 10 GPa for untreated HSS to 18 GPa after nitrogen PIII treatment. During PIII treatment a nitrogen diffusion constant of $1.75x10^{-9}$ cm^{2}s^{-1}, well within the range reported for nitrogen in b.c.c. Fe, was observed from the concentration profiles. After annealing at 400°C for 1 h, neither a change in the diffusion length nor in the retained dose is observed. The quality of the fits was considerably increased when the free carbon, not trapped in carbide precipitates is additionally included in the fits. Possibly, the implanted nitrogen is bound in the diffusion layer in microprecipitates at grain boundaries and dislocations. This view is corroborated by the enhanced contrast seen in the SEM cross-sections, whereas these precipitates would not contribute to an XRD signal as the size is too small.

E. Richter
R. Günzel
S. Mändl

Nitrogen and boron double implantation into austenitic stainless steel

Nitrogen and boron double implantation into austenitic stainless steel (SS-316L) were performed to enhance further the beneficial properties of nitrogen implantation, especially to reduce the brittleness of the near surface region. Nitrogen was implanted at first using PIII at a temperature below 400°C. The formation of a solid solution of nitrogen in the stainless steel ("expanded austenite" or "S-phase") has been characterized by XRD measurements. Boron was subsequently implanted in this first experiment using a conventional ion implanter. The effects of the boron implantation were compared with the expanded austenite samples annealed for the same duration as the boron implantation. No significant diffusion of the boron is observed, whereas the pre-implanted nitrogen shows additional diffusion during the boron implantation. The boron implanted specimens exhibit an even higher wear resistance (factor of 2) correlated with a slightly decreased surface hardness, than the already excellent values for expanded austenite.

Semiconductor Materials

SiC / Diamond

V. Heera
J. Stoemenos*
B. Pecz**

Epitaxial aluminium carbide formation in 6H-SiC by high dose Al$^+$ implantation

The phase formation after high dose Al ion implantation into single crystalline 6H-SiC at elevated temperature has been investigated by combined planar view and cross-section TEM. Fluences of 1×10^{17}cm^{-2} and 3×10^{17}cm^{-2} Al$^+$ ions at an energy of 350 keV have been implanted into (0001)-oriented 6H-SiC single crystalline substrates at a temperature of 500°C. Aluminium carbide and Si precipitates were detected around the maximum of the Al depth distribution at a fluence of 3×10^{17}cm^{-2} ions. Precipitation was not observed at a fluence of 1×10^{17}cm^{-2}. This means that Al implantation into 6H-SiC at 500°C leads to the decomposition of SiC into Al$_3$C$_4$ and Si if the Al concentration exceeds a threshold value which is between 5 and 15 at.%. Surprisingly, all of the Al$_4$C$_3$ and most of the Si precipitates are epitaxially aligned with the surrounding SiC matrix. Transition metal carbides have a high electrical conductivity and thermal stability. Therefore, epitaxial layers of Al$_4$C$_3$ in SiC could be interesting for contact formation and wiring.
Collaboration: *Aristotle University of Thessaloniki, Greece; **Research Institute for Technical Physics and Materials Science Budapest, Hungary

V. Heera
M. Voelskow
W. Skorupa

Inhomogeneity of amorphous SiC layers produced by ion implantation

Amorphous (a) surface layers in SiC produced by ion implantation at room temperature are thicker than predicted from the critical energy density model. Annealing below the recrystallization temperature of about 900°C causes an interfacial regrowth which stops after a short distance. This is obviously the consequence of a layer substructure. One idea to explain this inhomogeneity is that the low-temperature-annealable part of the a-layer was amorphized at lower damage energy because it is stabilized by the implanted impurity atoms. In order to test this idea the regrowth behaviour of the a-layer during low temperature annealing is investigated as a function of implantation temperature. Amorphous surface layers were produced in 6H-SiC by 200 keV Ge$^+$ implantation with a fluence of 1×10^{15} cm^{-2} at temperatures of 100 K, 200 K and 310 K. They were subsequently annealed at 500°C for 1h. The thicknesses of the a-layers in the as-implanted state as well as in the annealed state were measured by RBS/C. A dramatic effect of the implantation temperature is found on the regrowth behaviour during low temperature annealing. The regrowth distance increases with decreasing implantation temperature. According to this result there is no correlation between the impurity profile and the low-temperature-annealable part of the a-layer.

F. Eichhorn
N. Schell
W. Matz
R. Kögler

Formation of 3C-SiC particles in Si after implantation of C

Implantation of C ions with an energy of 195 keV into Si wafers heated up to 800°C results in an elastic distortion of the Si host lattice and in the formation of crystalline SiC particles or their prestages depending on implantation dose and temperature. Synchrotron XRD at the Rossendorf beamline in Grenoble (ROBL) was used to reveal phase formation and the correlated lattice strain changes. A strong Si lattice deformation was observed if the fluence does not exceed 5×10^{15}ions/cm^2. After implantation of C ions up to

$4 \times 10^{17} \text{cm}^{-2}$ at a temperature of 500°C prestages of Si-C and an altered state of Si lattice deformation are found. By implantation of 4×10^{17} ions/cm² at 800°C small particles of the 3C-SiC (β-SiC) phase grow. They are aligned in such a way with the Si matrix, that the cubic crystallographic axes of matrix and particles coincide within an accuracy of 3°.
Collaboration: ROBL-CRG, ESRF Grenoble

W. Fukarek
R.A. Yankov
M. Voelskow
V. Heera
G. Brauer
W. Anwand

Damage in 6H-SiC induced by RBS analysis

Damage in SiC generated by ion implantation or irradiation is usually analyzed by RBS/C using MeV He⁺ ions, a technique which is considered to be largely non-destructive. Swelling of 6H-SiC induced by He⁺ implantation is observed at fluences commensurate with, or lower than those commonly used for obtaining RBS/C spectra of desirable statistics. The swelling increases by about 40% if the He⁺ ions are implanted in a non-channeling direction. An optical damage depth-profile, with distinct optical properties corresponding to the regions of electronic and nuclear stopping, is obtained from a fit to PIRR data and compared to TRIM calculation. In addition, the formation of high concentrations of deep-reaching (μm range) defects due to RBS/C is confirmed by SPIS measurements. AES shows that the specific color of the implanted area is not due to the deposition of a thin surface film during He⁺ implantation, and the swelling is not related to chemical reactions in the near-surface region. The formation of additional disorder from RBS/C may corrupt the respective data obtained subsequently by other analytical techniques.

W. Anwand
G. Brauer
P.G. Coleman*
M. Voelskow
W. Skorupa

Characterization of defects in ion implanted SiC by SPIS and RBS methods

A buried $(SiC)_{1-x} (AlN)_x$ layer has been prepared by ion co-implantation of N⁺ and Al⁺ into a 6H-SiC n-type wafer. The substrate temperature during implantation was varied from 200°C to 800°C in order to reduce the damage created by ion implantation. The obtained structures have been investigated by SPIS and RBS/C. Both methods are sensitive to different kinds of defects and give complementary information. Damage seen by RBS/C after implantation at 200°C is commonly defined as 100 % and extends from surface to a depth of about 270 nm. By SPIS it is revealed, that the dominating defect up to this depth are vacancy agglomerates consisting of about five Si-C divacancies. At higher implantation temperatures, RBS/C reveals a decrease of damage in the implanted region to about 80 %, whereas the damage between surface and the implanted region drastically decreases to 10 %. From SPIS it can be seen that now the dominating defect in the implanted region is the Si-C divacancy, whereas in a narrow layer of about 50 nm close to the surface very large agglomerates are formed consisting of up to 21 Si-C divacancies.

supported by
DFG and SMWK

Collaboration: *School of Physics, University of East Anglia, UK

G. Brauer
H. Wirth
W. Skorupa
M. Gong*
C.V. Reddy*
C.D. Beling*

Deep level traps in the extended tail region of ion implanted n-type 6H-SiC

SPIS has revealed the existence of deep reaching vacancy-type defects, most probably mono-vacancies, far beyond the ion implantation range calculated by TRIM code in 6H-SiC. This unexpected finding initiated the search for these defects and their description by an independent method, i.e. deep level

S. Fung*

transient spectroscopy (DLTS). DLTS studies have been performed in the tail region of boron as well as aluminium-implanted n-type 6H-SiC which is of technological importance. In boron-implanted material DLTS show the existence of the D center consisting of boron-vacancy complexes. In Al-implanted material a more complicated family of implantation damages, including the inequivalent occupation of cubic and hexagonal lattice sites by Al atoms, is found which probably is vacancy-related.

Collaboration: *University of Hong Kong

T. Gebel
D. Panknin

Spreading resistance measurements on 6H-SiC
SR-measurements at bevelled samples are used as a standard method to determine charge carrier profiles in silicon. However, for wide bandgap semiconductors the high contact resistance determines the measured resistance. With a selective influence on the surface states the contact barrier can be lowered. Therefore, after the bevelling procedure methods like polishing with diamond emulsion of different grain sizes, vacuum annealing (1300 - 1400°C, 5- 10 min) or ion sputtering (3 keV Ar ions) have been carried out in order to check their influence to surface states. It was found that after a vacuum annealing process (1350°C, 10 min) the barrier resistance decreased but fluctuations of the measured resistance increased. Best results were achieved after sputtering with 3 keV Ar ions. A decrease of the contact resistance of up to two orders of magnitude was obtained and fluctuations dropped drastically. A first calibration of the SR-equipment for further measurements on SiC was achieved using Hall effect data taken at 6H-SiC samples.

D. Panknin
H. Wirth
A. Mücklich
W. Skorupa

Electrical and microstructural effects in highly boron implanted 6H-SiC
B^+ ions were implanted at 400°C into 6H-SiC EPI layers to form a buried (100 nm) 500 nm thick layer with plateau concentrations up to $1.5 \times 10^{21} cm^{-3}$. The electrical and microstructural effects were investigated using temperature dependent Hall measurements, XTEM and SIMS analysis. After annealing at temperatures between 1550 and 1750°C (10 min) for boron concentrations above the solubility extraordinary boron out-diffusion and Ostwald ripening is observed forming extended boron clusters. For boron concentrations near the solubility the out-diffusion is reduced. These effects are confirmed by Hall effect measurements showing a stagnation of the hole concentration with increasing boron concentration above $1.5 \times 10^{19} cm^{-3}$. The electrical activation is limited by the solubility of boron in SiC at about 1600°C. Higher boron concentrations as well as higher annealing temperatures, inclusive during short time annealing at about 2000°C, do not lead to higher activation.

F. Fontaine
J. von Borany
F. Blum*

Self-consistent calculations of the hole concentration in diamond and silicon carbide
In the case of highly doped-highly compensated semiconductors, the widely used Boltzman hole-statistics is not able to describe the temperature dependent hole concentration. With the aim of better understanding the doping properties of p-type diamond and p-type 6H-SiC, we have adapted a model which was originally developed for n-type silicon. The model is based on a

full Fermi hole-statistics and further takes into account (i) the screened interaction between free holes and ionised acceptors, which leads to the upward shift of the valence band-edge; (ii) the local potential fluctuations due to the random distribution of acceptors and donors, which smears out valence states into the band-gap; and (iii) the interaction between nearest neighbouring acceptors, which spread the acceptor level into an impurity-band. In diamond, because the hole effective-mass is not precisely known, we could only compare the calculations with the experimental activation energies. Quantitative agreement was obtained for acceptor concentrations up to 10^{20} cm^{-3} and for compensation ratios up to 64%. In 6H-SiC we could benefit from a better knowledge of the hole effective-mass. The calculations correctly described the experimental hole concentrations, even for low dopant concentrations-high compensation ratios as well as high dopant concentrations-low compensation ratios. Finally, we could determine the compensating donor concentration in the case of low acceptor concentrations, which was previously not possible using other models.

Collaboration: *FernUniversität Hagen, Fachbereich Elektrotechnik

F. Fontaine
J. von Borany
F. Blum*
S. Waidman**

Ion implantation into diamond at elevated temperatures
Natural diamond substrates (IIa-type, DRUKKER) were implanted wit B ions at temperatures between RT and 1300°C. RBS/C investigations reveal reduced damage above 400°C and no distortion of the crystalline order (within the sensibility of RBS) for implantation temperatures above 800°C. The examination of the implantation profiles by SIMS and RBS indicates that there is no significant boron diffusion even for 1300°C implantation temperature. Without any further annealing a doping effect could be observed after an implantation at 1300°C. The mobility was measured to be about 90 cm^2/Vs. In addition, CVD diamond films deposited onto Si substrates were implanted with B or Li ions at 1000°C. Due to the structure of the CVD films (columnar grains separated by conductive grain boundaries) the electrical conduction of the diamond film is shunted via the Si substrate and could not be measured.

Collaboration: *FernUniversität Hagen, Fachbereich Elektrotechnik; **Institut für Festkörper- und Werkstofforschung Dresden

Defects and Gettering in Silicon

M. Posselt

Development of a novel method to study defect production and evolution during and after ion implantation into silicon
The as-implanted defect structure in silicon is still not fully understood. However, its precise knowledge is decisive for the detailed understanding of the interplay between damage accumulation and channeling effects during implantation and of defect-assisted processes at post-implantation annealing. State-of-the-art atomistic simulations of these effects employ phenomenological models as "substitute" for the lacking information about the as-implanted damage. In order to estimate the extent of the as-implanted damage created by keV ions under realistic implantation conditions time-ordered computer simulations based on the binary collision approximation (BCA) and classical molecular dynamics (MD) simulations were combined. BCA simulations are applied to ballistic processes with energies above several

10 eV. Processes with lower characteristic energies are treated by MD simulations. They yield the as-implanted defect structure formed several 10 ps after ion impact. The combined method guarantees realistic initial conditions for MD calculations. It becomes practicable since statistical considerations are used enabling that MD simulations need to be performed only in regions which are smaller than the entire volume of the collision cascade of a keV ion. First results on the type and amount of defects created on average per incident ion were obtained for 30 keV P^+, 15 keV As^+, and 15 keV B^+ implants.

R. Kögler
F. Eichhorn
A. Mücklich
W. Skorupa
A.B. Danilin*

Metal gettering at the borders of a buried amorphous layer in Si
Gettering of metal impurities is known to be a powerful tool for the detection of point defects remaining in ion-implanted and annealed Si. In this study a buried amorphous layer, created by Ge^+ ion implantation, has been investigated by means of Cu gettering before and after recrystallization. Cu atoms have been subsequently introduced, and their depth distribution was measured by SIMS. The results show an accumulation of Cu atoms in a very narrow layer at the crystalline side of the two amorphous-to-crystalline (a/c) interfaces. After recrystallization of the amorphous layer Cu gettering occurs as well outside of the former amorphous layer, mainly at the interfaces. Si lattice expansion has been observed by XRD just in this region in which the Cu is trapped. Such regions, containing a high concentration of self-interstitials, have a much higher gettering capability for Cu atoms than extended defects formed for higher annealing temperatures (T>800°C). Cu gettering can be taken as an indication of a high supersaturation of self-interstitials in the corresponding region.
Collaboration: *CAS Moskau

R. Kögler
A. Peeva
Y. Gueorguiev
D. Panknin
W. Skorupa
A.B. Danilin*

Metal gettering in MeV-ion-implanted and annealed Si beneath the projected ion range, (R_P):"Trans-R_P-effect"
Damaged layers in Si remaining after MeV ion implantation and annealing can be detected by means of metal gettering. Recently a damaged layer at about half of the projected ion range ($R_P/2$) has been detected beside the well known damage layer at R_P. Now a further damage region is discovered well beneath R_P which is called the "Trans-R_P-layer". For an ion implantation of 3.5 MeV, $1x10^{15}$ P^+cm^{-2} with R_P=2.7 µm into n-type silicon the "Trans-R_P-layer", ob-served after annealing at 900°C, is situated at about 4 µm. Due to its high trapping ability for metal impurities this layer could be detected by SIMS profiling of intentionally introduced Cu. The formation of this layer cannot be simply explained by ion channelling effects. Point defect diffusion and agglomeration play a key role. The mobility of the point defects seems to be enhanced by a field drift during annealing because the "Trans-R_P-effect" is not observed for implantation of Si^+ ions instead of the P^+ ions which act as a dopant in Si.
Collaboration: *CAS Moskau

W. Fukarek
J.R. Kaschny*

Cavities in He implanted and annealed Si wafers characterized by spectroscopic ellipsometry

The formation of He induced cavities in silicon during rapid thermal annealing is analyzed. Specimens implanted with 40 keV He$^+$ ions to a fluence of 5×10^{16} cm^{-2} are heat treated at 800°C for times of 1 s to 1200 s. Spectroscopic ellipsometry (SE) is employed to obtain quantitative information on the free volume depth profiles. A newly developed formula is used to model the optical multilayer depth profiles. The free volume is found to increase during annealing for about 300 s and to decrease for longer annealing times. Over this characteristic time a marked change in the He loss occurs which has been reported only recently. Swelling of the He implanted and annealed silicon is analyzed using an AFM. Step heights are consistent with the free volume per unit area obtained from SE data analysis. The number density of cavities is found to be independent of depth in the central part of the cavity layer. The density of cavities after annealing for 600 s is calculated to be 1.2×10^{17} cm^{-3}, about 50 % higher than previously estimated based on TEM analysis.

Collaboration: *Instituto de Fisica, UFRGS, Porto Alegre, Brazil

A. Peeva
R. Kögler
P. Werner*
W. Skorupa

Injection of Si self-interstitials during ion milling for TEM sample preparation

Ion milling is the final step of TEM sample preparation. In conventional ion milling the parameters (ion energy and current, incidence angle) are optimized to achieve high sputtering rate and to minimize the depth of radiation damage. However, recent experiments showed that ion bombardment of Si during ion milling can influence the defect state of the sample. In the present investigation we try to observe the defects responsible for the so called "$R_p/2$ effect". Using "Gatan Duo Mill 600" with 4 keV Ar$^+$ ions (1 mA) under 13° incidence angle we observe small interstitial loops (20-30 nm) located only in the $R_p/2$ region. The size and the density of these loops are controlled by the milling parameters. This is taken as evidence that self-interstitials are injected far beyond the surface during ion milling. The presence of injected Si interstitials may trigger the modification of the existing point defects and small defect clusters to bigger defects which can be observed by XTEM.

Collaboration: *MPI für Mikrostrukturphysik, Halle

B.K. Panda
G. Brauer

Positron affinities and deformation potentials in cubic semiconductors

Positron affinities and deformation potentials are calculated in cubic bulk semiconductors using the density functional theory. The electron energies are calculated in the first principles pseudopotential method where the exchange-correlation energy functional is treated in both local density approximation (LDA) and generalized gradient approximation (GGA). In order to refer the electron and positron energies to the same average of the Coulomb potential, the electron energies are corrected by the pseudo-core factor and the positron ion-core potential is treated in the point-core approximation. The positron correlation energies are also treated using both the LDA and GGA schemes. While the GGA correction on the positron energy is found to be quite significant, the GGA correction on the electron energies is negligibly small.

Our calculated affinity in SiC -3.92 eV in the positron GGA scheme is found to be close to the measured value of (-3.83 ± 0.45) eV whereas the linear-

muffin-tin orbital method predicts -5.61 eV in disagreement with measurement. The calculated positron affinity in diamond -2.20 eV is found to be higher than the measured value of -1.2 eV as the effect of the boron impurity on the positron energy is not considered in the calculation. The positron affinity in BN is found to be close to diamond which suggests that it can be tested as a positron moderator. The calculated positron deformation potential in Si -6.51 eV is in good agreement with -6.19 eV obtained in the previous LMTO-ASA method and experimental value of (-6.2 ± 0.3) eV.

Focused Ion Beam

S. Hausmann
L. Bischoff
J. Teichert
H. Fuhrmann*

Dwell-time effects in focused ion beam synthesis of $CoSi_2$: Reflectivity measurements

$CoSi_2$ layers were produced by 70 keV Co^{2+} FIB implantation into Si(111) at temperatures of about 400°C and subsequent annealing. The $CoSi_2$ layer quality depends on pixel dwell-time and substrate temperature. Only properly chosen parameters result in a continuous layer. The dwell-time (1-250 µs) and substrate temperature (355-400°C) dependence was investigated by SEM, reflectivity measurements and RBS/C. The results show that the irradiation damage increases with dwell-time and decreases with temperature, indicating an interaction between the damage creation rate and the dynamic annealing rate. Already after implantation of less than a tenth part of the dose required for continuous layer formation, the quality of the resulting $CoSi_2$ layer is predetermined.

Collaboration: *Paul-Scherrer-Institut, Zürich, Switzerland

J. Teichert
S. Hausmann
L. Bischoff
M. Voelskow
H. Hobert*

Micro-Raman spectroscopy and ion channeling analysis of crystal damage in Si due to FIB Co implantation

The damage produced by Co ions in Si were investigated since layer and interface quality of the $CoSi_2$ formed by ion beam synthesis strongly depend on the degree of irradiation damage. Implantation was performed with Co^{2+} ions of 70 keV in n-type Si(111) with fluences of $6.7 \times 10^{15} cm^{-2}$ and $1.2 \times 10^{16} cm^{-2}$ varying the pixel dwell-time (1-250 µs) and the target temperature (RT, 355-415°C). The irradiation damage was measured by means of Micro-Raman spectroscopy and RBS/C. Although the fluence was constant, a higher degree of damage was found for longer dwell-times. Above a critical dwell-time which increases with implantation temperature the Si becomes amorphous. The dwell-time dependence of the damage can only be understood if an interaction of disordered zones occurs during FIB implantation. From the critical dwell-time the typical time for dynamic annealing can be estimated to be in the order of 10^{-6}s. The study of the temperature dependence provides an activation energy of 3 eV.

Collaboration: *Friedrich-Schiller-Universität, Institut für Physikalische Chemie, Jena

L. Bischoff
J. Teichert
S. Howitz*
G. Fuhr**

Direct FIB patterning of electrostatic trap structures for the handling of biological cells

The handling of living biological cells (i.e. virus or bacteria) in an optical microscope is possible by applying an electrostatic potential at microstructures with dimensions of the cell size. A four layer device was designed consisting of a first metal film (10 nm Ti + 100 nm Pt), a 1 μm PECVD-Si_3N_4 layer, a second metal film and a 1 μm polymer-insulator. Test structure pattern has been realized using a thin TiPt metal film deposited on a glass substrate by means of standard optical lithography up to a level of 5 μm feature size. The final structuring was done by writing focused ion beam milling down to the sub-μm level using the FIB system IMSA-100. The gap size as well as the shape of the electrodes were varied using an Auto CAD aided pattern design.

Collaboration: *GeSiM mbH Rossendorf; **Humboldt‒Universität Berlin, Institut für Biologie

J. Teichert
L. Bischoff
H. Felsmann
B. Köhler*

FIB preparation and characterization of SEM and TEM samples

FIB sputtering represents a promising preparation technique for microstructural characterization. Cross-section cuts for SEM inspection can be performed and TEM lamellas can be prepared. Compared to conventional methods there are some advantages as improved position accuracy, less time consuming, and applicability to very hard or very sensitive materials. The preparation has been carried out with the Orsay Physics Dual Beam System applying a Ga ion source. XTEM samples of stainless steel were prepared in two steps: fabrication of a T-shape sample with a wafer saw and FIB milling of the TEM lamella. Cross-section cuts were carried out from a variety of metallic multilayer systems. Inspection were done with the scanning electron or ion beam. The ion images with lateral resolution of about 10 nm were found to be fuller in contrast and more informative with respect to the grain structure of the layers.

supported by
SMWK

Collaboration: *Fraunhofer-Institut für zerstörungsfreie Prüfverfahren, Außenstelle EADQ, Dresden

L. Bischoff
J. Teichert
G.L.R. Mair*

Investigation of the emission characteristics of alloy LMISs as a function the source temperature

Liquid metal ion sources (LMIS) are very important components in FIB technology. The temperature behaviour of the sources is essential to know in order to operate the LMIS in a stable emission regime with a long life time. LMIS's wetted with $Au_{73}Ge_{27}$, $Au_{77}Ge_{14}Si_9$ and $Co_{36}Nd_{64}$ alloys were investigated. The temperatures of the needle tip, the droplet and the filament tungsten wire were measured with an optical pyrometer through a window of the vacuum chamber as a function of the heating current in the range of 650°C to 1200°C. The calibration at the melting points ($T_{AuGeSi,AuGe} \approx 365$°C, $T_{CoNd} = 566$°C) was performed visually by microscopy. For the AuGe and CoNd emitters the extraction voltage decreases with temperature according to theoretical predictions with the square root of the surface tension. In the case of the AuGeSi emitter, a completely different behaviour was found. The

extraction voltage increases with temperature up to 800°C and then decreases slowly caused by a phase transition of the alloy in this temperature range.

Collaboration: *University of Athens, Department of Physics, Greece

L. Bischoff
*R. Mühle**
J. Teichert
W. Probst
G. Hofmann

Energy and mass distribution of alloy LMISs depending on the emission current

The mass-resolved retarding field energy analyser was used for the investigation of alloy liquid metal ion sources (LMIS). The energy resolution of the equipment was determined to be about 1 eV, using a Ga-LMIS from which the energy spread is well known. The mass resolution $m/\Delta m$ was estimated from the separation of the isotopes of the single charged Ge and amounts to more than 75. Then the energy spread and the mass spectra of $Au_{73}Ge_{27}$, $Au_{77}Ge_{14}Si_9$ and $Co_{36}Nd_{64}$ alloy LMISs were analysed as a function of emission current in the range of 1 to 50 µA. In general, the energy spread is increasing with increasing emission current due to Coulomb interactions. For the Co^+-line an energy spread of ΔE_{FWHM}=7.6 eV was measured and for the Co^{2+}-line a value of 8.8 eV at an emission current of 1 µA. Then the intensities of all emitted species were measured as a function of emission current. In the case of the AuGe alloy LMIS the results were compared with those obtained with a TOF equipment where a reasonable agreement was found.

Collaboration: *ETH Zürich, Institut für Teilchenphysik

L. Bischoff
J. Teichert
*W. Knapp**

Investigation of solidified alloy LMIS as a regenerative electron emitter

Solidified liquid metal ion sources (LMIS) can be used as high intensity regenerative electron point sources for UHV applications. $Au_{73}Ge_{27}$ and $Au_{77}Ge_{14}Si_9$ alloy LMISs were operated at first in the ion emission mode and quenched abruptly by switching off the heating current. During this process a micro-emitter is formed on top of the needle tip. The radii of the micro-emitter tips were in the range of tens of nm measured by SEM (i.e. $r \le 20$ nm for 10 µA quench current). The solidified LMIS was used as an electron source by switching over the voltage potentials. The I-V characteristics were analyzed using the Fowler-Nordheim plot. It was found that by lowering the quenching currents an improvement of the electron emission characteristic can be obtained due to the reduction of the supertip radius. From 0,2 to 3 µA a stable electron field emission was found limited at higher currents by space charge effects. An *in-situ* regeneration of the electron emission properties under vacuum conditions is given by the formation of a new tip after operating the LMIS in the ion-emission mode.

Collaboration: *Otto-von-Guericke Universität Magdeburg, Abt. Vakuumphysik und -technik

Nanoclusters

L. Rebohle
R.A. Yankov
W. Skorupa
I.E. Tyschenko*
H. Fröb**
K. Leo**

The mechanism of photoluminescence of ion implanted silicon dioxide layers

PL studies were performed at 500 nm thick SiO_2 films thermally grown on [100]-oriented, n-type Si substrates, implanted with Si^+-, Ge^+- or Sn^+-ions and annealed in the temperature range of 400°C to 1200°C. The PL spectra of the implanted SiO_2 layers consist of an UV peak around 4.3 eV and a blue-violet peak between 2.7 eV and 3.3 eV depending on the implanted element. These peaks were found to be due to the radiative deexcitation from the first excited singlet (UV peak) and first excited triplet state (blue-violet peak) to the ground state of a molecule-like luminescence centre. For the substitution of one atom by an isoelectronic but heavier atom the heavy-atom-effect predicts a strong increase in the PL intensity, a slight increase of the emission energy and a decrease of the decay time of the triplet-to-singlet transition. These predictions are in excellent correspondence with the experimental results. In the order of Si, Ge and Sn the PL intensity of the blue-violet PL peak increases and its position is shifted to higher energies. Furthermore, first measurements of time dependent PL reveal a decay time in the order of 100 μs for Ge and of 8 μs for Sn. We suggest that the observed PL is due to the neutral oxygen vacancy typical for Si-rich SiO_2 and similar Ge- and Sn-related defects in Ge^+- and Sn^+-implanted silicon dioxide, respectively.

Collaboration: *Institute of Semiconductor Physics, Novosibirsk, Russia; **Institut für Angewandte Photophysik, TU Dresden

T. Gebel
J. von Borany
W. Skorupa
H.-J. Thees*
M. Wittmaack*

Electrical characterization of Si- and Ge- implanted SiO_2-layers for memory applications

Ion beam synthesized Ge or Si nanoclusters in SiO_2 layers have recently attracted much attention because of their possible use for non-volatile memory applications. MOS capacitors were prepared using thermally grown SiO_2 of 20 nm thickness and subsequently implanted with 20 keV Ge^+ ions or 12 keV Si^+ ions to fluences in the range of $1-5x10^{15}cm^{-2}$. RTA processing at 950°C, 30s, N_2 was applied for annealing. The contacts were formed by patterned n^+- doped poly-Si dots of 300 nm thickness. Current-voltage measurements showed that the conductivity mechanism of the implanted oxides is mainly determined by Fowler-Nordheim tunneling. The effect of charge trapping inside the clusters has been derived from high frequency capacitance-voltage (CV) characteristics. After charging and discharging by applying positive or negative stress voltage pulses the CV curve was shifted to positive and negative voltages, respectively. A fluence of $3x10^{15}cm^{-2}$ already shows a re-markable shift in the CV curve. For the highest implanted fluence ($5x10^{15}cm^{-2}$) a programming window size of 2.0 V (Ge implant) and

supported by
SMWK and SMWA

180 mV (Si implant) was found (6V/100 ms voltage pulses).
Collaboration: * Zentrum Mikroelektronik Dresden

B. Schmidt
K.-H. Heinig
A. Markwitz

Control of the annealing ambient impact on Ge-cluster evolution

The annealing behaviour of Ge implanted SiO_2 strongly depends on the in-diffusion of different species (O_2 or a few ppm of moisture) from the annealing ambient (N_2 or Ar) due to their reaction with dissolved and/or clustered Ge. The resulting multimodal Ge redistribution observed after annealing

could be largely suppressed by the deposition of a 20 nm thick film of LPCVD-Si_3N_4 (diffusion barrier) on top of the SiO_2 layer before implantation. Up to annealing temperatures of 1000°C in N_2 the Ge nanocluster distribution follows the implanted Gaussian profile of Ge as measured by RBS and TEM. Only at T≥1100°C near the SiO_2 surface a small amount of oxidized Ge was observed. Furthermore, the accumulation of Ge at the SiO_2/Si interface was substantially lowered probably due to the absence of hydrogen from the moisture. The lower Ge concentration at the SiO_2/Si interface was observed also after annealing in pure O_2. This effect can be explained by the high concentration of O_2, which decreases the concentration of free hydrogen within the SiO_2.

H. Seifarth
A. Markwitz
B. Schmidt

PVD preparation of Si-nanocluster monolayers within a SiO_2 matrix

Si or Ge nanocrystals embedded into thin SiO_2 films exhibit superior charge-storage properties and may be favoured for future nonvolatile EPROM memory devices. Besides LPCVD and ion beam synthesis the fabrication of such nanocluster layers by sputtering is a promising preparation method. First experiments have shown that 5 nm thick SiO_x layers (x ≈ 1) can be deposited between thin SiO_2 films by reactive sputtering. The as-deposited SiO_x layers with x < 2 are amorphous with a random mixture of $Si-Si_nO_{4-n}$ tetrahedra, which distribution depends on x and n (n = 1...4). During subsequent annealing at T=1000°C for 1h in N_2 atmosphere, the exceeding Si of the SiO_x layer forms a Si nanocrystal monolayer in the surrounding SiO_2 network. The lattice structure of the Si nanocrystals have been observed by HRTEM.

M. Klimenkov
J. von Borany
K.-H. Heinig
W. Matz

Formation of As nanoclusters in a thermally grown SiO_2 layer

In order to understand the conditions for the formation of semiconductor and metallic nanoclusters embedded in a dielectric matrix different elements as Si, Ge, Sn, Au and others are investigated. In a new experiment we have synthesized As nanoclusters near the SiO_2/Si interface in thermally grown thin (65 nm) SiO_2 films. The creation of nanoclusters was performed using implantation of As^+ ions at 50 keV, $1 \times 10^{16} As^+/cm^2$ fluence and subsequent annealing at 1300 K during 30 min in N_2. The XTEM examination reveals a line of clusters with average size of 6 nm in a distance of 9 nm from SiO_2/Si interface. The cluster density was estimated to $2 \times 10^{11} cm^{-2}$. HRTEM and dark field micrographs give no suggestions on a crystalline order of these nanoclusters. Additionally, the formation of small clusters of about 3 nm size in the volume of the SiO_2 film has been obtained, which are hardly to detect due to the very week Z-contrast. The STEM-EDX line-scan across the SiO_2 film show quite homogeneous As distribution from 20 nm depth to interface with a 30% higher As concentration near interface. The latter is correlated with the line of bigger clusters while the flat distribution supports the existence of small cluster observed in HRTEM measurements.

K.-H. Heinig
B. Schmidt
A. Markwitz
J. von Borany
M. Klimenkov

Formation of δ-layers of Ge nanocrystals in SiO_2

Under specific conditions XTEM images of Ge^+ implanted and subsequently annealed SiO_2 films (30...500 nm thick) on Si show a "δ-like" nanocluster layer of a few nm thickness which is located close to but well-separated (~5 nm) from the SiO_2/Si interface. Guided by theoretical predictions, systematic

series of experiments have been designed and performed (i) because this phenomenon seems to be based on an interesting interplay between irradiation effects and thermodynamics, and (ii) the properties of this self-organizing nanocluster δ-layer fulfil the requirements for new nanocluster memory devices. It has been confirmed that controlled Ge ion implantation with about one displacement per atom at the SiO_2/Si interface results in the formation of a nanocluster δ-layer during annealing. STEM-EDX measurements of as-implanted samples have confirmed that the nanocluster δ-layer evolves from a thin interface-layer of sub-stoichiometric SiO_{2-x}. It should be emphasized that during annealing the formation of nano-cluster δ-layers is a transient stage. However, the δ-layers can be frozen in by finishing the annealing at an appropriate time.

V.A. Borodin*
K.-H. Heinig
B. Schmidt

Non-local mean-field modeling of Ge nanocluster evolution in ion implanted SiO_2 layers

An analytical model has been developed for the microstructural evolution in ion implanted layers during high-temperature annealing in an ambient with reactive components. The model has been applied to Ge redistribution in a 500 nm thick silicon dioxide layer during annealing at 950°C in dry oxygen, which allowed to reproduce the main features found experimentally for the Ge nanocluster evolution kinetics. It has been found that the kinetics of impurity redistribution accompanied by chemical reactions in the annealed layer is quite sensitive to the choice of parameters. Hence, the comparison of simulation predictions with experimental date allowed to estimate a number of currently uncertain thermodynamic parameters of diffusing species, in particular of oxygen and germanium in SiO_2. Moreover, the application of this theoretical approach to the choice of appropriate experimental parameters can noticeably facilitate nanoscale engineering during ion-beam synthesis of nanocluster structures.
Collaboration: *Kurchatov Institute, Moscow, Russia

K.-H. Heinig
M. Strobel
B.Schmidt

Modeling and computer simulation of precipitation at 2D sinks applied to self-organization of Ge nanoclusters

A model has been developed which can be applied to the formation of void layers parallel to grain boundaries or of narrow nanocluster layers parallel to interfaces. Based on that model computer simulations have been performed which have been proven to have sufficient predictive power to support the design of experiments for a controlled fabrication of narrow layers of Ge nanoclusters in SiO_2 at the Si/SiO_2 interface. The model requires an optimum ion implantation damage of SiO_2 in the region of the Si/SiO_2 interface (~1 dpa), resulting in free oxygen which diffuses towards the Si/SiO_2 interface leaving behind a thin SiO_2 layer with silicon excess. The silicon excess has been calculated by TRIM and rate-equation calculations. For the subsequent annealing step the model considers the diffusion and nucleation of both, the implanted Ge as well as of the superstoichiometric Si which has been accumulated due to oxygen out-diffusion during ion implantation. Starting with such initial conditions and taking into account Si-Si, Si-Ge and Ge-Ge bond strengths from literature, kinetic 3D Monte Carlo simulations show the evolution of a narrow nanocluster band close to but well-separated from the interface, which is in excellent agreement with TEM images.

M. Klimenkov
J. von Borany
W. Matz

Crystallisation of nanoclusters under electron irradiation in TEM

Nanoclusters were created in very thin (20 nm) thermally grown SiO_2 film using ion implantation of Ge at 12 keV and a fluence of $7x10^{15}cm^{-2}$ followed by a thermal treatment at 1230 K for 30 s in N_2 atmosphere. XTEM examination shows a Ge cluster band around the middle of the oxide. The observed cluster density was estimated to $8x10^{11}cm^{-2}$ with an average cluster size of 4 nm. As the clusters are in the amorphous state it is not possible to decide whether the clusters consist of elementary Ge or Ge-oxide. Thermal emission guns used in this TEM study have an estimated beam current density of $1-2x10^7A/cm^2$ in the HRTEM regime. This current density has no major influence on the clusters. In additional studies of the same sample in a TEM equipped with a field electron emitter (electron beam density $1-2x10^8A/cm^2$) *in-situ* crystallisation of clusters during TEM investigation has been obtained. The explanation of the crystallisation as a thermal effect or an influence of electronic interaction remains an open question. The detected lattice planes have a distance of 0.324 nm which is in good agreement to elementary Ge(111) (0.326 nm). Further electron irradiation leads to no additional changes in the system after crystallisation. The formation of crystalline Ge clusters under irradiation favours the model that the firstly observed amorphous clusters are from pure Ge rather than from GeO_x.

K.-H. Heinig
M. Strobel
M.-O. Ruault*
H. Bernas*

CoSi$_2$ nanocrystal evolution in silicon during Co$^+$ ion implantation

It has been found that under Co^+ ion implantation the growth mode of $CoSi_2$ nanocrystals embedded in a silicon matrix depends strongly on the ion implantation temperature. At low temperatures (e.g. 400°C) the crystal size increases with time as $t^{1/3}$, whereas at high T (e.g. 650 °C) a $t^{1/2}$ behaviour has been observed. At intermediate temperatures the growth starts initially (for small mean crystal radii) with $t^{1/3}$ and switches at a certain crystal size to a $t^{1/2}$ behaviour. The growth speed of the $CoSi_2$ nanocrystals obeys an Arrhenius-type temperature dependence with $E_a \approx 1$ eV at lower T, whereas for higher temperatures $E_a \approx 4$ eV have been found. This complex behaviour could be understood by an unified theoretical modeling of ion deposition, ion beam mixing and diffusion processes. It has been shown that the growth exponentials $\square$ and ½ cannot be used as a proof for diffusion and reaction controlled Ostwald ripening, as it is usually done. A much more sophisticated evaluation of the experimental data was required. With a fundamental modeling taking into account all processes involved it became possible to extract from the experimental data the Si/CoSi$_2$ interface energy, a very important physical parameter for nanocluster evolution which has not been measured precisely up to now.

Collaboration: *CSNSM, Paris-Orsay, France

R.A. Zuhr*
C.W. White*
L.C. Feldman**
M. Strobel
K.-H. Heinig

Nanostructured arrays formed by finely focused ion beams

In conventional ion beam synthesis colloids are formed by blanket implantation and, if necessary, by a subsequent thermal annealing. Due to the governing physical processes like nucleation and in particular Ostwald ripening, the colloids are not uniform in size, resulting in dimi-nution of the size dependent optical properties. Using kinetic 3D lattice Monte Carlo simulations it has been predicted theoretically that more uniform size particles arranged in a 2-dimensional lattice can be formed by using a finely focused

ion beam to implant identical ion doses only into nanometer size regions located at each point of a rectangular lattice. Initial work has been done with a 30 keV Ga beam implanted into Si. Particle formation as a function of implant conditions as analyzed by RBS, XRD, AFM, SEM and TEM shows that aggregation of the roughly Gaussian implanted profile into a single particle at each lattice site has not been achieved. However, it is clear that Ga is retained in the substrate and does form small crystalline colloids. For Ga the dose and energy of implanted ions appear to be critical in formation of larger single particles, since the Ga ions must be implanted into a relatively undisturbed region of the substrate in order to form a single colloid. However, high doses drill holes into the substrate surface, leaving Ga spread around the wall and bottom of the hole, which produces an unsuitable geometry from which to diffuse the Ga into a single particle. Based on the current work an optimization in the dose region of 10^{16} ions/cm^2 is required.

Collaboration: *Solid State Division, Oak Ridge National Laboratory, Oak Ridge, USA; **Vanderbilt University, Nashville; USA

M.T. Pham
J. Schöneich
W. Matz
S. Oswald*

Films of CdS nanocrystals

Nanometer-sized CdS has potential applications in optoelectronics and photocatalysis. Cd$^+$ and S$^+$ were implanted into a 100 nm thick SiO$_2$ layer followed by a heat treatment process at 500°C in N$_2$ for 10-80 min to form CdS nanocrystals. The formation of CdS depending on the annealing time was studied by XRD and XPS. The starting as-implanted surface presents a mixed phase comprising CdS, CdO, Cd, and S embedded within the SiO$_2$ matrix. The 10 min annealing results in a substantial conversion into CdS. The completion in terms of crystallinity and crystallite size falls in the range between 20 and 40 min. In this time range, the depth profiles remain unchanged, indicating the immobility of the compound CdS. Shorter annealing times produce a CdS phase mixed with unreacted Cd and S. A loss of CdS is evident upon a long-lasting annealing.

Collaboration: *Institut für Festkörper- und Werkstofforschung, Dresden

Biotechnological Materials

M.T. Pham
J. Schöneich
W. Matz
H. Reuther
E. Richter
E. Wieser
S. Oswald*

CaO - P$_2$O$_5$ - containing titanium and titanium oxide surfaces

Ca$^+$ (1.5×10^{17}cm^{-2} at 25 - 55 keV) and P$^+$ (1.5×10^{17} or 7×10^{16} cm^{-2} at 20 - 40 keV) were implanted in pure Ti and TiO$_2$ substrates (200 nm TiO$_2$ sputter de-posited on an oxidized Si substrate). A subsequent oxidation was conducted at 400, 600, and 800°C for 40 min in an oxygen atmosphere. The conversion of Ca and P into their oxides was studied by XPS and XRD measurements. In the as-implanted state, Ca and P are uniformly distributed over a dominant implantation depth in a Ca/P-ratio of about 2 for TiO$_2$ substrate and about 1 for Ti substrate consistent with the nominal applied ion fluence. Ca is present as Ca^{2+} in CaO, while P remaining predominantly as elemental P. The 600°C oxidation converts nearly completely P into P^{5+}. The further oxidation at 800°C does not produce significant alterations in terms of the distribution and P oxidation. The conformal distribution of Ca and P, with a slight broadening toward bulk suggests (i) an oxygen uptake responsible for the P oxidation and, (ii) some degree of undergoing reactions

between CaO and P_2O_5. There are no crystalline Ca and P containing phases. With pure Ti substrates, the oxidation occurs for both P and the matrix Ti. TiO_2 crystallizes to rutile with increasing temperatures.

Collaboration: *Institut für Festkörper- und Werkstofforschung, Dresden

M.T. Pham
J. Schöneich
W. Matz
H. Reuther
E. Richter
E. Wieser
S. Oswald*
G. Steiner**

Surface bioreactivity of ion implanted Ti

Ion implanted Ti was examined for its surface bioreactivity by mineralization, to form bone-like hydroxyapatite precipitates, in a simulated body fluid containing soluble calcium and phosphate ions. The experiments were carried out in a fluid cell at 37°C by exposing samples to the solution and *in situ* recording the surface with an optical microscope. Samples under test were pure Ti (control sample) and Ti implanted either with Ca or P or Ca and P. The comparison reveals a drastically different behaviour of two types of surface, showing the active involvement of implantation incorporated species in interfacial reactions. All ion implanted surfaces exhibit enhanced apatite formation, evidently reflected in the early stages of exposure to solution. The rate of mineralization increases with the implantation fluence. The precipitates on implanted surfaces are populated laterally more homogeneously than on the control sample. The prevalent interfacial process is the hydroxyapatite precipitation while no surface degradation is observed. The surface reactivity is related to surface-incorporated CaO and P_2O_5 supplying mineral-forming precursors Ca^2 and PO_4^3.

Collaboration: *Institut für Festkörper- und Werkstofforschung, Dresden; **Institut für Analytische Chemie, TU Dresden

I. Zyganov*
E. Wieser
W. Matz
H. Reuther
E. Richter

Phase formation and mechanical properties in Al-implanted Ti

Within a programme to improve the surface properties of Ti for medical applications Al was implanted into pure Ti at 195 keV with doses from 1×10^{17} Al/cm² to 1×10^{18} Al/cm² resulting in Al depth distributions with maximum concentrations from about 10 to 55 at.% Al. By double implantation with 100 and 195 keV of 1×10^{18} Al/cm² for both energies a layer extending from the surface to about 500 nm with a maximum concentration 60 at.% Al was formed. XRD shows that for Al concentrations < 50 at.% only precipitates of Ti_3Al are formed. For a maximum Al content of 50-55 at.% up to an annealing temperature of 500°C only Ti_3Al is found, however, after annealing at 700°C also TiAl is observed. The Al double implantation results already in the as-implanted state in a disordered fcc (TiAl) phase beside Ti_3Al which transforms by annealing 600°C into tetragonal TiAl. The hardness of the implanted layer increases with increasing Al dose up to a factor 2 for the double implantation. For samples with Ti_3Al precipitates only by annealing at 500°C a hardness decrease is observed. This hardness decrease becomes negligible if TiAl is formed during annealing.

Collaboration: *Lipetsk State Technical University, Russia

M.T. Pham
I. Zyganov*
W. Matz
H. Reuther
E. Richter
E. Wieser

Corrosion behaviour of high-dose Al-implanted Ti

Surface alloying of Ti was prepared by consecutively implanting 1×10^{18} Al⁺/cm² at 200 and 100 keV in pure Ti or with pre-implanted V⁻ (2×10^{17} cm⁻² at 200 keV). The implanted surfaces were examined for their corrosion behaviour in 5 M HCl by recording the corrosion-time curves and potentiodynamic polarization curves. Before corrosion test the surfaces were characterized

by XRD and AES. The corrosion rate is about 8 times lower, and the process occurs at a moderately unnoble potential, compared with a control sample of pure Ti with its natural passivating oxide barrier. These characteristics are also different from those of a pure Al surface. At anodic potentials greater than 20 mV (NHE) an increase of the current density due to dissolution of surface Al is observed. Both the corrosion and the anodic dissolution occur on the barrier-free surface. Our observations suggest that the corrosion is determined by titanium aluminides, the inter-metallic compounds generated by ion implantation. Two such compounds were revealed by XRD: the hcp Ti_3Al and a disordered fcc TiAl at the as-implanted state. The surface Al concentrations of 25-65 at.% determined by AES fall within the compositional ranges of the specified compounds.

Collaboration: *Lipetsk State Technical University, Russia

Ion Beam Analysis

U. Kreissig
P. Skeldon*
R. Grötzschel
E. Wieser

TOF-ERDA, RBS and TEM studies of corrosion barrier film formation on Al-4.5Mg-0.05Cu alloy

TOF-ERDA has been used to determine the distribution of B, O and Mg in corrosion barrier films formed by anodic oxidation on an electropolished Al-4.5Mg-0.05Cu alloy. The results are in reasonable agreement with those of RBS and EDX analysis in TEM. Magnesium are incorporated into the film at the alloy/film interface, migrate outwards in the film at approximately twice the rate of Al^{3+} ions, and are ejected into the ammonium penta-borate electrolyte. As a consequence of the faster migration rate of Mg, its concentration in the alumina layer is less than that in the alloy. Boron originating from the electrolyte was found to be limited to the outer 40% of the film thickness. A copper enrichment of $1.3x10^{15}Cu$ atoms/cm^2 at the alloy/film interface could be found by RBS as a result of the electropolishing pretreatment of the alloy. During the formation of the anodic film, voids develop at the alloy/film interface, which are attributed to the 30% lower oxide volume of MgO compared to Al_2O_3.

Collaboration: *Corrosion and Protection Centre, University of Manchester Institute of Science and Technology, Manchester, UK

J. Piekoszewski*
R. Grötzschel
E. Wieser
H. Reuther
Z. Werner*
E. Christalle

Analysis of Al_2O_3 surfaces modified by pulsed plasma beam modifi-cation

Single crystalline sapphire and polycrystalline Al_2O_3 ceramics were irradiated with intense plasma pulses generated in a rod plasma injector (RPI) to obtain elemental mixing of surface near layers. The RPI works in a regime referred to as deposition by pulsed erosion (DPE) providing plasma beams consisting of gaseous (nitrogen, argon, xenon) and metal ions (titanium or molybdenum) in controlled fractions. Sequences of single pulses with energy densities of about 6 J/cm^2 and durations in the µs-range were applied to melt a thin layer of the substrate and get a deep mixing. RBS, AES and SEM were used to study the depth profiles of the metals. The investigations revealed a pecularity of the mechanism of the DPE. The metal ions are hardly acceler-ated and reach the sample only after resolidification of the surface, causing a deposition of a thin layer, which is molten by the following pulse. In this

mode it is possible to obtain mixing with Ti. No mixing, but surface droplet formation was observed for Mo, probably due to the large difference in surface tension between Mo and substrate.

Collaboration: * Soltan Institute for Nuclear Problems, Swierk, Poland

St. Jankuhn*
D. Grambole
F. Herrmann
T. Reinert*

Nuclear microprobe analyses of ancient human bone

In order to get more information about the relationship between biological development, health status, and living conditions of our ancestors, osteo-densitometrical methods are coupled with ion beam techniques. Femoral cross sections of ancient human bones of the Merowingian period (6-8th century AD) were analysed by lateral-resolved micro-PIXE at the Rossendorf nuclear microprobe using a 3 MeV proton beam of $(3x3)\mu m^2$ at 200 pA. The cross sections were scanned radially from the outer edge (Periost) in the direction to the middle of the bone (Endost) over a distance of 1.55 mm at maximum. A different behaviour of the radial distributions of the main and trace elements like P, Ca, Mn, Fe, Zn, Br, and Sr was observed. In the case of Zn, a possible explanation for these characteristic profiles is that Zn enrichment in the centres of bone formation is superim-posed onto a diffusion profile of Zn from the environment into the bone. These results indicate post mortem mineral exchange processes and dia-genetic alteration during burial of bone tissue in soil. However, these processes are limited to the region near the surface (up to a maximum of 1 mm).

Collaboration: *Institut für Experimentelle Physik II, Universität Leipzig

U. Reibetanz*
D. Grambole
F. Herrmann
T. Reinert*

Element distribution analysis in articular cartilage by means of micro-PIXE

The investigation of structure and mechanical properties of the articular cartilage is important to the understanding of abnormal and pathological changes of the joints. The elemental distributions of P, S, Cl, K and Ca over an area of $(1x1.5)$ mm^2 from the bone-cartilage-interface to the articular surface were measured with micro-PIXE by means of the Rossendorf nuclear microprobe. The samples were freeze-dried sagittal sections of a knee joint from a juvenile domestic pig. Particularly, we focused on differences in elemental distributions of mechanically loaded and unloaded cartilage samples. The distributions of S and K are not affected by mechanical loading. Due to the excretion with the cartilage water Cl suffered a loss of 25% without loading. The most interesting results could be found in the distributions of P and Ca. The loaded samples revealed an increase of 35% of the contents of Ca and P slightly below the articular surface in a 25 µm tangential ribbon. The reason is probably the flux of cartilage water due to the loading, that brings calciumphosphates to the surface region where they are trapped in the narrower tangential collagenous network. This enrichment of Ca and P could be the reason for increased formation of microcrystals that effect destructive arthrotic changes of the cartilage.

Collaboration: *Institut für Experimentelle Physik II, Universität Leipzig

S. Rößler*
D. Grambole
F. Herrmann
D. Scharnweber*

Investigation of the hydrogen content in Ti alloys

Titanium and its alloys show good biocompatibility and are therefore increasingly used as biomaterials. Using electrochemical processes grow mechanism and thickness of the oxide can be controlled over a wide range

because the oxide has n-semiconducting properties and the ion charge number of the cation (Ti^{4+}) and anion (O^{2-}) are very different. A two layer model can be used for describing electrochemically formed oxide layers (inner barrier layer, outer gel-like porous layer). The aim of this investigation is to get more information about the structure and composition (water content) of the oxide layer.

Specimens of Ti6Al4V were oxidized in neutral phosphate buffer solution at 37°C under galvanostatic and potentiostatic conditions. The water content was investigated as a function of time at constant current density and as a function of the anodisation conditions by measuring the hydrogen content using the resonant nuclear reaction $^1H(^{15}N,\alpha\gamma)^{12}C$. Due to the observed strong hydrogen loss during the measurements the γ-yield was measured in dependence on the ^{15}N ion fluence and than fitted by an exponential function to get the yield value at the beginning of the analysis. First results for thick oxide layers (160 nm) show that the water content, as judged by the H-impulses, depends strongly on the electrochemically conditions. The oxide formed under potentiostatic conditions contains only a small amount of water, which was found in the 1/8 of the oxide, whereas the galvanostatic formed oxide contains water throughout the whole outer porous layer (80-100 nm).

Collaboration: *TU Dresden, Institut für Werkstoffwissenschaft

M. Friedrich
W. Pilz
N. Bekris*
R.D. Penzhorn*
R. Hellborg**
S. Mattssonn**
R. Vesanen***

Tritium detection by accelerator mass spectrometry (AMS)
The activities for tritium depth profiling by AMS at the 3 MV Tandetron have been restarted on the base of a contract between the FZ Rossendorf and the FZ Karlsruhe/Germany. Samples from the wall material of the fusion experiment JET Culham/UK have been prepared in the tritium laboratory of the FZ Karlsruhe. The tritium contents of the investigated samples were one to two orders higher in comparison to the former measured samples from the fusion experiment ASDEX-upgrade of the Max-Planck-Institut für Plasmaphysik Garching/Germany. The problem of the detector overloading has been solved by installation of the detector at the end of the implantation beamline, which enables defined scanning of the tritium beam over an aperture in front of the detector. Additionally, first measurements have been made in collaboration with the Universities of Lund and Göteborg for the tritium detection by AMS for biomedical applications.

Collaboration: *Forschungszentrum Karlsruhe, **University of Lund/Sweden, ***University of Göteborg/Sweden

M. Mäder
C. Neelmeijer
M. Schreiner*

Composition analysis of medieval glass using PIXE
The resistivity of potash-lime-silica glass to environmental attacks is mainly determined by the contents of silicon oxide. Hence, the determination of the Si/K/Ca atomic ratios in the bulk of medieval glass objects of art helps to decide on the necessity of preventive atmospheric conditions for storage in the museum. Non-destructive PIXE studies of the glass bulk, however, are possibly modified by the presence of a leached surface layer pretending high concentrations of Si and low concentrations of K and Ca. To evaluate those effects PIXE measurements were carried out on synthetic glass samples of medieval composition covered by leached coatings of different thickness. The

compositions of the leached layers obtained from the PIXE spectra were simulated using the GUPIX code. In the case of thin altered surface layers, knowledge about the layer structure gained by artificial leaching or natural glass corrosion plus the individual GUPIX model calculations allow to correct the measured values to get the real composition of the glass bulk.

Collaboration: *Institut für Farbenchemie, Akademie der Bildenden Künste Wien, Österreich; Bundesanstalt für Materialforschung und -prüfung Berlin; Fraunhofer-Institut für Silicatforschung Bronnbach

supported by
BMBF

R. Behrisch*
D. Grambole
U. von Toussant*
W. von der Linden**

Surface layer destruction during ion beam analysis

A mathematical evaluation for the signal decrease in ion beam analyses has shown that the decrease depends critically on the lateral distribution of the analysing ion beam. We will assume a single step distraction process and no dependence on the current density. For a nearly uniform current distribution an exponential decrease of the analysing signal is expected, while for a "bell shaped" or Gaussian current distribution the measured signal should decrease with the total number of incidence ions Φ as $(R^2/\rho^2\Phi)[1-\exp(-\Phi(\rho/R)^2]$. Here $\pi\rho^2$ is the destruction cross section and $2R$ the half width of the current distribution. The decrease of the Au PIXE signal as measured during the analysis of an Au layer of 75 nm on graphite using 10 MeV Si ions could be well fitted to the above dose dependence giving a distraction cross section of 0.012 nm^2 and indicating a Gaussian current distribution. With this distraction cross section a erosion yield of about $Y= 53$ Au-atoms/Si-ion can be deduced. In a micro-ERDA analysis of the hydrogen in a carbon sample using also 10 MeV Si ions the measured signal decrease could be described by a simple exponential function, indicating that the current distribution used was very uniform on the beam spot. The decrease gave a desorption cross section of about $\pi\rho^2= 1nm^2$.

Collaboration: *Max Planck Institut für Plasmaphysik, EURATOM Association, Garching bei München; **Institut für Theoretische Physik, Universität Graz, Österreich

Other Activities

J. Noetzel
A. Handstein*
A. Mücklich
F. Prokert
H. Reuther
E. Wieser

Co/Cu solid solution prepared by ion implantation

Granular samples of the immiscible system Co/Cu attracted large research activity because of their giant magneto resistance (GMR) behaviour. To get a sample with high GMR one has to prepare a solid solution of Co in Cu, which is difficult due to the positive heat of mixing of the system. Afterwards, one uses the spinodal decomposition of Co/Cu upon annealing. In this project, Co is directly implanted into Cu at 200 keV with a maximum fluence of 2×10^{17} cm^{-2}. AES shows a nearly rectangular depth distribution of Co in Cu. The maximum Co concentration is about 25 at.%. The formation of a solid solution without Co clusters is shown by XRD, TEM and magnetic measurements. XRD shows only fcc-Cu-peaks that are slightly shifted towards fcc-Co for low angles of incidence. No clusters could be found by

TEM investigations and an EDX mapping showed a homogeneous Co distribution in the implanted area. SQUID measurements of the magnetic moment at low temperatures and low external fields (H_{ext}=5 mT) confirmed a spinglass behaviour, indicating that ferro- and antiferro-magnetic interactions exist in random distribution. The presence of Co clusters would lead to superparamagnetic properties.

Collaboration: * Institut für Festkörper- und Werkstofforschung Dresden

U. Hornauer
G. Schumacher*
H. Reuther
W. Matz
E. Wieser
E. Richter
M. Schütze*

Influence of Si ion-implantation on the microstructure and oxidation kinetics of Ti50Al

The application of intermetallic Ti50Al above 700°C fails due to low oxidation resistance. In this investigation Si was implanted at 1 MeV to reduce the high temperature oxidation. The fluence was varied from 2.5×10^{16} to 8×10^{17} cm^{-2} resulting in a local concentration of Si between 1 at.% and 35 at.% at a projected range of 1 µm. After implantation an increase of the α_2-Ti$_3$Al phase is found. Isochronal annealing in Ar and in air for different temperatures was performed. For the highest fluence AES depth profiling shows that titanium starts to diffuse at 650°C into the implanted region, whereas the Si- profile remains unchanged. XRD proves the formation of Ti$_5$Si$_3$. After 750°C a pronounced oxidation starts. The depth profile for 850°C shows an almost constant oxygen distribution up to the Si profile, which acts as a diffusion barrier. XRD shows the existence of a mixed TiO$_2$/Al$_2$O$_3$ scale, the Ti$_5$Si$_3$ pha-se is still detectable. Long term TGA oxidation tests at 900°C in air show a positive effect in the beginning of oxidation for the fluence of 8×10^{17} Si/cm^2. After a few hours the oxidation kinetic is similar to unimplanted Ti50Al, but the mass gain after 100 h is still 30 % smaller.

Collaboration: *Karl-Winnacker-Institut der DECHEMA e.V., Frankfurt a.M.

A. Turos*
G. Gawlik*
W. Matz
R. Grötzschel
J. Jagielski*
A. Wierzchucka*
A. Stonert*

Ion Beam Mixing of the ZrO$_2$/Fe System

Stabilised zirconia (SZ) layers (ZrO$_2$ stabilised with 12 mol-% Y$_2$O$_3$) were deposited by sputtering on 200 nm thick Fe layers on SiO$_2$/Si substrates. The thickness of the SZ layers ranges from 35 to 100 nm. Ion beam mixing of these structures by Kr ions of 300 keV and 1.5 MeV was studied for implantation temperatures ranging from 100 K to 300 K. According to the XRD analysis the as-deposited SZ and Fe layers were characterized by very small grains (10-20 nm). Upon ion bombardment at RT no crystallite growth was observed. But the tetragonal crystalline structure of as-deposited SZ layers transforms into the cubic one with the lattice constant of 4% larger than the standard value. Ion bombardment with 300 keV Kr ions produces continuous decrease of the XRD Fe signal with increasing ion dose indicating the partial amorphization of the Fe layer. At fluences exceeding 1×10^{16} at/cm^2 the formation of the rare FeO phase (wuestite) was observed. RBS analysis revealed important atomic transport across the SZ/Fe interface. Kinetics of the new phase formation and mixing efficiency were determined. Ion beam mixing was substantially suppressed at low temperatures. High energy ion bombardment produces only transformations of the crystalline structure without any visible atomic transport.

Collaboration: *Institute of Electronic Materials Technology, Warsaw, Poland

M.T. Pham
J. Schöneich
W. Matz
S. Oswald*

Electrocatalytic activity of Ni-implanted Ti surfaces

There is a great interest in obtaining model surfaces for a systematic study of the electrocatalytic activity of Ni. Ni^+ ions were implanted into a polished Ti surface at 40-55 keV to fluences ranging from 5×10^{16} to $3.2\times10^{17}cm^{-2}$. The surfaces were characterized by AES / XPS, XRD, and optical microscopy. The electrocatalytic activity was examined by oxidation of glucose in 0.1 M NaOH using cyclic voltammetry measurements. The Ni concentration reaches a maximum value of ca. 60 at.% at 50 nm from surface, with Ni^{2+} present on the outermost surface and elemental Ni incorporated underneath the surface. The Ni phase is finely dispersed or amorphous. The matrix substrate composes a TiO_2 surface film gradually replaced by pure Ti toward bulk. For Ni^+ fluences $> 1\times10^{17}cm^{-2}$, the surface becomes textured and rugged. The catalytic activity shows (i) a variation over 3 orders of magnitude by changing the Ni^+ fluence between 5×10^{16} and $3.2\times10^{17}cm^{-2}$, (ii) a greater efficiency, and (iii) greater stability compared with a polished pure Ni surface.

Collaboration: *Institut für Festkörper- und Werkstofforschung, Dresden

G. Brauer
E.-M. Nicht
R. Franke*
G. Tempus**

Study of the alloy Al-2024 by positron annihilation spectroscopy

These investigations were part of a larger program established by AIRBUS Industries to characterize the ageing behaviour of the alloy Al-2024 used in the fabrication of the aircraft 'Airbus'. The ageing properties of samples taken from an aircraft 'Airbus A300', being in operation for 18 years, have been compared to a reference material which was artificially aged.

The results of positron annihilation spectroscopy show that there are no significant differences in both materials. This finding is in agreement with the results obtained from other methods within the scope of the general research program mentioned above which points to a materials behaviour as predicted for a safe operation of this type of aircraft.

supported by
SMWK and
AIRBUS Bremen

Collaboration: *Fraunhofer-Institut für Angewandte Materialforschung Dresden, **AIRBUS Bremen

F. Eichhorn
F. Prokert
J. Sass*
K. Mazur*

Characterization of highly rough surfaces by X-ray reflectometry

Wafers with a controlled highly rough surface allow to grow quasi-epitaxial layers with only small strain values in comparison to their growth on flat surfaces. The growth conditions for mismatched layers are weakened so that a greater variety of layer material can be grown on wafers treated in such way. Two different surface profiles were studied: (i) The surface of a Si wafer consists of mesas with a mean distance of 2 µm and valleys of 2 µm depth between them. The top surfaces of all the mesas are flat and in the same height. The specular reflectivity shows a clear range of total reflection and from the critical angle follows a density value of 46 % of the Si bulk density. The rms-roughness of the top layer was found to be small, comparable with the quality of a flat Si wafer surface (0.01 nm r.m.s.). (ii) By anisotropic etching a GaAs wafer a hilly structure with moderate gradients is formed. The distance between the bottom to the top of the profile is approximately 2.5 µm. The mean surface misorientation varies in the range of 1.4°.

The X-ray reflectivity curve doesn't show any total reflection range; it can be described by a model assuming a material with a monotonic increasing mass density from the surface to the bulk of the sample.
Collaboration: *Institute of Electronic Materials Technology, Warsaw

M. Dobler
H. Reuther
A. Mücklich

Ion beam induced epitaxial crystallization of FeSi$_2$ studied by CEMS
The formation of different FeSi$_2$ phases was investigated using the IBIEC process. Si (111) substrates were implanted with 200 keV Fe ions at RT and fluences ranging from $7x10^{15}$cm^{-2} to $1x10^{17}$cm^{-2}. The concentration profiles have maximum iron concentrations from 0.7 at.% for the lowest fluence up to 14.2 at.% for the highest fluence at around 100 nm depth as determined by AES sputter profiling. After implantation completely amorphized Si top layers with thicknesses of about 300 nm are found by TEM. The CEMS spectra of all samples show a similar broad electric quadrupole doublet which could not be attributed to any known amorphous or crystalline iron silicide phases. The subsequent irradiation with $1x10^{16}$cm^{-2} Si ions with an energy of 500 keV at 350°C induce the formation of different FeSi$_2$ phases due to the IBIEC process. For the samples implanted within the low fluence range of $(0.7-5)x10^{16}$cm^{-2} the metastable γ-FeSi$_2$ is present whereas for the fluence of $1x10^{17}$cm^{-2} the formation of α- and β-FeSi$_2$ phase mixture is found.

M. Dobler
*M. Walterfang**
*S. Kruijer**
H. Reuther
*W. Keune**

Depth selective Mössbauer studies of FeSi$_2$ layers produced by ion beam synthesis
For the ion beam synthesis of FeSi$_2$ a fluence of $3x10^{17}$cm^{-2} Fe ions were implanted with an energy 200 keV into Si(111) at 350°C. The sample was subsequent rapid thermal annealed at 900°C for 30 s. The depth distributions of the α- and β-FeSi$_2$ phases were investigated non-destructively by depth-selective CEMS. In the as-implanted case an equal-distributed mixture of α- and β-FeSi$_2$ is found and the total amount is correlated to the Fe depth profile determined by AES sputter profiling. The subsequent annealing leads to a structured Fe profile correlated to the formation of different FeSi$_2$ phases. In a first layer between 20 nm and 130 nm precipitates of α- and β-FeSi$_2$ are formed. In the region around the previous implantation maximum from 130 nm to 240 nm pure β-FeSi$_2$ is obtained.
Collaboration: *University of Duisburg

T. Hauschild
K.-H. Heinig
*M. Jentschel**
*H.-G. Börner**

Study of the interatomic potentials in zinc sulfide (ZnS)
At the high-flux neutron reactor in Grenoble Crystal-GRID experiments have been performed with ZnS single crystals in two different orientations (<111> and <110>) with respect to the axis of the spectrometer. This method allows to get information about the interatomic solid state potentials by fitting the parameters of analytical potential energy functions to the experimental Doppler broadening lines. Molecular dynamics (MD) simulations have been performed to the special situation of GRID where, due to neutron capture and the first photon emission, the recoiling atrom starts with a kinetic energy of about 500 eV within the crystal.

For a first time the theoretically predicted asymmetric line shape could be verified experimentally for the crystal aligned with their <111> direction along the spectrometer axis. At the current state of data evaluation, it seems to be clear that the lifetime of the 3221 keV level in ^{33}S is longer than the value of (40 ± 12) fs reported in literature. For this reason the line shapes are much less structured than predicted by computer simulations using the reported lifetime, i.e. less information can be extracted for the investigation of the potentials. Nevertheless the clearly visible structure of the line shape allows the extraction of improved nuclear lifetimes and parameters of ion-solid interactions. A further improvement is expected from a recently accepted measurement with <100> aligned crystals.

Collaboration: ILL Grenoble, France

Equipment

M. Friedrich
S. Turuc
W. Bürger

Operation and development of the electrostatic accelerators

All three electrostatic MeV accelerators have been operating very reliably.

The *2 MV VdG* has been applied exclusively for RBS measurements. A new charging belt from the IPPE Obninsk/Russia has been tested. It has shown a high electric stability, but after 300 and 600 h of operation the belt had to be repaired due to discharge tracks.

The *5 MV Tandem* has been applied to ion beam analysis, high energy implantation, basic ion-solid interaction research and detector development. Two openings of the pressure vessel were necessary for maintenance (voltage divider and belt recharging system in the terminal). At the injector an additional duoplasmatron (NIIEFA St. Petersburg/Russia) has been installed for generation and acceleration of He ions.

The *3 MV Tandetron* has been used for high energy ion implantation, ion beam synthesis and ion beam analysis. Only one opening of the pressure vessel was necessary due to some destroyed needle bearings. A new precise digital control unit for the acceleration voltage has improved the control and stability of the acceleration voltage.

J. von Borany
M. Friedrich
W. Bürger
S. Turuc

New beamline for high energy ion implantation for industrial service purposes

For high-energy ion implantation into semiconductor wafers, in particular for high-power devices, a new beamline has been constructed and commissioned at the 5 MV Tandem accelerator. The two dimensional electrostatic scanning system (20 kV plate to plate voltage, scanning frequencies of about 1 kHz) enables a homogeneous implantation up to 15 cm x 15 cm area for singly charged protons and alphas up to 8.5 MeV energy. The implantation chamber has volume of about 150 l containing 14 irradiation positions for Si wafers with a diameter up to 5". Due to a large rotary pump (65 m³/h) and a very effective combination of a 1500 l/s turbomolecular pump and the APG Cryogenics Aqua Trap© system the evacuation time down to operation vacuum conditions ($< 1\times10^{-6}$ mbar) is below 10 min. Different ion beam sources

(sputter source, duoplasmatron) supply a typical ion beam density of 5-20 nA/cm^2 at the target position. The beam current density is measured by four Faraday cups situated at the corners of the irradiation field behind the wafer plane to avoid contaminations due to sputtering at the cup edges.

B. Schmidt

New clean-room laboratory

Since August 1998, the institute provides for a new clean-room facility of in all 320 m^2. The aim of this facility is to make available excellent preparation techniques for the research tasks in the fields of ion beam modification of semiconductors and corresponding ion beam analysis.

The facility includes laboratories and technical rooms at three floors: the basement floor with the media equipment for ultrapure water and gases as well as for the sewage treatment, the ground floor with the clean-room area, and the second floor with the air conditioning. The clean-room itself offers 118 m^2 of class 100.000 area with measuring and test equipment, 136 m^2 class 10.000 service area, 35 m^2 class 1000 operator area and 35 m^2 local working spots of class 100, warranting a good basis for semiconductor processing.

The clean-room enables the following preparation techniques: wet chemical processing (cleaning and etching), photolithography (2 μm level), thermal processing (furnace and rapid thermal treatment in the temperature range 300...2000°C for oxidation, diffusion and annealing), physical thin film deposition and fluorine based reactive ion etching or plasma etching.

The preparation equipment in the new 100 class clean-room is permanently used in wafer and sample preparation for the semiconductor related research tasks of the institute: high energy ion implantation, defect engineering by ion beams, high temperature treatment for defect annealing and electrical activation of dopands in Si, SiC and diamond as well as cleaning, etching and thin film deposition for the demands of ion beam analysis and electron microscopy. It comprises the pre- and after-ion-beam-treatment, the fabrication of test structures and samples for different analytical and experimental investigations as well as industrial customer based semiconductor wafer processing and device development.

Etching and annealing steps are accomplished to form $CoSi_2$ silicide layers after FIB implantation in silicon. At present, main emphasis is directed to the fabrication of semiconductor nanoclusters in thin dielectric layers by ion beam synthesis for optoelectronic and memory circuit applications. This research activity requires the deposition of thin films, different annealing processes under very well defined conditions (temperature, atmosphere) and the fabrication of MOS- or optoelectronic device structures. Within this topic a new PVD process has been developed, which allows the growth of stacked Si-nanocluster monolayers in SiO_2 applying the deposition of SiO_x films by reactive magnetron sputtering and appropriate subsequent annealing. The well developed wet chemical anisotropic etching of Si is mainly applied to the fabrication of crystalline Si membranes for transmission ion beam experiments, and to the fabrication of Si cantilevers, which are used for optical in situ stress measurements during the deposition of BN-layers by the IBAD process.

The clean-room gives a significantly improved basis for device preparation. Industrial customer based development and device fabrication are focused to the fabrication of silicon radiation detectors for environment radiation monitoring and silicon electron detectors, which are used for the diagnostics of the electron beam in electron beam lithography equipment for the ULSI technology.

List of Abbreviations

Analytical Methods

AES	Auger electron spectroscopy
AFM	Atomic force microscopy
AMS	Accelerator mass spectroscopy
CEMS	Conversion electron Mössbauer spectroscopy
EDX	Energy dispersive X-ray spectroscopy
ERDA	Elastic recoil detection analysis
FTIR	Fourier transform infrared spectroscopy
GRID	Gamma-ray induced Doppler-broadening
GDOS	Glow discharge optical spectroscopy
HRTEM	High resolution transmission electron microscopy
NRA	Nuclear reaction analysis
PAS	Positron annihilation spectroscopy
PIRR	Polarized infrared reflection spectroscopy
PIXE	Proton induced X-ray emission
RBS	Rutherford backscattering spectroscopy
RBS/C	Rutherford backscattering spectroscopy under channeling conditions
SE	Spectroscopic ellipsometry
SEM	Scanning electron microscopy
SIMS	Secondary ion mass spectroscopy
SQUID	Superconductive quantum interference detection
SPIS	Slow positron implantation spectroscopy
STEM-EDX	Scanning TEM with EDX-analysis
TEM	Transmission electron microscopy
XPS	X-ray excited photoelectron spectroscopy
XRD	X-ray diffraction
XTEM	Cross-section transmission electron microscopy

Preparation Techniques

CVD	Chemical vapour deposition
FIB	Focused ion beam
IBAD	Ion beam assisted deposition
LPCVD	Low pressure chemical vapour deposition
MOS	Metal-oxide-semiconductor
PECVD	Plasma enhanced chemical vapour deposition
PIII	Plasma immersion ion implantation
RTA	Rapid thermal annealing

Supporting Institutions

BMBF	Bundesministerium für Bildung und Forschung
DAAD	Deutscher Akademischer Austauschdienst
DFG	Deutsche Forschungsgemeinschaft
EU	European Union
SMWA	Sächsisches Staatsministerium für Wirtschaft und Arbeit
SMWK	Sächsisches Staatsministerium für Wissenschaft und Kunst
TMR	European Programm „Training and Mobility of Researchers"

Statistics

Publications

Albe, K., Möller, W.,
Modelling of boron nitride: atomic scale simulations on thin film growth,
Computat. Mat. Sci. 10 (1998) 111

Anwand, W., Parascandola, S., Richter, E., Brauer, G., Coleman, P.G., Möller, W.,
Slow positron implantation spectroscopy of high current ion nitrided austenitic stainless steels,
Nucl. Instr. Meth. B136-138 (1998) 768

Assmann, W., Dobler, M., Avasthi, D. K., Kruijer, S., Mieskes, H. D., Nolte, H.,
Swift heavy ion induced formation of α-FeSi$_2$,
Nucl. Instr. Meth. B146 (1998) 271

Barth, K.L., Fukarek, W., Maucher, H.P., Plass, M.F., Lunk, A.,
In situ characterization of cubic boron nitride film growth in the IR spectral region,
Thin Solid Films 313-314 (1998) 697

Behrisch, R., Grigull, S., Kreissig, U., Grötzschel, R.,
Influence of surface roughness on measuring depth profiles and the total amount of implanted ions by RBS and ERDA,
Nucl. Instr. Meth. B136-138 (1998) 628

Bonhaus, J., Harlander, T., Borchert, D., Ecke, G., Fontaine, F., Fahrner, W.R.,
High sensitive thermal sensors in heat spreading diamond for industrial application,
IEEE International Symposium on Industrial Electronics, Proceedings vol. 1,2 (1998) p. 157

Brauer, G., Anwand, W., Coleman, P.G., Störmer, J., Plazaola, F., Campillo, J.M., Pacaud, Y., Skorupa, W.,
Post-implantation annealing of SiC studied by slow positron spectroscopies,
J. Phys.: Condens. Matter 10 (1998) 1147

Brenscheidt, F., Matz, W., Wieser, E., Möller, W.,
Tribological properties and hardness of silicon nitride ceramics after ion implantation and subsequent annealing,
Surf. Coat. Technol. 110 (1998) 188

Brenscheidt, F., Piekoszewski, J., Wieser, E., Langner, J., Grötzschel, R., Reuther, H.,
Modification of silicon nitride ceramics with high intensity pulsed ion beams,
Mat. Sci. Eng. A253 (1998) 86

Brückner, J., Günzel, R., Richter, E., Möller, W.,
Metal plasma immersion ion implantation and deposition (MPIIID): chromium on magnesium,
Surf. Coat. Technol. 103-104 (1998) 227

Dobler, M., Reuther, H., Möller, W.,
Phase formation of iron silicides by ion implantation,
Hyperfine Interactions (c) 3 (1998) 145

Dobler, M., Reuther, H., Möller, W.,
Microdisperse iron silicide structures produced by implantation of iron ions in silicon,
Hyperfine Interactions 112 (1998) 185

Dvurechenskii, A.V., Karanovich, A.A., Grötzschel, R., Herrmann, F., Kögler, R., Rybin, A.V.,
Depth distribution of point defects in Si bombarded by high-energy N^{5+} and Si^{5+} ions,
Phys. Solid State 40 (1998) 195

Fichtner, P.F.P., Kaschny, J.R., Kling, A., Trinkaus, H., Yankov, R.A. Mücklich, A., Skorupa, W.,
Zawislak, F.C., Amaral, L., da Silva, M.F., Soares, J.C.,
Nucleation and growth of platelet bubble structures in helium implanted silicon,
Nucl. Instr. Meth. B136-138 (1998) 460

Fukarek, W., Yankov, R.A., Anwand, W., Heera, V.,
Damage in silicon carbide induced by Rutherford backscattering analysis,
Nucl. Instr. Meth. B142 (1998) 561

Fung, S., Gong, M., Beling, C.D., Brauer, G., Wirth, H., Skorupa, W.,
Aluminium-implantation induced deep levels in n-type 6H-SiC,
J. Appl. Phys. 84 (1998) 1152

Ganetsos, Th., Tsamakis, D., Panknin, D., Mair, G.L.R., Teichert, J., Bischoff, L., Aidinis, C.,
$Si_{1-x}Ge_x$ structures fabricated by focused ion beam implantation,
J. de Phys. IV 8 (1998) Pr3-109

Gong, M., Reddy, C.V., Beling, C.D., Fung, S., Brauer, G., Wirth, H., Skorupa, W.,
Deep-level traps in the extended tail region of boron-implanted n-type 6H-SiC,
Appl. Phys. Lett. 72 (1998) 2739

Groß, B., Marion, St., Hempelmann, R., Grambole, D., Herrmann, F.,
Proton conducting $Ba_3Ca_{1.18}Nb_{1.82}O_{8.73}/H_2O$: Sol-gel preparation and pressure/composition isotherms,
Solid State Ionics 109 (1998) 13

Hausmann, S., Bischoff, L., Teichert, J., Grambole, D., Hermann, F., Möller, W.,
Investigation of dwell-time effects on the cobalt disilicide formation using focused ion beam
implantation,
Microelectr. Eng. 41/42 (1998) 233

Hausmann, S., Bischoff, L., Teichert, J., Voelskow, M., Grambole, D., Herrmann, F.,
Möller, W.,
Dose rate effects in focused ion beam synthesis of cobalt disilicide,
Appl. Phys. Lett. 72 (1998) 2719

Heera, V.,
Comment on "Amorphization and defect recombination in ion implanted silicon carbide",
J. Appl. Phys. 83 (1998) 3935

Henkel, T., Heera, V., Kögler, R., and Skorupa, W.,
In-situ laser reflectometry study of the amorphization of 6H-SiC by MeV ion implantation,
J. Appl. Phys. 84 (1998) 3090

Höfgen, A., Heera, V., Eichhorn, F., and Skorupa, W.,
Annealing and recrystallization of amorphous silicon carbide produced by ion implantation,
J. Appl. Phys. 84 (1998) 4769

Jäger, H.U., Weiler, M.,
Molecular-dynamics studies of a-C:H film growth by energetic hydrocarbon molecule impact,
Diamond Relat. Mat. 7 (1998) 858

Jankuhn, St., Butz, T., Flagmeyer, R.-H., Reinert, T., Vogt, J., Barckhausen, B., Hammerl, J., Protsch von Zieten, R., Grambole, D., Herrmann, F., Bethge, K.,
Ion microprobe analyses of ancient human bone,
Nucl. Instr. Meth. B136-138 (1998) 329

Kachurin, G.A., Leier, A.F., Zhuravlev, K.S., Tyschenko, I.E., Gutakovsky, A.K., Volodin, V.A., Yankov, R.A., Skorupa, W.,
Effect of ion dose and annealing mode on the photoluminescence from SiO_2-layers implanted with Si-ions,
Phys. Techn. Semiconductors (in Russian) 32 (1998) 1371

Kaschny, J.R.A., Fichtner, P.F., Mücklich, A., Kreißig, U., Yankov, R.A., Skorupa, W.,
Helium bubbles in silicon: study of the residual helium content using elastic recoil detection analysis,
Nucl. Instr. Meth. B136-138 (1998) 583

Kharlamov, V.S., Kulikov, D.V., Trushin, Yu.V., Yankov, R.A.,Voelskow, M., Pezoldt, J., Skorupa, W.,
Computer simulation and RBS/C studies of high dose N^+ and Al^+ co-implantation in 6H-SiC,
Proc. SPIE-The Int.Society for Optical Engineering 3345 (1998) 260

Kleinsorge, B., Ilie, A., Chowalla, M., Fukarek, W., Milne, W.I., Robertson, J.,
Electrical and optical properties of boronated tetrahedrally bonded amorphous carbon (ta-C:B),
Diamond and Related Mat. 7 (1998) 472

Kögler, R., Yankov, R.A., Kaschny, J.R., Posselt, M., Danilin, A.B., Skorupa, W.,
Spatial distribution of defects in ion-implanted and annealed Si,
Nucl. Instr. Meth. B142 (1998) 493

Krähenbühl, U., Noll, K., Döbeli, M., Grambole, D., Herrmann, F., Tobler, L.,
Exposure of Allan Hills 84001 and other achondrites on the Antarctic ice,
Meteoritics and Planetary Science 33 (1998) 665

Kreissig, U., Grigull, S., Lange, K., Nitzsche, P., Schmidt, B.,
In situ ERDA studies of ion drift processes during anodic bonding of alkali-borosilicate glass to metal,
Nucl. Instr. Meth. B136-138 (1998) 674

Kruijer, S., Nikolov, O., Keune, W., Reuther, H., Weber, S., Scherrer, S.,
Depth analysis of phase formation in α-Fe after high-dose Al ion implantation,
J. Appl. Phys. 84 (1998) 6570

Kruijer, S., Dobler, M., Reuther, H., Keune, W.,
Depth analysis of Fe-silicide formation after Fe-implantation into Si by DCEMS,
Hyperfine Interactions (c) 3 (1998) 149

Küchler, R., Richter, E.,
Ultrasonic surface waves for studying the properties of thin films,
Thin Solid Films 315 (1998) 29

Kulikov, D.V., Trushin, Yu.V., Yankov, R.A., Pezoldt, J., Skorupa W.,
Theoretical description of high-temperature implantation of 6H-SiC with N^--and Al^--ions,
Tech. Phys. Lett. 24 (1998) 17

Mäder, M., Grambole, D., Herrmann, F., Neelmeijer, C., Schreiner, M., Woisetschläger, G.,
Non-destructive evaluation of glass corrosion states,
Nucl. Instr. Meth. B136-138 (1998) 863

Mändl, S., Günzel, R., Möller, W.,
Sheath and presheath dynamics in plasma immersion ion implantation,
J. Phys. D 31 (1998) 1109

Mändl, S., Günzel, R., Richter, E., Möller, W.,
Nitriding of austenitic stainless steels using plasma immersion ion implantation,
Surf. Coat. Technol. 100-101 (1998) 372

Mändl, S., Günzel, R., Rauschenbach, B., Hilke, R., Knösel, E., Künanz, K.,
Characterization of drills implanted with nitrogen plasma immersion ion implantation,
Surf. Coat. Technol. 103-104 (1998) 167

Manova, D., Dimitrova, V., Fukarek, W., Karpuzov, D.,
Investigation of d.c.-reactive magnetron-sputtered AlN thin films by electron microprobe analysis, X-ray
photoelectron spectroscopy and polarized infra-red reflection,
Surf. Coat. Technol. 106 (1998) 205

Mantl, S., Kappius, L., Antons, A., Löken, M., Klinkhammer, F., Dolle, M., Zhao, Q.T., Mesters, S.,
Buchal, C., Bay, H.L., Kabius, B., Trinkaus, H., Heinig, K.-H.,
Growth, patterning and microelectronic applications of epitaxial cobaltdisilicide,
MRS Symp. Proc. 514 (1998) 145

Markwitz, A., Matz, W., Waldschmidt, M., Demortier, G.,
Investigation of the atomic interdiffusion and phase formation in ion beam-irradiated thin Cu-Al and Ag-
Al multilayers by in-situ RBS and XRD,
Surf. Interf. Anal. 26 (1998) 160

Markwitz, A., Schmidt, B., Matz, W., Grötzschel, R., Mücklich, A.,
Microstructural investigation of ion beam synthesised germanium nanoclusters embedded in SiO$_2$ layers,
Nucl. Instr. Meth. B 142 (1998) 338

Markwitz, A., Matz, W., Schmidt, B., Grötzschel, R.,
Depth profile analysis: STEM-EDX vs. RBS,
Surf. Interf. Anal. 26 (1998) 359

Markwitz, A., Prokert, F., Waldschmidt, M., Demortier, G.,
X-ray reflectivity investigation of near-surface density changes induced in Al-Au multilayers by high-
current ion beam bombardment,
Nucl. Instr. Meth. B143 (1998) 422

Markwitz, A., Matz, W.,
Phase formation in ion beam bombarded Al-Au multilayers using high-current 2.0 MeV ^{4}He$^+$ ions,
Surf. Interf. Anal. 26 (1998) 650

Matz, W., Pham, M.T., Mücklich, A.,
Nanometre-sized silver halides entrapped in SiO$_2$ matrices,
J. Mat. Sci. 33 (1998) 155

Matz, W.,
Rossendorfer Beamline an der ESRF,
Phys. Bl. 54 (1998) 785

Matz, W., Schell, N., Funke, H., Bernhard, G.,
ROBL (German Beamline) on BM20: Structural and radiochemical investigations,
ESRF- Newsletter, April 1998, 45

Mazur, K., Sass, J., Eichhorn, F.,
X-ray high resolution diffraction and reflectivity studies of the mechanical treatment related defects in
NdGaO$_3$ single crystals,
J. Phys.: Condens. Matter 10 (1998) 6065

Mieskes, H. D., Assmann, W., Brodale, M., Dobler, M., Glückler, H., Hartung, P., Stenzel, P.,
Measuring sputtering yields of high energy heavy ions on metals,
Nucl. Instr. Meth. B146 (1998) 162

Moelle, C., Werner, M., Szüczs, F., Wittorf, D., Sellschop, M., Borany, J. von, Fecht, H.-J., Johnston, C.,
Specific heat of single-, poly- and nanocrystalline diamond,
Diamond and Rel. Mat. 7 (1998) 499

Möller, W., Fukarek, W., Grigull, S., Kruse, O., Parascandola, S.,
Dynamic in situ diagnostics using high-energy ion beam analysis,
Nucl. Instr. Meth. B136-138 (1998) 1203

Möller, W., Richter, E.,
Praktische Anwendungen der Ionenimplantation,
Galvanotechnik 89 (1998) 858

Müller, M., Herzer, G., Mattern, N., Grahl, H., Schnell, B., Reibold, M., Reuther, H.,
Structure and magnetic properties in the low temperature annealing range of FeZrBCu-base alloys,
J. Phys. IV 8 (1998) Pr 2-187

Murthy, C.S., Posselt, M., Feudel, T.,
Physically-based modeling of two-dimensional and three-dimensional implantation profiles: influence of
damage accumulation,
J. Vac. Sci. Technol. B16 (1998) 440

Neelmeijer, C., Mäder, M., Jarjis, R., Calligaro, T., Salomon, J., Schreiner, M., Gantz, T.,
Initial inter-laboratory testing of the Rossendorf-Oxford (ROX97) secondary standard for X-ray analysis,
Nucl. Instr. Meth. B136-138 (1998) 902

Neelmeijer, C., Hüller, J., Mäder, M., Borchers, B., Jarjis, R.A.,
A simple paper-based secondary standard for energy dispersive X-ray analysis,
Nucl. Instr. Meth. B140 (1998) 191

Nitzsche, P., Lange, K., Schmidt, B., Grigull, S., Kreissig, U., Thomas, B., Herzog. K.,
Ion drift processes in PYREX-type alkali-borsilicate glass during anodic bonding,
J. Electrochem. Soc. 145 (1998) 1755

Noll, K., Döbeli, M., Grambole, D., Herrmann, F., Krähenbühl, U.,
Fluorine enrichement on the surface of antarctic C30 and H chondrites by nuclear reaction analysis
(NRA) and the sources of this terrestrial fluorine,
Meteoritics and Planetary Science 33 (1998) Supplement, A118

Otte, K., Lippold, G., Grambole, D., Herrmann, F., Schlemm, H., Schindler, A., Bigl, F.,
Hydrogen incorporation into Cu-III-VI2 chalcopyrite semiconductors,
Mat. Res. Soc. Symp. Proc. 513 (1998) 275

Parascandola, S., Günzel, R., Grötzschel, R., Richter, E. Möller, W.,
Analysis of deuterium induced nuclear reactions giving criteria for the formation process of expanded
austenite,
Nucl. Instr. Meth. B136-138 (1998) 1281

Perez-Rodriguez, A., Gonzalez-Varona, O., Calvo-Barrio, L., Morante, J. R., Wirth, H., Panknin, D., Skorupa, W.,
Raman scattering analysis of defects in 6H-SiC induced by ion implantation,
Mat. Sci. Forum 258 - 263 (1998) 727

Pezoldt, J., Yankov, R.A., Voelskow, M., Brauer, G., Anwand, W., Heera, V., Skorupa, W., Coleman, P.G.,
Studies of buried $(SiC)_{1-x}(AlN)_x$ layers formed by co-implantation of N^+ and Al^+ ions into 6H-SiC,
Proc. 7th Int. Conf. Defect Recognition and Image Processing of Semicond. (DRIP VII)
Inst. Phys. Conf. Ser. No 160 (1998) IOP Publishing Ltd. Bristol, 1998, 335

Pham, M.T., Zyganow, I., Matz, W., Reuther, H., Oswald, S., Richter, E., Wieser, E.,
Corrosion behavior and microstructure of titanium implanted with α and β stabilizing elements,
Thin Solid Films 310 (1997) 25

Pham, M.T., Möller, D., Matz, W., Mücklich, A., Oswald, S.,
CdS nanocrystals entrapped in thin SiO_2 films,
J. Phys. Chem. B21 (1998) 4081

Pilz, W., Borany, J. von, Grötzschel, R., Jiang, W., Posselt, M., Schmidt, B.,
Dependence of the silicon detector response to heavy ions on the direction of incidence: computer simulations versus experimental data,
Nucl. Instr. Meth. A419 (1998) 137

Posselt, M.,
Computer simulation of channeling profile analysis of implantation damage,
Mat. Res. Soc. Symp. Proc. 532 (1998) 133

Prokert, F., Ritter, H., Ihringer, J.,
X-ray diffraction study of phase transitions in $Sr_{0.75}Ba_{0.25}Nb_2O_6$ between 20 K and 400 K,
Ferroel. Lett. 24 (1998) 1

Rebohle, L., Borany, J. von, Grötzschel, R., Markwitz, A., Schmidt, B., Tyschenko, I. E., Skorupa, W., Fröb, H., Leo, K.,
Strong blue and violet photo- and electroluminescence from Ge- and Si-implanted silicon dioxide,
Phys. Stat. Sol. (a) 165 (1998) 31

Rebohle, L., Tyschenko, I.E., Borany, J. von, Schmidt, B., Grötzschel, R., Markwitz, A., Yankov, R.A., Fröb, H., Skorupa, W.,
Strong blue and violet light emission from silicon- and germanium-implanted silicon-dioxide films,
Mat. Res. Soc. Symp. Proc. 486 (1998) 175

Reinert, T., Butz, T., Flagmeyer, R.-H., Jankuhn, St., Vogt, J., Gründer, W., Kanowski, M., Wagner, M., Werner, A., Grambole, D., Herrmann, F.,
Investigation of the calcium content in joint cartilage: Is it connected with (early arthrotic) changes in cartilage structure?,
Nucl. Instr. Meth. B136-138 (1998) 936

Reuther, H., Betzl, M., Matz, W., Richter, E.,
Investigation of Fe-Mg-alloys produced by ion implantation,
Hyperfine Interactions 112 (1998) 165

Reuther, H., Betzl, M., Matz, W., Richter, E.,
Alloying by high dose ion implantation of iron into magnesium and aluminium,
Hyperfine Interactions 113 (1998) 391

Reuther, H., Behr, G., Dobler, M., Teresiak, A.,
Angle dependent Mössbauer spectroscopy on β-FeSi$_2$ single crystals,
Hyperfine Interactions (c) 3 (1998) 385

Richter, E., Günzel, R.,
Härtung von Edelstahl ohne Korrosionsverlust,
Vakuum in Forschung und Praxis 10 (1998) 198

Schmidt, B., Nitzsche, P., Lange, K., Grigull, S., Kreissig, U., Thomas, B., Herzog, K.,
In situ investigation of ion drift processes in glass during anodic bonding,
Sensors and Actuators A67 (1998) 191

Schmidt, Br., Posselt, M., Strecker, N., Feudel, T.,
Atomistic simulation of ion implantation into 2D structures,
Computat. Mat. Sci. 11 (1998) 87

Schmidt, Br., Posselt, M., Strecker, N., Feudel, T.,
Atomistic modeling of ion implantation within a 2D process simulator,
Mat. Res. Soc. Symp. Proc. 490 (1998) 21

Schneider, M., Nocke, K., Richter, E.,
Untersuchungen zum Korrosionsverhalten von Magnesium nach Ionenimplantation,
Galvanotechnik 80 (1998) 2524

Seifarth, H., Grötzschel, R., Markwitz, A., Matz, W., Nitzsche, P., Rebohle, L. ,
Preparation of SiO$_2$ films with embedded Si nanocrystals by reactive rf-magnetron sputtering,
Thin Solid Films 330 (1998) 202

Soltani-Farshi, M., Baumann, H., Anwand, W., Brauer, G., Coleman,P.G., Richter, E., Kreißig, U.,
Bethge, K.,
Positron Studies of defects in nitrogen and carbon implanted titanium,
Mat. Res. Soc. Symp. Proc. 527 (1998) 81

Soltani-Farshi, M., Baumann, H., Rück,D., Richter, E., Kreissig, U., Bethge,K.,
Content of hydrogen in boron-, carbon-, nitrogen-, oxygen-, fluorine- and neon-implanted titanium,
Surf. Coat. Technol. 103-104 (1998) 299

Spaeth, C., Richter, F., Grigull, S., Kreissig,U.,
Conversion algorithm for ERDA multielement spectra and its application to thin-film problems,
Nucl. Instr. Meth. B140 (1998) 243

Strobel, M., Heinig, K.-H., Möller, W.,
A combination of atomic and continuum models describing the evolution of nanoclusters,
Computat. Mat. Sci. 10 (1998) 457

Teichert, J., Voelskow, M., Bischoff, L., Hausmann, S.,
RBS and channeling analysis of cobalt disilicide layers produced by focused ion beam implantation,
Vacuum 51 (1998) 261

Teichert, J., Bischoff, L., Hausmann, S.,
Ion beam synthesis of cobalt disilicide using focused ion beam implantation,
J. Vac. Sci. Technol. B16 (1998) 2574

Turos, A.,Wierzchowski, W.,Wieteska, K., Wendler, E., Wesch,W., Graeff, W., Grötzschel, R., Strupinski,W.,
Ion bombardment induced relaxation of strained AlGaAs/GaAs heterostructures studied by the complementary use of RBS-channeling and X-ray synchrotron radiation,
Nucl. Instr. Meth. B136-138 (1998) 1062

Wang, X., Charlamov, V., Kolitsch, A., Posselt, M., Trushin, Y., Möller, W.,
Study of ion beam assisted deposition of Al/AlN multilayers by comparison of computer simulation and experiment,
 J. Phys. D31 (1998) 2241

Wang, X., Kolitsch, A., Prokert, F., Möller, W.,
Ion beam assisted deposition of AlN monolithic films and Al/AlN multilayers: a comperative study,
Surf. Coat. Technol. 103-104 (1998) 334

Werninghaus, T., Zahn, D.R.T., Yankov, R.A., Mücklich, A., Pezoldt, J.,
Cross-sectional micro-Raman Spectroscopy: a tool for structural investigations of thin polytypic SiC layers,
Mat. Sci. Forum 264-268 (1998) 661

Wesch, W., Karmann, A., Börner, H.G., Jentschel, M., Heinig, K.-H.,
GRID spectroscopy - a new nuclear method for lattice site localization of foreign atoms,
 Nucl. Instr. Meth. B136-138 (1998) 494

Wieser, E., Grötzschel, R., Mücklich, A., Prokert, F.,
Microstructure and tribological properties of aluminium implanted with high doses of nickel ,
Nucl. Instr. Meth. B134 (1998) 365

Wieser, E., Richter, E., Grötzschel, R., Mücklich, A., Prokert, F.,
Microstructure and wear behaviour of aluminium implanted with nickel,
Surf. Coat. Technol. 103-104 (1998) 353

Wieser, E., Tsyganov, I., Matz, W., Reuther, H., Oswald, S., Pham, T., Richter, E.,
Modification of titanium by ion implantation of calcium and/or phosphorus,
Surf. Coat. Techn. 111 (1998) 103

Wirth, H., Anwand, W., Brauer,G., Voelskow, M., Panknin, D., Skorupa,W., Coleman, P.G.,
Investigation of ion-implantation induced damage in 6H-SiC by RBS/C and PAS,
Mat. Sci. Forum 264-268 (1998) 729

Yankov, R.A., Fukarek, W., Hatzopoulos, N., Voelskow, M., Kreißig, U., Brauer, G., Anwand, W., Heera,V., Skorupa, W.,
Ion beam synthesis: a novel method of producing $(SiC)_{1-x}(AlN)_x$ layers,
Mat. Sci. Forum 264-268 (1998) 753

Conference Contributions

Albe, K. (invited),
Computersimulationen zu Struktur und Wachstum von Bornitrid,
Workshop "Molekulare Dynamik" des SFB 438 der Universität Augsburg, Herrsching, April 24, 1998

Albe, K., (invited)
Computer simulations on thin film growth of superhard materials,
4th Int. Conf. on Computer Simulation of Radiation Effects in Solids, Okayama, Japan,
Sept. 15-19, 1998

Anwand, W., Brauer, G., Coleman, P.G., Voelskow, M., Skorupa, W.,
Characterisation of defects in ion implanted SiC by slow positron implantation spectroscopy and
Rutherford backscattering,
8th Int. Workshop on Slow Positron Beam Techniques for Solids and Surfaces (SLOPOS-8),
Cape Town, Sept. 6- 12, 1998

Anwand, W., Brauer, G., Coleman, P.G., Voelskow, M., Skorupa, W.,
Characterisation of defects in ion implanted SiC by slow positron implantation spectroscopy and
Rutherford backscattering,
30th Polish Seminar on Positron Annihilation, Jarnoltowek, Sept. 17-21, 1998

Anwand, W., Brauer, G., Coleman, P.G., Yankov, R., Skorupa, W.,
Characterisation of vacancy-type defects in Al^+ and N^+ co-implanted SiC by slow positron implantation
spectroscopy (SPIS),
30th Polish Seminar on Positron Annihilation, Jarnoltowek, Sept. 17-21, 1998

Anwand, W., Brauer, G., Coleman, P.G., Yankov, R., Skorupa, W.,
Characterisation of vacancy-type defects in Al^+ and N^+ co-implanted SiC by slow positron implantation
spectroscopy (SPIS),
8th Int. Workshop on Slow Positron Beam Techniques for Solids and Surfaces (SLOPOS-8),
Cape Town, Sept 6-12, 1998

Bischoff, L., Hausmann, S., Voelskow, M., Teichert, J.,
Dwell-time dependence of the defect accumulation in focused ion beam synthesis of $CoSi_2$,
E-MRS'98, Strasbourg, France, June 16-19, 1998

Bonhaus, J., Harlander, T., Borchert, D., Ecke, G., Fontaine, F., Fahrner, W.R.,
High Sensitive Thermal Sensors in Heat Spreading Diamond for Industrial Application,
IEEE Int. Symp. on Industrial Electronics (ISIE `98), Pretoria, South Africa, July 7 - 10, 1998

Borany, J. von, Grötzschel, R., Heinig, K.-H., Markwitz, A., Schmidt, B., Skorupa, W., Thees, H.-J.,
The formation of narrow nanocluster bands in Ge-implanted SiO_2-layers,
E-MRS'98, Strasbourg, France, June 16-19, 1998

Borany, J. von, (invited)
New aspects in the design of silicon detectors for particle spectroscopy,
1ˢᵗ Dresden Protection Symposium on „New Aspects of Radiation Measurements, Dosimetry and
Alphaspectrometry", Dresden , March, 4-6, 1998

Borodin, V.A., Heinig, K.-H., Schmidt, B.,
Non-local approach to modeling of nanocluster evolution in ion implanted layers,
E-MRS'98, Strasbourg, France, June 16-19, 1998

Brauer, G., Ley, R., Schneider, H., Arnold, W.,
Concept of an intense positron source at the new superconducting LINAC 'ELBE',
15th Int. Conf. on the Application of Accelerators in Research and Industry (CAARI '98), Denton/TX,
Nov. 4-7, 1998

Deshkovskaya, A.A., Richter, E.,
Einfluß der Ionenimplantation auf die Festigkeit von Quarzglas,
28. Int. Konf. Physik der Wechselwirkung geladener Teilchen mit kristallinen Materialien, Moskau,
May 25- 27, 1998

Deshkovskaya, A.A., Richter, E.,
Ion bombardment stimulated phase formation in quartz glasses,
11.th Int. Conf. on Ion Beam Modification of Materials, Amsterdam, Netherlands,
Aug. 31 - Sept. 4, 1998

Dobler, M., Reuther, H.,
Untersuchung der Eisendisilizidbildung nach der Implantation von Fe in Si,
10. Arbeitstagung Angewandte Oberflächenanalytik AOFA 10, Kaiserslautern, Sept. 6-10, 1998

Dobler, M.,
CEMS-Eisendisilizide-Ionenstrahlverfahren,
IX. Mößbauerkolloquium Freiberg, Sept. 28-30, 1998

Eichhorn, F., Sass, J., Mazur, K.,
X-ray studies of silicon wafers implanted with MeV Ge^{++} ions,
4th Europ. Conf. on High Resolution X-ray Diffraction and Topography, Durham/GB, Sept. 9-12, 1998

Fichtner, P.F.P., Kaschny, J. R., Behar, M., Yankov, R., Mücklich, A., Skorupa, W.,
The effects of annealing temperature on the formation of helium filled structures in silicon,
11th Int. Conf. on Ion Beam Modification of Materials (IBMM'98), Amsterdam, Aug. 31 - Sept. 4, 1998

Fichtner, P.F.P., Kaschny, J.R., Yankov, R.A., Mücklich, A., Skorupa, W.,
Temperature effect on the morphology of helium bubble clusters in silicon,
14th Int. Conf. On Electron Microscopy, Cancum, Mexico, Aug. 31-Sept.5, 1998

Fischer, C.G., Connell, S.H., Coleman, P.G., Anwand, W., Malik, F., Brauer, G., Britton, D.T.,
Sellschop, J.F.P.,
A slow positron beam investigation of positron-defect interactions in single crystalline synthetic type IB
diamonds and a natural type IIB diamond,
8th Int. Workshop on Slow Positron Beam Techniques for Solids and Surfaces (SLOPOS-8),
Cape Town , Sept. 6-12, 1998

Fukarek, W., (invited)
Applications of infrared spectroscopy in materials research,
33. Holzhau-Meeting, March 30 – April 3, 1998

Fukarek, W., Möller, W.,
In plane anisotropy of IBAD t-BN films,
Gordon Research Conference on Plasma Processing Science, Tilton School, New Hampshire, USA,
Aug. 9–14, 1998

Fukarek, W., Möller, W.,
Investigation of in-plane anisotropy of IBAD t-BN films,
DACH - Kolloquium, Giengen, Oct. 6-8, 1998

Fukarek, W., Möller, W.,
Analysis of mechanisms in ECR-PECVD of BN films using in situ ellipsometry,
DACH - Kolloquium, Giengen, Oct. 6-8, 1998

Ganetsos, Th., Tsamakis, D., Panknin, D., Mair, G.L.R., Teichert, J., Bischoff, L., Aidinis, C.,
$Si_{1-x}Ge_x$ structures fabricated by focused ion beam implantation,
Conference in Low Temperature Devices, Toscane, Italy, June 1998

Gong, M., Beling, C.D., Fung, S., Brauer, G., Wirth, H.D., Skorupa, W., You, Z.-P.,
Ions and electron-irradiation induced deep levels in n-type and p-type 6H-SiC,
MRS 1998 Spring Meeting, San Francisco, April 13-17, 1998

Grambole, D., Herrmann, F., Behrisch, R., Hauffe, W.,
Hydrogen and deuterium depth profiling in divertor tiles of a fusion experiment by micro-ERDA,
6th Int. Conf. on Nucl. Microprobe Technology and Applications, Stellenbosch, South Africa,
Oct. 11 -16, 1998

Grigull, S., Behrisch, R. Parascandola, S.,
Nitrogen implantation into carbon: retention, release and target erosion process,
13.th Int.Conf. on Plasma Surface Interactions in Controlled Fusion Devices, San Diego,
May 18-22, 1998

Grötzschel, R., Kreissig, U., Kruse, O., Grigull, S., Parascandola, S., Schmidt, B., (invited)
ERDA in-situ studies of atomic transport processes in various materials,
Int.Conf. on Swift Heavy Ions in Materials Engeneering and Characterization (SHIMEC-98), New Delhi,
Oct. 19 - 22, 1998

Groß, B., Marion, St., Lind, K., Hempelmann, R., Grambole, D., Herrmann, F.,
Proton conducting $Ba_3Ca_{1.18}Nb_{1.82}O_{8.73}$ /H_2O: Pressure/compositions isotherms in terms of Fermi-Dirac-Statistics,
9th Int. Conf. on Solid State Protonic Conductors (SSSPC-9), Bled, Slovenia, Aug. 17 -21, 1998

Günzel, R.,
An integrated high voltage modulator for plasma immersion ion implantation,
4th Int. Workshop on PBII, Dearborn, June 2-4, 1998

Günzel, R., Richter, E., Uglov, V., V., Khodasevich, A., K., Kuleshov, A., K., Fedotova, J., A.,
Rusalsky, D.,
Plasma immersion ion implantation for improvement of mechanical properties of AISI M2 steel,
4th Int. Workshop on PBII, Dearborn, June 2-4, 1998

Günzel, R., Brückner, J., Richter, E., Möller, W.,
Plasma-Immersions-Implantation – ein modernes Verfahren zur Modifizierung von
Werkstückoberflächen, Werkstoffwoche München, Oct. 12 – 15, 1998

Günzel, R., Mändl, S., Möller, W., Hilke, R., Knösel, E., Künanz, K.,
Phasenbildung und Standzeiterhöhung von HSS-Bohrern nach Plasma-Immersions-Implantation,
Werkstoffwoche München, Oct. 12 –15, 1998

Günzel, R., Mändl, S., Richter, E., Liu, A., Tang, B., Y., Chu, P., K.,
Corrosion protection of titanium by deposition of niobium thin films,
PSE98, Garmisch-Partenkirchen, Sept. 14-18, 1998

Hausmann, S., Bischoff, L., Voelskow, M., Teichert, J., Möller, W., Fuhrmann, H.,
Dwell-time effects in the focused ion beam synthesis of cobalt disilicide: reflectivity measurements,
11th Int. Conf. on Ion Beam Modification of Materials, Amsterdam, Aug. 31 – Sept. 4, 1998

Heera, V., Stoemenos, J., Kögler, R., Voelskow, M., Skorupa, W.,
Crystallization and surface erosion of SiC by ion irradiation at elevated temperatures,
ECSCRM '98 (2nd European Conf. on Silicon Carbide and Related Materials), Montpellier,
Sept. 2-4, 1998

Heinig, K.-H., Schmidt, B., Markwitz, A., Grötzschel, R., Strobel, M., Borany, J. von, (invited)
Nanocrystal formation in SiO_2: experiments, modelling and computer simulations,
E-MRS'98, Strasbourg, France, June 16-19, 1998

Heinig, K.-H., Börner, H.G., Jentschel, M., (invited)
Application of high-resolution γ-spectroscopy (GRID method) in solid state physics,
Int. Workshop on Applications of High-Precision γ-Spectroscopy, University of Notre Dame,
Notre Dame, IL, USA, July 1-3, 1998

Heinig, K.-H., Strobel, M.,
A combination of computer simulation methods to predict quantum dot evolution during ion beam
synthesis,
4th Int. Conf. on Computer Simulation of Radiation Effects in Solids, Okayama, Japan,
Sept. 15 -19, 1998

Hempel, A., Saneyasu, M., Tang, Z., Hasegawa, M., Brauer, G., Plazaola, F., Yamaguchi, S.,
Effects of neutron irradiation on Fe-Cu model alloys and RPV steels probed by positron annihilation and
hardness measurements,
19th Symp. on Effects of Radiation on Materials, Seattle/WA, June 16-18, 1998

Herrmann, S., Mahnke, H.-E., Spellmeyer, B., Wienecke, M., Reinhold, B., Yankov, R.A.,
Gumlich, H.-E.,
Pd diffusion in ZnTe and CdTe,
E-MRS'98, Strasbourg, June 16-19, 1998

Höfgen, A., Heera, V., Eichhorn, F., Skorupa, W.,
Annealing and recrystallization of amorphous silicon carbide produced by ion implantation,
ECSCRM '98 (2nd European Conf. on Silicon Carbide and Related Materials), Montpellier,
Sept. 2-4, 1998

Hornauer, U., Richter, E., Wieser, E., Möller, W.,
Improvement of the high temperature oxidation resistance of Ti50Al via ion implantation,
11th Int. Conf. on Ion Beam Modification of Materials, Amsterdam, the Netherlands,
Aug. 31 - Sept. 4, 1998

Huber, H., Assmann, W., Karamian, S.A., Mieskes, H.D., Nolte, H., Gazis, E., Kokkoris, M.,
Kossionides, Vlastou, R., Grötzschel, R., Mücklich, A., Prusseit, W.,
Heavy-Ion induced damage of crystalline Ge and W at 0.5 to 8 MeV/u range,
Int. Conf. on Swift Heavy Ions in Matter (SHIM-98), Berlin, May 1998

Jankuhn, St., Butz, T., Flagmeyer, R.-H., Reinert, T., Vogt, J., Barckhausen, B., Hammerl, J., Protsch von
Zieten, R., Grambole, D., Herrmann, F., Bethge, K.,
Untersuchung historischer menschlicher Knochen mit Ionen-Mikrosonde,
Frühjahrstagung der Fachverbände Chemische Physik, Kurzzeitphysik, Plasmaphysik, Polymerphysik,
Bayreuth, March 9 - 13, 1998

Jäger, H.U.,
Growth of ion-beam deposited a-C and a-C:H films: molecular-dynamics simulations using empirical many-body potential expressions,
9th Europ. Conf. on Diamond, Diamond-Like Materials, Nitrides and Silicon Carbide, Crete, Greece, Sept. 13-18, 1998

Jagielski, J., Kopcewicz, M., Turos, A., Eichhorn, F.,
Structural analysis of Si/Fe and Mo/Fe ion-beam mixed layers,
11th. Int. Conf. on Ion Beam Modification of Materials, Amsterdam, The Netherlands,
Aug. 31 - Sept. 4, 1998

Jentschel, M., Börner, H.G., Heinig, K.-H., Doll, C.,
The GRID technique: current status and new trends,
Int. Workshop on Applications of High-Precision γ-Spectroscopy, University of Notre Dame,
Notre Dame, IL, USA, July 1-3, 1998

Karmann, A., Wesch, W., Börner, H.G., Jentschel, M., Heinig, K.-H.,
Lattice site location of foreign atoms measured by the GRID method,
Int. Workshop on Applications of High-Precision γ-Spectroscopy, University of Notre Dame,
Notre Dame, IL, USA, July 1-3, 1998

Koch, T., Heinig, K.-H., Jentschel, M., Börner, H.G.,
Study of interatomic potentials in ZnS - Crystal-GRID experiments versus ab initio calculations,
Int. Workshop on Applications of High-Precision γ-Spectroscopy, University of Notre Dame,
Notre Dame, IL, USA, July 1-3, 1998

Krieger, K., Maier, H., Grambole, D., Schleussner, D., Franzen, P.,
Hydrogen isotope inventories in plasma facing components of ASDEX UPGRADE,
17th IAEA Fusion Energy Conference, Yokohama, Japan, Oct. 19 -24, 1998

Kachurin, G.A., Leier, A.F., Zhuravlev, K.S., Tyschenko, I.E., Gutakovsky, A.K., Volodin, V.A., Yankov, R.A., Skorupa, W.,
Effect of ion dose and annealing mode on the photoluminescence from SiO_2-layers implanted with Si-ions,
11th Int. Conf. on Ion Beam Modification of Materials, Amsterdam,The Netherlands,
Aug. 31 - Sept. 4, 1998

Kappius, L., Antons, A., Dolle, M., Trinkaus, H., Mesters, S., Bochem, H.-P., Mantl, S., Heinig, K.-H.,
Nanopatterning of thin $CoSi_2$ layers by local oxidation,
MRS Spring Meeting, San Francisco, CA, USA, April 13-17, 1998

Kaschny, J.R., Fichtner, P.F.P., Yankov, R.A., Fukarek, W., Mücklich, A., Kreißig, U., Peeva, A., Danilin, A.B., Skorupa, W.,
Gettering of iron and oxygen at cavities formed by helium ion implantation in Czochralski and float-zone silicon,
E-MRS´98, Strasbourg, June 16-19, 1998

Knapp, W., Bischoff, L., Teichert, J.,
Electron emission characteristics of solidified gold alloy liquid metal ion sources,
2nd Int. Vacuum Electron Source Conf., Tsukuba, Japan, July 7 - 10, 1998

Kögler, R., Eichhorn, F., Mücklich, A., Skorupa, W., Danilin, A.B.,
Distribution of gettering centres at a buried amorphous layer in Si,
11th Int. Conf. on Ion Beam Modification of Materials, Amsterdam,The Netherlands,
Aug. 31 - Sept. 4, 1998

Kögler, R., Yankov, R.A., Posselt, M., Danilin, A.B., Skorupa, W.,
Defects remaining in MeV-ion-implanted Si away from the peak of the nuclear energy deposition,
E-MRS´98, Strasbourg, June 16-19, 1998

Kögler, R., Yankov, R.A., Skorupa, W.,
Defect agglomeration in ion implanted silicon away from R_P,
XIIth Int. Conf. Ion Implantation Technology (IIT´98), Kyoto, Japan, June 22-26, 1998

Kögler, R., Eichhorn, F., Mücklich, A., Skorupa, W., Danilin, A. B.,
Spatial distribution of gettering centres in ion-implanted and annealed silicon ,
11th. Int. Conf. on Ion Beam Modification of Materials, Amsterdam, The Netherlands,
Aug. 31 - Sept. 4, 1998

Kolitsch, A., Wang, X., Manova, D, Fukarek, W. Oswald, S., Möller, W.,
Effects of Ti and Al incorporations on the structure of boron nitride films,
9th Europ. Conf. on Diamond, Diamond-Like Materials, Nitrides and Silicon Carbide DIAMOND, Crete,
Greece, Sept. 1998

Kolitsch, A., Wang, X., Möller, W.,
BN based multilayers by ion beam assisted deposition,
MRS Fall Meeting 1998, , Boston, USA, Dec. 1998

Kolitsch, A., Schöneich, J.,
Development of a user data base system for ion implanter operation,
5th DANFYSIK User Meeting, Brindisi, Italy, Sept. 1998

Kolitsch, A., Wang, X., Möller, W.,
Deposition of nanoscaled multilayer structures by ion beam assisted deposition,
5th DANFYSIK User Meeting, Brindisi, Italien, Sept. 1998

Kruijer, S., Walterfang, M., Keune, W., Dobler, M., Reuther, H.,
Tiefenselektive Phasenanalyse der Fe-Silizidbildung in Fe-ionenimplantiertem Si mittels DCEMS,
DPG-Frühjahrstagung, Regensburg, March 23-27, 1998

Kruse, O., Grötzschel, R.,
Dynamic in-situ diagnostics using ERD analysis,
ION'98, Kazimierz Dolny, Poland, June 16 - 19, 1998

Kulikov, D.V., Pezoldt , J., Rybin, P.V., Skorupa, W., Trushin, Yu.V., Yankov, R.A.,
Theoretical and experimental studies of $(AlN)_{(1-x)}(SiC)_x$ layer structures formed by N^+ and Al^+
co-implantation 6H-SiC,
Int.Workshop Nondestructive Testing and Computer Simulations in Science and Engineering,
E2, St.Petersburg, Russia, June 8-12, 1998

Kulikov, D.V., Trushin, Yu.V., Yankov, R.A., Kreißig, U., Fukarek, W., Mücklich, A., Skorupa, W.,
Pezoldt J.,
Modeling high temperature co-implantation of N^+-and Al^+-ions into SiC: the effects of stress on the
implant and damage distributions,
E-MRS´98, Strasbourg, June 16-19, 1998

Mäder, M., Neelmeijer, C., Schreiner, M.,
Composition analysis of medieval glass using PIXE,
8th. Int. Conf. on PIXE and its Analytical applications, Lund, Sweden, June 14-18, 1998

Mäder, M., Neelmeijer, C., Schreiner, M.,
Vorsorgeuntersuchung an historischem Glas,
Jahrestagung der GDCh, Archäometrie und Denkmalpflege, Würzburg, Sept. 23 -25, 1998

Mändl, S., Günzel, R., Richter, E., Möller, W.,
Nitrogen and boron implantation into austenitic stainless steel,
4th Int. Workshop on PBII, Dearborn, June 2-4, 1998

Mändl, S., Richter, E., Günzel, R., Möller, W.,
Nitrogen plasma immersion ion implantation into high speed steel,
11th Int. Conf.on Ion Beam Modification of Materials, Amsterdam, The Netherlands,
Aug. 31 - Sept. 4, 1998

Markwitz, A., Rebohle, L., Skorupa, W.,
Homogeneously size distributed Ge-nanoclusters embedded in SiO_2-layers produced by ion beam
synthesis,
E-MRS'98, Strasbourg, June 16-19, 1998

Matz, W. (invited),
Introduction to X-ray diffraction at synchrotron light sources,
Euroconf. and NEA Workshop on Speciation Techniques and Facilities for Radioactive Materials at
Synchrotron Light Sources, Grenoble, Oct. 4-6, 1998

Möller, W. (invited),
Plasma immersion implantation for diffusive treatment,
PSE'98, Garmisch-Partenkirchen, Sept. 14 - 18, 1998

Möller, W. (invited),
Plasma based ion implantation (4 lectures),
NATO ASI, "Advanced Technologies Based on Wave and Beam Generated Plasmas",
Sozopol, Bulgaria, May 28 - 30, 1998

Möller, W. (invited),
Schichtanalyse mit Ionenstrahlen,
W. E.-Heraeus-Ferienkurs, Chemnitz, Sept. 7, 1998

Möller, W. (invited),
Plasma-Immersions-Ionenimplantation,
Sommerschule "Nukleare Sonden und Ionenstrahlen", Bad Blankenburg, Sept., 1998

Mrotschek, I., Günzel, R., Matz, W. Möller, W., Anishchik, V.,
Beam line implantation of boron into hard metals,
ION'98, Kazimierz Dolny, Poland, June 16-19, 1998

Narojczyk, J., Piekoszewski, J., Richter, E., Werner, Z.,
Wear properties of TiN coated cutting tools implanted with nitrogen ions,
ION'98, Kazimierz Dolny, Poland, June 16-19, 1998

Näser, A., Gehlhoff, W., Overhof, H., Yankov, R.A.,
EPR identification of a shallow donor state of cadmium in silicon,
8th Int. Conf. on Shallow Level Centres in Semiconductors, Montpellier, France, July 27-30, 1998

Näser, A., Gehlhoff, W., Yankov, R.A.,
Paramagnetische Störstellen in Si nach Implantation von Pd,
DPG-Tagung, Regensburg, Germany, March 23, 1998

Neelmeijer, C., Mäder, M., Pietsch, U., Ulbricht, H., Walcha, H.-M.,
Johann Gregorius Höroldt fecit?
Jahrestagung der GDCh, Archäometrie und Denkmalpflege, Würzburg, Sept. 23 - 25, 1998

Noetzel, J., Geisler, H., Gorbunov, A., Dietsch, R., Mai, H., Mensch, A., Möller, W., Pompe, W.,
Reuther, H., Toselev, A., Wieser, E., Worch, H.,
Structure of laser-deposited Fe/Al multilayers,
6th Int. Symp. on Trends and New Applications of Thin Films, Regensburg, March 1998

Otte, K., Schlemm, H., Schindler, A., Bigl, F., Lippold, G.,Grambole, D.,Herrmann, F.,
Hydrogen incorporation into Cu-III-VI$_2$ chalcopyrite semiconductors,
MRS Spring Meeting, San Francisco, USA, April 13 -17, 1998

Panda, B.K., Brauer, G.,
Positron affinities and deformation potentials in cubic semiconductors,
30th Polish Seminar on Positron Annihilation, Jarnoltowek, Sept. 17-21, 1998

Panknin, D., Wirth, H., Mücklich, A., Skorupa, W.,
Correlation of electrical and microstructural properties after high dose aluminium implantation into 6H-
SiC,
ECSCRM '98 (2nd European Conf. on Silicon Carbide and Related Materials), Montpellier,
Sept. 2-4, 1998

Parascandola, S., Kruse, O., Richter, E. Möller, W.,
Nitrogen transport during plasma ion nitriding of austenitic stainless steel - the role of the native surface
oxide layer,
Int. Conf. on Metallurgical Coatings and Thin Films, San Diego, April 27 - May 1, 1998

Parascandola, S., Kruse, O., Richter, E., Möller, W.,
Nitriding stainless steel at moderate temperature - time- and depth-resolved characterization of the near
surface composition during the nitriding process,
4th Int.Workshop on PBII, Dearborn, June 2-4, 1998

Parascandola, S., Kruse, O., Richter, E. Möller, W.,
Nitriding of stainless steel by low energy ion implantation - the nitriding kinetics,
11th Int. Conf. on Ion Beam Modification of Materials, Amsterdam, The Netherlands,
Aug. 31 - Sept. 4, 1998

Pezoldt, J., Yankov, R.A., Mücklich, A., Fukarek, W., Reuter, H., Skorupa, W.,
A novel (SiC)$_{1-x}$(AlN)$_x$ compound synthesized using ion beams,
E-MRS'98, Strasbourg, June 16-19, 1998

Pezoldt, J., Yankov, R.A., Fukarek, W., Mücklich, A., Fontaine, F., Skorupa, W., Werninghaus, T.,
Zahn, D.R.T.,
Structural and compositional characterisation of N$^+$ and Al$^+$ co-implanted 6H-SiC using optical methods,
9th Europ. Conf. on Diamond, Diamond-like Materials, Nitrides, and Silicon Carbide, Crete, Greece,
Sept. 13-18, 1998

Piekoszewski, J., Werner, Z., Wieser, E., Langner, J., Grötzschel, R., Reuther, H., Jagielski, J.,
Formation of surface Pd-Ti alloys using pulsed plasma beams,
ION'98, Kazimierz Dolny, Poland, June 16-19, 1998

Piekoszewski, J., Wieser, E., Groetzschel, R., Reuther, H., Werner, Z., Langner, A.,
Pulsed plasma beam mixing of Ti and Mo on Al$_2$O$_3$ substrates,
11th Int. Conf. on Ion Beam Modification of Materials, Amsterdam, The Netherlands,
Aug. 31 - Sept. 4, 1998

Posselt, M.,
Microscopic processes of damage production during ion implantation studied by combining time-ordered
BCA with MD simulations,
MRS Spring Meeting, San Francisco, CA, USA, April 13-17, 1998

Posselt, M.,
Computer simulation of channeling profile analysis of implantation damage,
MRS Spring Meeting, San Francisco, CA, USA, April 13-17, 1998

Posselt, M.,
Defect production and evolution during and after ion implantation studied by a combination of time-
ordered BCA with MD simulations,
XIIth Int. Conf. Ion Implantation Technology (IIT'98), Kyoto, Japan, June 22-26, 1998

Prokert, F., Betzl, M., Eichhorn, F., Matz, W., Schell, N.,
The Installations for Materials Research on ROBL at the ESRF,
Jahrestagung DGK, Karlsruhe, März 1998

Rebohle, L., Borany, J. von, Skorupa, W., Tyschenko, I.E., Fröb, H.,
Photoluminescence and electroluminescence investigations at Ge-rich SiO$_2$ layers,
E-MRS'98, Strasbourg, June 16-19, 1998

Rebohle, L., Borany, J. von, Markwitz, A., Skorupa, W.,
Is there still any hope for blue luminescence from silicon?
E-MRS'98, Strasbourg, June 16-19, 1998

Rebohle, L., Borany, J. von, Tyschenko, I.E., Skorupa, W.,
Strong blue electroluminescence from Ge-rich silicondioxide-on-silicon formed by ion beam synthesis,
XIIth Int. Conf. Ion Implantation Technology (IIT'98), Kyoto, Japan, June 22-26, 1998

Reuther, H.,
Charakterisierung von durch Ionenimplantation hergestellten Fe-Al-Schichten mittels Augerelektronen-
und Mößbauerspektroskopie,
10. Arbeitstagung Angewandte Oberflächenanalytik AOFA 10, Kaiserslautern, Sept. 6-10, 1998

Reuther, H.,
Temperaturverhalten von durch Hochdosisimplantation hergestellten Al-Fe-Legierungen,
IX. Mößbauerkolloquium, Freiberg, Sept. 28-30, 1998

Schmidt, B., Heinig, K.-H., Markwitz, A., Grötzschel, R., Strobel, M., Oswald, S.,
Precipitation, ripening and chemical effects during annealing of Ge$^+$ implanted SiO$_2$ layers,
11th Int. Conf. on Ion Beam Modification of Materials, Amsterdam, The Netherlands,
Aug. 31 - Sept. 4, 1998

Schreiner, M., Mantler, M., Neelmeijer, C., Mäder, M.,
Non-destructive analysis of elements with low atomic numbers (Na – K) in artifacts using X-ray
fluorescence analysis,
31th Int. Symp. on Archaeometry, Budapest, Hungary, April 27 - May 1, 1998

Sendezera, E.J., Davidson, A.T., Fischer, C.G., Connell, S.H., Sellschop, J.F.P., Anwand, W., Brauer, G., Nicht, E.-M.,
Characterisation of Al-implanted LiF by a monoenergetic positron beam,
8th Int. Workshop on Slow Positron Beam Techniques for Solids and Surfaces (SLOPOS-8),
Cape Town, Sept. 6-12, 1998

Serre, C., Perez-Rodriguez, A., Romano-Rodriguez, A., Morante, J.R., Fonseca, L., Acero, M.C., Esteve, J., Kögler, R., Skorupa, W.,
Bonding and etch-back of ion beam synthesized beta-SiC for SiCOI formation,
NATO Advanced Workshop "Perspectives, Science and Technologies for Novel Silicon on Insulator Devices", Kiev, Ukraine, Oct. 1998

Serre, C., Romano-Rodriguez, A., Perez-Rodriguez, A., Morante, J.R., Fonseca, L, Acero, M.C., Kögler, R., Skorupa, W.,
Beta-SiC on SiO_2 formed by ion implantation and bonding for micromechanical applications,
E-MRS'98, Strasbourg, France, June 16 - 19, 1998

Skorupa, W., (invited)
Ion beam processing for silicon-based light emission,
XIIth Int. Conf. Ion Implantation Technology (IIT'98), Kyoto, Japan, June 22-26, 1998

Smirnov, V.K., Kibalov, D. S., Krivlevich, S.A., Lepshin, P.A., Potapov, E.V., Ynakov, R.A., Skorupa, W., Danilin, A. B., Makarov, V. V.,
Wave-ordered nanostructures formed on silicon-on-insulator wafers by means of reactive ion beams,
E-MRS'98, Strasbourg, France, June 16 - 19, 1998

Soltani-Farshi, M., Baumann, H., Anwand, W., Brauer, G., Coleman, P.G., Richter, E., Kreissig, U., Bethge, K.,
Positron studies of defects in nitrogen and carbon implanted titanium,
1998 Spring Meeting, San Francisco/CA, April 13-17, 1998

Soltani-Farshi, M, Baumann, H., Richter, E., Kreißig, U., Bethge, K.,
The behaviour of hydrogen in titanium after ion implantation,
CAARI'98, Denton, USA, December 1998

Stölzel, M., Born, R., Scharnweber, D., Worch, H., Pham, M.T., Wieser, E.,
In vitro Charakterisierung modifizierter ionenimplantierter Titanoberflächen,
Werkstoffwoche, München, Germany, Oct. 12-15, 1998

Strobel, M., Heinig, K.-H., Möller, W., Meldrum, A., Zhou, D.S., White, C.W., Zuhr, R.A.,
Ion beam synthesis of gold nanoclusters in SiO_2: computer simulations versus experiments,
E-MRS Spring Meeting, Strasbourg, France, June 16-19, 1998

Strobel, M., Heinig, K.-H., Möller, W.,
Can core/shell nanocrystals be formed by sequential ion implantation? Predictions from kinetic lattice Monte Carlo simulations,
11th Int. Conf. on Ion Beam Modification of Materials, Amsterdam, The Netherlands,
Aug. 31 - Sept. 4, 1998

Strobel, M., Heinig, K.-H., Moeller, W.,
Computer simulation studies of the competition between nucleation and ion mixing in ion beam synthesis of nanoclusters,
4th Int. Conf. on Computer Simulation of Radiation Effects in Solids, Okayama, Japan,
Sept. 15-19, 1998

Teichert, G., Schleicher, L., Knedlik, Ch., Voelskow, M., Skorupa, W., Yankov, R.A., Pezoldt, J.,
Thermal wave analysis: a tool for non-invasive testing ion beam synthesis of wide band gap materials,
MRS Fall Meeting., Boston, USA, Nov. 30 - Dec. 4, 1998

Turos, A., Gawlik, G., Jagielski, J., Stonert, A., Matz, W., Grötzschel, R.,
Ion Beam Mixing of the ZrO_2/Fe System ,
11Int. Conf. on Ion Beam Modification of Materials, Amsterdam,The Netherlands,
Aug. 31 - Sept. 4, 1998

Tyschenko, I.E., Kachurin, G.A., Rebohle, L., Yankov, R.A., Skorupa, W., Misiuk, A.,
The effect of annealing under hydrostatic pressure on the visible photoluminescence from Si^+-implanted
SiO_2 films,
E-MRS´98, Strasbourg, June 16-19, 1998

Tyschenko, I.E., Kachurin, G.A., Rebohle, L., Skorupa, W.,
Room temperature visible photoluminescence from Ar^+- and Ge^+-implanted Si_3N_4- and SiO_XN_Y-films,
E-MRS´98, Strasbourg, June 16-19, 1998

Tyschenko, I.E., Kachurin, G.A., Zhuravlev, K.S., Rebohle, L., Skorupa, W.,
Effect of hydrostatic pressure annealing on visible photoluminescence from Si^+- and Ge^+-implanted SiO_2
films,
11th Int. Conf. on Ion Beam Modification of Materials, Amsterdam, The Netherlands,
Aug. 31 - Sept. 4, 1998

Uglov, V., V., Rusalsky, D., P., Kholmetskii, A., L., Khodasevich, V., V., Ruebenbauer, K., Günzel, R.,
Richter, E., Wilbur, P., J., Wei, R.,
Surface modification of AISI M2 steel by nitrogen plasma immersion ion implantation,
11th Int. Conf. on Ion Beam Modification of Materials, Amsterdam, The Netherlands,
Aug. 31 - Sept. 4, 1998

Waidmann, S., Bartsch, K., Endler, I., Fontaine, F., Arnold, B., Knupfer, M., Leonhardt, A., Fink, J.,
Electron energy-loss spectroscopy in transmission of undoped and doped diamond films,
E-MRS'98, Strasbourg, France, June 16 - 19, 1998

Walterfang, M., Kruijer, S., Keune, W., Dobler, M., Reuther, H.,
Tiefenselektive Phasenanalyse Si-ionenimplantierter α-Fe-Oberflächen mittels DCEMS,
DPG-Frühjahrstagung, Regensburg, March 23-27,1998

Wang, X., Kolitsch, A., Zhao, J.P., Möller, W.,
Similarity of energetic depositions of cubic boron nitride and titanium nitride thin films,
MRS Fall Meeting 1998, Boston, USA, Nov. 30 - Dec.4, 1998

Wirth, H., Anwand, W., Mücklich, A., Panknin, D., Voelskow, M., Brauer, G., Skorupa, W., Gonzalez-
Varona, O., Perez-Rodriguez, A.,
Ion-implantation induced damage In 6H-SiC: the influence of substrate temperature,
40th Electronic Materials Conference (EMC'98), Charlottesville, Virginia, USA,June 24-26, 1998

Wirth, H., Panknin, D., Perez-Rodriguez, A., Brauer, G., Anwand, W., Voelskow, M., Skorupa, W.,
Electrical and microstructural effects in highly doped 6H-SiC after Al-implantation,
40th Electronic Materials Conference (EMC'98), Charlottesville, Virginia, USA, June 24-26, 1998

Zappe, S., Obermeier, E., Stoemenos, J., Möller, H., Krötz, G., Wirth, H., Skorupa, W.,
Stabilisation of the 3C-SiC/SOI system by an intermediate Si_3N_4 layer,
ECSCRM '98 (2nd European Conf. on Silicon Carbide and Related Materials), Montpellier,
Sept. 2-4, 1998

Zuhr, R.A., Budai, J.D., Datskos, P.G., Meldrum, A., Thomas, K.A., Warmack, R.J. White, C.W., Feldman, L.C., Strobel, M., Heinig, K.-H.,
Nanostructured arrays formed by finely focused ion beams,
MRS Fall Meeting, Boston, USA, Nov. 30 - Dec. 4, 1998

Lectures

Borany, J. von,
Abschlußseminar zum SMWA-Verbundprojekt:
Miniaturisiertes Analysesystem für die Gewässerüberwachung,
Dresden, 30.06.1998

Brauer, G.,
Characterization of vacancy-type defects in ion implanted SiC by positron annihilation spectroscopy,
University of the Witwatersrand (Schonland Research Centre for Nuclear Sciences), Johannesburg,
12.01.1998

Brauer, G.,
Comparative study of ion implanted SiC by slow positron implantation and Rutherford backscattering/
channeling spectroscopies,
Texas Christian University (Department of Physics), Ft. Worth/TX, 02.11.1998

Brauer, G.,
Comparative study of ion implanted SiC by slow positron implantation and Rutherford backscattering/
channeling spectroscopies,
University of Texas at Arlington (Physics Department), Arlington/TX, 03.11.1998

Brauer, G.,
Charakterisierung leerstellenartiger Defekte in ionenimplantiertem SiC mit Positronen,
FZ Rossendorf, Zentrumsseminar, 10.12.1998

Dobler, M.,
Untersuchung der Bildung der Eisendisilizide während der Ionenstrahlsynthese und der ionenstrahl-
induzierten Phasenbildung,
Institutsseminar IIM, Februar 1998

Eichhorn, F., Matz, W., Prokert, F.,
Möglichkeiten der Röntgenuntersuchungen an Wafern in Rossendorf und an der ESRF,
WACKER Siltronic, Burghausen, 14.10.98

Fontaine, F., von Borany, J.,
Hochtemperatur-Implantation von Diamant,
2. Statusseminar zum BMBF-Verbundprojekt 'Sensorcluster für extreme Umgebungsbedingungen',
Fernuniversität Hagen, 2./3. Juni 1998

Grötzschel, R.,
In-situ -Ionenstrahlanalytik während der Ionenstrahlmodifikation dünner Schichten,
ETH Zürich, 9.6.1998

Günzel, R.,
Verschleißfester Edelstahl durch Plasmaimmersions-Ionenimplantation,
Robert Bosch AG, Crailsheim, March 9, 1998

Günzel, R., Richter, E.,
Plasma-Immersions-Implantation – ein modernes Verfahren zur Modifizierung von Werkstück-oberflächen,
Werkstoffforum der Hannover Messe, April 20 – 22, 1998

Günzel, R.,
Anlagentechnik für die Plasmaimmersions-Ionenimplantation,
Anwenderforum AWS, Meisdorf, December 12, 1998

Heinig, K.-H.,
Nanokristalle: Ein neues Material der Opto- und Halbleiterelektronik?
Physikalisches Institut der Universität Kaiserslautern, Jan. 19, 1998

Heinig, K.-H.,
Ion beam synthesis of nanocrystals - fundamentals and experiments,
Oak Ridge National Laboratory, Solid State Division, Oak Ridge, TN, USA, June 26, 1998

Heinig, K.-H.,
Ion beam synthesis of nanocrystals in SiO_2: experiments, modeling and computer simulations,
Vanderbilt University, Nashville, TN, USA, June 29, 1998

Herrmann, F., Grambole, D.,
Anwendungen der Rossendorfer Kernmikrosonde als Schwerionenmikroskop,
Arbeitstreffen Forschung mit nuklearen Sonden und Ionenstrahlen, Leipzig, 5. - 7. Okt. 1998

Höfgen, A.,
Ionenstrahlinduzierte Rekristallisation von amorphen SiC-Schichten,
Institut für Physik, TU Chemnitz, May 11, 1998

Kögler, R.,
Implantation defects in Si at half of the projected ion range (1/2 R_P),
Fed. Univ. of Rio Grande dol Sul, Porto Alegre, Brasilien, Nov.17, 1998

Kolitsch, A., Möller, W.,
Preparation of CN_x films by ion beam assited deposition
Kick-off Meeting of the TMR Project "New carbon based hard materials", Stockholm, Sweden, January, 1998

Kolitsch, A., Möller, W.,
Analytical methods of CN_x film investigations in Rossendorf – results,
Kick-off Meeting of the TMR Project "New carbon based hard materials", Stockholm, Sweden, January 1998

Matz, W., Betzl, M., Schell, N., Eichhorn, F., Prokert, F.,
Materialforschungsmeßplatz bei ROBL - erste Ergebnisse und Möglichkeiten,
Programmseminar des IIM, Rossendorf, Mai 1998

Matz, W.,
Die deutsche Beamline in Grenoble - Vom Radionuklidverhalten in der Umwelt bis zu Festkörper-untersuchungen,
1. BEAMline Seminar, Bundesanstalt für Materialprüfung Berlin, 12.-13. November 1998

Möller, W.,
Forschung mit Ionenstrahlen: Grundlagen und Anwendungen,
MPI für Plasmaphysik, Garching, April 17, 1998

Möller, W.,
Neue Technologien der Ionenimplantation,
Ruhr-Universität Bochum, Fakultät für Physik, April 20, 1998

Möller, W.,
Forschung mit Ionenstrahlen: Grundlagen und Anwendungen,
FernUniversität Hagen, April 21, 1998

Möller, W.,
Plasma immersion ion implantation for diffusive treatment,
Joint Research Center Ispra, Institute of Applied Physics, Italy, Oct. 16, 1998

Möller, W.,
Plasma immersion and low-energy ion implantation for the nitriding of metal surfaces,
Charles University Prag, Dept. of Polymer Physics, Oct. 26, 1998

Mrotschek, I.,
Oberflächenmodifizierung von Hartmetallen mittels Bor-Implantation,
Weißrussische Universität Minsk, July 28, 1998

Neelmeijer, C. (invited),
The scientific analysis of Böttger stoneware at the Research Center Rossendorf (Dresden, Germany),
1st Int. Workshop on the non-destructive characterisation of Böttger stoneware, J. Paul Getty Museum - Los Angeles/Cal., Nov. 1998

Parascandola, S.,
Nitriding of stainless steel at moderate temperature - time- and depth-resolved characterization of the near surface composition during the nidtriding process,
Colorado State University, Dept. of Mechanics and Enegineering, Fort Collins, USA, May 12, 1998

Peeva, A.,
Spatial distribution of defects in ion-implanted and annealed Si: the $R_p/2$ effect,
Fed. Univ. of Rio Grande dol Sul, Porto Alegre, Brasilien, Oct.27, 1998

Posselt, M.,
Theoretische Beschreibung von Implantationsprozessen: Grundlagen, Methoden, Anwendungen,
Sommerschule "Nukleare Sonden und Ionen", Bad Blankenburg, Germany, Sept. 21-25, 1998

Posselt, M.,
Computersimulation der Ionenimplantation in der Si-Technologie: Wechselspiel zwischen Kanalisierung und Defektbildung,
Physikalisches Institut der Universität Münster, July, 3, 1998

Rebohle, L.,
Photoluminescence and electroluminescence investigations at Ge-rich SiO_2 layers,
Sommerschule "Enrico Fermi", Varenna, Italy, 21-31 July 1998

Richter, E., Möller, W.,
Nitrierung von Leichtmetallen durch Ionenimplantation,
ATW-Tagung, Freiberg, April 15-16, 1998

Richter, E., Günzel, R.,
Härtung von Edelstahl ohne Korrosionsverlust,
2. Workshop Anwendungen moderner Oberflächentechnologien in der Medizintechnik, Tübingen, May 14, 1998

Skorupa, W.,
Ion beam processing of single crystalline SiC,
UK-User Meeting of the Ion Beam Laboratory at the School of Mathematics, Physics and Engineering,
University of Surrey, UK, April 1-3, 1998

Skorupa, W.,
Advanced ion beam processing of semiconductor materials,
Advanced Lectureship Program, Dept. of Appl. Phys., Univ. of Barcelona, Spain, May 11, 1998

Skorupa, W.,
Photo- and electroluminescence studies at ion beam synthesized Ge-rich SiO_2-layers,
Advanced Lectureship Program, Dept. of Appl. Phys., Univ. of Barcelona, Spain, May 12, 1998

Skorupa, W.,
Single event and soft error effects in silicon based device configurations,
AMD (Advanced Micro Devices) Saxony GmbH, Dresden, Oct. 15, 1998

Skorupa, W.,
Ion beam processing of single crystalline SiC,
Institut für Elektrotechnik, RWTH Aachen, Oct.19, 1998

Skorupa, W.,
Ion beam processing of single crystalline SiC,
Fed. Univ. of Rio Grande dol Sul, Porto Alegre, Brasilien, Nov.5, 1998

Skorupa, W.,
Ion beam synthesis of Ge-rich SiO_2-layers for photo-and electroluminescence,
Fed. Univ. of Rio Grande dol Sul, Porto Alegre, Brasilien, Nov. 13, 1998

Reports

Bischoff, L., Teichert, J.,
Focused ion beam sputtering of silicon and related materials,
Report FZR-217, March 1998

Borany, J. von, Gehring, T.,
Mikrofluidhandlingsystem für die chemische Analytik und Biotechnologie,
Abschlußbericht zum SMWA-Projekt, FKZ: 42-4333.15, June 1998

Borany, J. von, Gehring, T.,
Miniaturisiertes Analysensystem für die Gewässerüberwachung,
Abschlußbericht zum SMWA-Verbundprojekt, FKZ: 42-4333.16, June 1998

Borany, J. von, Fontaine, F.,
Implantationsdotierung von Diamant,
Zwischenbericht zum Verbundprojekt: Sensorcluster für extreme Umgebungsbedingungen, BMBF -
FKZ: 16 SV 548/2, February 1998

Brauer, G.,
Materialforschung mittels Positronen-Annihilationsspektroskopie,
SMWK: 4-7533-70-FZR/705, Zwischenberichte 22.01.1998, 14.07.1998

Brauer, G., Nicht, E.-M.,
Abschlußbericht 'PAS-Untersuchungen an 2024-Blechen' (Stand: 18.12.1998)
Industrie-Projekt Nr. 3448109

Rück, D.M., Schminke, A., Schmidt, H., Soltani-Farshi, M., Baumann, H., Fink, U., Richter, E.;
Tribological investigations of surface treated Ti6Al4V, GSI-98-29

Wirth, H.,
Elektrische und mikrostrukturelle Effekte in hochdotiertem 6H-SiC nach Ionenimplantation,
Report FZR-236, October 1998

Laboratory Visits

Betzl, M.,
European Synchrotron Radiation Facility, Grenoble, France,
May 4 - 12, June 7 - 9, Sept. 8 - 18, 1998

Bischoff, L., Teichert, J.,
Orsay Physics, Fuveau, France
Nov. 9 - 11, 1998

Brauer, G.,
University of the Witwatersrand (Schonland Research Centre for Nuclear Sciences), Johannesburg,
South Africa, Jan. 5 - 13, 1998

Brauer, G.,
Institut für Physik, Johannes-Gutenberg-Universität Mainz,
March 16-18, 1998

Brauer, G.,
Fachbereich Elektrotechnik, Fachhochschule Fulda,
May 19-20, 1998

Brauer, G.,
Physics Department, University of Texas at Arlington, Arlington/TX, USA,
Jun 22-Jul 6, 1998

Bürger, W.,
University of Helsinki, Dept. of Physics, Finland,
Dec. 8-12,1998

Eichhorn, F.,
European Synchrotron Radiation Facility, Grenoble, France,
Feb. 8 - 16, March 23 - April 3, June 7 - 9, Oct. 26 - Nov. 2, 1998

Eichhorn, F.,
Institute of Electronic Materials Technology, Warsaw, Poland,
June 29 - July 4, 1998

Günzel, R.,
City University of Hong Kong,
Nov. 4- 13, 1998

Heinig, K.-H.,
Universität Kaiserslautern,
Jan. 19 - 20, 1998

Heinig, K.-H.,
ILL Grenoble, France,
May 10 - 13, 1998

Heinig, K.-H.,
Oak Ridge National Laboratory, Solid State Division,Oak Ridge, TN, USA,
June 25 - 28, 1998

Heinig, K.-H.,
Vanderbilt University, Nashville, TN, USA,
June 28 - 30, 1998

Kögler, R.,
Fed. Univ. of Rio Grande do Sul, Porto Alegre, Brasil,
Nov. 2-25, 1998

Matz, W.,
European Synchrotron Radiation Facility, Grenoble, France,
Jan. 26 - 30, March 23 - 26, June 5 - 12, July 1 - 8, Oct. 3 - 8, Dez. 7 - 11, 1998

Matz, W.,
Bundesanstalt für Materialprüfung und -forschung, Berlin,
Nov. 12 - 13, 1998

Neelmeijer, C.,
National Centre for Scientific Research Demokritos, Athenes, Greek,
March 5 - 7, 1998

Neelmeijer, C.,
University of Oxford, Department of Materials, Oxford, UK,
Nov. 19 - 21, 1998

Neelmeijer, C.,
The J. Paul Getty Conservation Centre, Los Angeles, USA,
Nov. 2 - 4, 1998

Panda, B.K.,
Laboratory of Physics, Helsinki University of Technology, Finland,
Dec 7-31, 1998

Panknin, D.,
Institut für Elektrotechnik, Rheinisch-Westfälische TH Aachen,
Oct.19-20, 1998

Parascandola, S.,
Colorado School of Mines, Dept. of Physics, Golden, USA,
May 2 - 31, 1998

Peeva, A.,
Fed. Univ. of Rio Grande do Sul, Porto Alegre, Brasil,
Sept. 30 - Dec. 1, 1998

Posselt, M.,
Physikalisches Institut der Universität Münster,
July 3-4, 1998

Prokert, F.,
European Synchrotron Radiation Facility, Grenoble, France,
Jan. 28 - Feb. 6, May 4 - 12, Sept. 2 - 11, 1998

Reichel, P.,
European Synchrotron Radiation Facility, Grenoble, France,
March 19 - April 3, July 7 - 17, Sept. 8 - 18, 1998

Skorupa, W.,
Institut für Elektrotechnik, Rheinisch-WTH Aachen,
Oct.19-20, 1998

Skorupa, W.,
Fed. Univ. of Rio Grande do Sul, Porto Alegre, Brasil,
Nov. 2-18, 1998

Turuc, S.,
University of Helsinki, Dept. of Physics, Finland,
Dec. 8-12, 1998

Patents

Günzel, R.,
Modulator für die Plasmaimmersions – Ionenimplantation,
PCT/DE 98/00144

Parascandola, S., Günzel, R., Richter, E.,
Stickstoffhaltige Randschicht auf Bauteilen aus nichtrostendem Stahl und Verfahren zur Herstellung der Randschicht,
DP 198 20 152.4

Wirth, H., Skorupa, W., Panknin, D., Niemann, E.,
Verfahren zur Herstellung eines mikroelectronischen Halbleiterbauelements,
DP 198 08 245.2

Wirth, H., Skorupa, W., Panknin, D., Niemann, E.,
Verfahren zur Herstellung eines mikroelectronischen Halbleiterbauelements,
DP 198 08 246.0

PhD Theses

Albe, K.,
Computersimulation zu Struktur und Wachstum von Bornitrid,
TU Dresden, April 1998

Dobler, M.,
Untersuchung der Bildung der Eisendisilizide während der Ionenstrahlsynthese und der ionenstrahlinduzierten Phasenbildung,
TU Dresden, 23. 01. 1998

Wirth, H.,
Elektrische und mikrostrukturelle Effekte in hochdotiertem 6H-SiC nach Ionenimplantation,
TU Dresden, 28.9.98

Diploma Thesis

Gebel, T,
Spreading Resistance Messungen an Siliziumkarbid (6H-SiC)
TU Dresden, 29.9.98

Awards

Strobel, M.,
Graduate Student Award of the European Materials Research Society,
EMRS'98, Strasbourg, France, June 16-19, 1998

Albe, K.,
Doktorandenpreis des FZ-Rossendorf 1998

Meetings organized by the institute

2nd Summer School "Nuclear Probes and Ion Beams", Bad Blankenburg, Thuringia, Sept. 1998
(FZ Rossendorf/HMI Berlin)

Guests

C. Allen,
Argonne National Lab., Chicago, USA, April 16-20, 1998

W. Arnoldbik,
Debye Institute, Utrecht, Netherlands, Nov. 14-15, 1998

N. Barradas,
Univ. of Surrey, UK, Jan. 5 - 16, 1998

M. Behar,
Dept. of Physics, Univ. of Rio Grande dol Sul, Porto Allegre, Brazil, Aug. 17-22, 1998

V.I. Belko,
Belorussian State University, Minsk, Belarus, Sept. 1- Nov. 30, 1998

H. Bernas,
CSNSM, Paris-Orsay, France, Nov. 7 - 13, 1998

V.A. Borodin,
RRC Kurchatov Institute, Moscow, Russia, May 16 -July 18

S. Coffa,
IMETEM Catania, Italy, Jan.31-Feb.3, 1998

A. Danilin,
Centre for Analysis of Substances, Moskau, Oct. 5-7, 1998

A. A. Deshkovskaya,
Belarussian State University for Informatics and Radio Electronics, Minsk (Belarus),
Nov. 25 – Dec. 11, 1998

S. El Sayed Soliman Mohamed,
Ain Shams University Cairo, Egypt, Jan 1 - Jul 30, 1998

J. Engeldinger,
Univ. des Saarlandes, July 20 - 24, 1998

C. Fischer,
Wits University Johannesburg, South Africa, Jul 9-26, 1998

H. Fuhrmann,
Paul-Scherrer-Institut Zürich, March 25-26, 1998

T. Ganetsos,
The University of Athens, Department of Physics, April 12-24, 1998

B. Groß,
Univ. des Saarlandes, July 20 - 24,1998

R. Hellborg,
University of Lund, Dept. of Physics, Sweden, Dec. 8-11, 1998

W. Jiang,
PNNL , USA , Sept. 7 - 18, 1998

J. Kaschny,
Dept. of Physics, Univ. of Rio Grande dol Sul, Porto Allegre, Brazil, July 15 - Sept. 30, 1998

W. Knapp,
Otto-von-Guericke-Universität Magdeburg, Abt. Vakuumphysik und -technik,
24.2.98, 26.-28.3.98, 24.-25.4.98

J. Krynicki,
Insitute for Nuclear Chemistry and Technology, Warsaw, Poland, Nov. 11- 13, 1998

G. Lövestam,
Chalmers University of Technology, Göteborg, Sweden, July 14 -17, 1998

A. Malygin,
IPPE Obninsk, Accelerator Laboratory, Russia, April 1 - May 31, 1998

K. Mazur,
Institute of Electronic Materials Technology, Warsaw, Poland, Nov. 16 - 20, 1998

P. Meheust,
Université de Potitiers, Dec. 6 - 19, 1998

K. Meyer,
K., NAC Faure, RSA, May 30 - June 13, 1998

R. Mühle,
ETH Zürich, Institut für Teilchenphysik, March 25-26, 1998

S. Nikiforov,
Beamex Ltd., St. Petersburg, Russia, Nov. 23 - 27, 1998

K. Noll,
Univ. Bern, CH, May 18 - June 19, 1998

A. Osipowicz,
Fachhochschule Fulda, Jul 20-22, 1998

J. Padayachee,
NAC Faure, RSA, May 10 - June 13, 1998

B.K. Panda,
Alexander-von-Humboldt-Stipendiat, Indien, Apr 29 - Dec 31, 1998

J. Peisl,
Ludwig-Maximillian-Universität München, Feb. 18 - 19, 1998

J. Piekoszewski,
Insitute for Nuclear Chemistry and Technology, Warsaw, Poland,
Feb. 25 - March 6, May 6 - 15, July 22 - 31, Nov. 25 - Dec. 5, 1998

T. S. Pugatscheva,
Technical State University of Tashkent, Uzbekistan, May 12 – April 15, 1998

U. Reibetanz,
Univ. Leipzig, Aug. 5 - 8, 1998

T. Reinert,
Univ. Leipzig, Aug. 5 - 8, 1998

A. Revesz,
Revesz Associates, Bethseda,MD & Naval Research Lab., Washington, D.C., USA,
April 15-20, 1998

J.-P. Riviere,
Université de Poitiers, France, Oct. 26 – 30, 1998

M.-O. Ruault,
CSNSM, Paris-Orsay, France, Nov. 7 - 13, 1998

B. K. Saikia,
Centre of Plasma Physics, Guwahati, India,
Sept. 7 – Oct. 12, 1998 and Nov. 6, 1998 – Jan. 06, 1999

J. Sass,
Institute of Electronic Materials Technology, Warsaw, Poland, Nov. 16 - 20, 1998

S. Scharnholz,
RWTH Aachen, April 23-24, 1998

E. Sendezera,
Wits University Johannesburg, South Africa, May 31 - Jun 14, 1998

A. Ster,
MTA-KFKI, Research Institute for Technical and Materials Science, Budapest, Hungary,
Sept. 1-12, 1998

V. Stundzia,
University of Vilnius, Lithuania, March 1 – May 31, 1998

T. A. Telbizova,
University of Sofia, Bulgary, Feb. 15 – June 30, 1998

P. Tikkanen,
University of Helsinki, Dept. of Physics, Finland, Dec. 8-12, 1998

A. Turos,
Institute of Electronic Materials Technology, Warsaw, Poland, Feb. 25 - 28, 1998

G. Voronin,
Efremov Institute, Accelerator Dept., St. Petersburg, Russia, Nov. 23 - 27, 1998

A. M. Vredenberg,
Debye Institute, Utrecht, Netherlands, Nov. 14.-15.,1998

K. Wahlstrom,
University of Helsinki, Dept. of Physics, Finland, Dec. 8-12, 1998

X. Wang,
Shanghai Institute of Metallurgy, Chinese Academy of Sciences, Shanghai, PR China,
Jan. 1 - June 24, 1998

S. Warchol,
Insitute for Nuclear Chemistry and Technology, Warsaw, Poland, Nov. 11 - 13, 1998

W.J. Weber,
PNNL, USA, Aug. 7- 9, 1998

P. Werner,
MPI für Mikrostrukturphysik, Halle, May 18 - 20, 1998

Z. Werner,
Soltan Institute for Nuclear Studies, Swierk-Otwock, Poland, Nov. 28 - Dec. 3, 1998

R. A.Yankov,
TU Ilmenau and Bulg.Acad. of Sciences., Sofia, Jan.1-May 31, 1998

E. Zhurkin,
St. Petersburg State University, Russia, April 14 – May 13, 1998

I. Zyganov,
Lipetsk State University, Lipetsk, Russia, April 27 – July 25, 1998

Seminar of the Institute

K. Albe
FZ Rossendorf, IIM
Computersimulation zu Struktur und Wachstum von Bornitrid
Jan. 15, 1998

Dr. Henne
DLR Stuttgart
Neue Entwicklungen bei und Anwendungen von Gleichstrom- und Hochfrequenzplasmabrennern zum
thermischen Beschichten
Jan. 29, 1998

Dr. X. Wang
FZ Rossendorf, IIM
Multilayer formation by ion beam assisted deposition
Feb. 12, 1998

M. Dobler
FZ Rossendorf, IIM
Phasenbildung der Eisensilizide während der Ionenstrahlsynthese
Feb. 26, 1998

Dr. S. Howitz
GESIM, Rossendorf
Mikrofluidische Komponenten und Systeme für die Molekularbiologie
April 16, 1998

Dr. G. Schiwietz
HMI Berlin
Quantenmechanische Berechnung des Energieverlustes leichter Ionen in Gasen und Festkörpern
April 23, 1998

Dr. A. Markwitz
FZ Rossendorf, IIM
Cross section TEM-Analyse von Germanium-Nanoclustern in SiO_2-Schichten
April 30, 1998

Dr. J. Lindner
Universität Augsburg
Ionenstrahlsynthese und Ionenstrahlmodifikation von vergrabenen SiC-Schichten
May 7, 1998

Dr. A. Vredenberg
Utrecht University, The Netherlands
Low-temperature nitridation and oxidation of iron
June 11, 1998

Prof. E. Pernicka
TU BA Freiberg
Physikalische Methoden in der Archäologie
June 18, 1998

M. Strobel
FZ Rossendorf, IIM
Computersimulationen zur Evolution von Nanostrukturen bei der Ionenstrahlsynthese
July 7, 1998

Dr. G. Kroesen
Eindhoven University, The Netherlands
Stability and surface chemistry of silicon substrates etched in a high density tool studied by in-situ
spectroscopic IR ellipsometry
July 9, 1998

M. Mäder
FZ Rossendorf, IIM
Spätmittelalterliche Buchmalerei - Pigmente erzählen
Nov. 5, 1998

Prof. A. Benninghoven
Universität Münster
Neue Entwicklungen in der Sekundärionen-Massenspektrometrie (SIMS)
Dec. 17, 1998

Project based on External Funds

The following overview is listed according to the starting dates and informs about the topic, the local project leader and the supporting institution. Additional projects with industrial partners are not included because of confidential agreements.

1.
10/1994 - 12/1998   Bundesministerium für Forschung und Technologie   **BMFT**
Quantitative detection of tritium by means of accelerator mass spectrometry
Dr. Manfred Friedrich; Tel.: (0351) 260-3284; m.friedrich@fz-rossendorf.de

2.
07/1995 - 03/1998   Bundesministerium für Bildung und Forschung   **BMBF**
Ion beam analysis at the Rossendorf accelerators by external groups
Dr. Rainer Grötzschel; Tel.: (0351) 260-3294; r.groetzschel@fz-rossendorf.de

3.
11/1995 - 03/1998   Deutsche Forschungsgemeinschaft   **DFG**
Permeable base transistor with cobalt disilicide gate produced by focused ion beam implantation
Dr. Jochen Teichert;   Tel.: (0351) 260-3445; j.teichert@fz-rossendorf.de

4.
04/1996 - 02/1998   Deutsche Forschungsgemeinschaft   **DFG**
Preparation and characterization of ion implanted oxygen ion conductors
Dr. Edgar Richter; Tel.: (0351) 260-3326; e.richter@fz-rossendorf.de

5.
04/1996 - 10/1998   Sächsisches Staatsministerium für Wissenschaft und Kunst   **SMWK**
Nitriding of stainless steel and aluminium alloys by low energy ion implantation
Dr. Edgar Richter; Tel.: (0351) 260-3326; e.richter@fz-rossendorf.de

6.
04/1996 - 03/1999   Bundesministerium für Bildung und Forschung   **BMBF**
Ion beam based characterization of silicatic materials for non-destructive analytical work on objects of historic glass and enamel
Dr. Christian Neelmeijer; Tel.: (0351) 260-3254; c.neelmeijer@fz-rossendorf.de

7.
08/1996 - 10/1999   Deutsche Forschungsgemeinschaft   **DFG**
Investigation of the corrosion behaviour of magnesium and magnesium alloys by oxygen ion implantation
Dr. Edgar Richter; Tel.: (0351) 260-3326; e.richter@fz-rossendorf.de

8.
09/1996 - 07/1999   Deutsche Forschungsgemeinschaft   **DFG**
Depth selective analysis of the metallurgical phase formation and phase composition in ion implanted iron-silicon surface layers by Mössbauer spectroscopy
Dr. Helfried Reuther; Tel.: (0351) 260-2898; h.reuther@fz-rossendorf.de

9.
01/1997 - 09/1998   Sächsisches Staatsministerium für Wirtschaft und Arbeit   **SMWA**
Diffusion and electrical activation for low temperature budget annealing for submicron silicon doping
Dr. Hans-Ulrich Jäger; Tel.: (0351) 260-3373; h.u.jaeger@fz-rossendorf.de

10.
01/1997 - 12/1998   Bundesministerium für Bildung und Forschung   **BMBF**
Doping of diamond and diamond films by ion implantation for microsystem applications
Dr. Johannes von Borany; Tel.: (0351) 260-3378; j.v.borany@fz-rossendorf.de

11.
01/1997 - 12/1998   Sächsisches Staatsministrium für Wissenschaft und Kunst   **SMWK**
Doped and undoped diamond films
Dr. Viton Heera; Tel.: (0351) 260-3343; v.heera@fz-rossendorf.de

12.
01/1997 - 12/1999   Deutsche Forschungsgemeinschaft (SFB 422)   **DFG**
Nanostructures in ion irradiated interfaces of multilayers prepared by pulsed laser deposition
Prof. Dr. Egbert Wieser; Tel.: (0351) 260-3096; e.wieser@fz-rossendorf.de

13.
03/1997 - 06/1998   Sächsisches Staatsministerium für Wirtschaft und Arbeit   **SMWA**
Physical modeling of diffusion and electrical activation of dopands for silicon doping
Dr. Hans-Ulrich Jäger; Tel.: (0351) 260-3373; h.u.jaeger@fz-rossendorf.de

14.
03/1997 - 02/1999   Deutsche Forschungsgemeinschaft   **DFG**
Plasma immersion ion implantation: experiments and simulation of the sheet layer dynamics
Prof. Dr. Wolfhard Möller; Tel.: (0351) 260-2245; w.moeller@fz-rossendorf.de

15.
03/1997 - 02/2000   Deutsche Forschungsgemeinschaft   **DFG**
Modification of the electrical and optical properties of implanted SiC layers by ion beam
induced epitaxial crystallization, annealing and activation
Dr. Viton Heera; Tel.: (0351) 260-3343; v.heera@fz-rossendorf.de

16.
05/1997 - 04/2001   European Union, within the BRITE-EURAM Project   **EU**
Plasma immersion ion implantation for enhancing high precision machining with tools of
complex geometry
Dr. Reinhard Günzel; Tel.: (0351) 260-2462; r.guenzel@fz-rossendorf.de

17.
07/1997 - 06/2000   Volkswagen-Stiftung   **VWSt.**
Improvement of the high-temperature oxidation behaviour of TiAl-based alloys by ion
implantation
Prof. Dr. Egbert Wieser; Tel.: (0351) 260-3096; e.wieser@fz-rossendorf.de

18.
07/1997 - 12/2000   Sächsisches Staatsministerium für Wissenschaft und Kunst   **SMWK**
Surface analysis of steels and silicon by positron annihilation spectroscopy
Dr. Gerhard Brauer; Tel.: (0351) 260-2117; g.brauer@fz-rossendorf.de

19.
08/1997 - 07/1999   European Union, within the Copernicus Research Program   **EU**
Development of heavy duty reactor windows for industrial scale removal of NO_x and SO_2
from flue gas by electron beam treatment
Prof. Dr. Egbert Wieser; Tel.: (0351) 260-3096; e.wieser@fz-rossendorf.de

20.
09/1997 - 06/2000   Sächsisches Staatsministerium für Wirtschaft und Arbeit   **SMWA**
Hardening of stainless steel using plasma immersion ion implantation
Dr. Edgar Richter; Tel.: (0351) 260-3326; e.richter@fz-rossendorf.de

21.
10/1997 - 10/1999   Deutsche Forschungsgemeinschaft   **DFG**
Deposition of c-BN layers with thickness in the micrometer scale: Diagnostics and modeling
of the film growth processes
Dr. Wolfgang Fukarek; Tel.: (0351) 260-2277; w.fukarek@fz-rossendorf.de

22.
01/1998 - 12/1998   *Deutscher Akademischer Austauschdienst*   **DAAD**
Nb/NbN-layers on Ti produced by plasma immersion ion implantation
Dr. Edgar Richter; Tel.: (0351) 260-3326; e.richter@fz-rossendorf.de

23.
01/1998 - 12/1999   Deutsche Forschungsgemeinschaft   **DFG**
Investigation of defects of the vacancy-type in ion beam treated silicon carbide
 by means of positron annihilation spectroscopy
Dr. Gerhard Brauer; Tel.: (0351) 260-2117; g.brauer@fz-rossendorf.de

24.
01/1998 - 12/1999   Deutscher Akademischer Austauschdienst   **DAAD**
Nucleation, growth and gettering behavior of helium induced cavities in silicon
Dr. Wolfgang Skorupa; Tel.: (0351) 260-3612; w.skorupa@fz-rossendorf.de

25.
01/1998 - 12/1999   Deutscher Akademischer Austauschdienst   **DAAD**
Implementation of a negative helium ion source for the operation at the Rossendorf tandem
accelerator
Dr. Manfred Friedrich; Tel.: (0351) 260-3612; m.friedrich@fz-rossendorf.de

26.
07/1998 - 06/2000   Sächsisches Staatsministerium für Wissenschaft und Kunst   **SMWK**
Physical and technological fundamentals for the engineering of nanoclustersfor nonvolatile
memories
Dr. Johannes von Borany; Tel.: (0351) 260-3378; j.v.borany@fz-rossendorf.de

27.
07/1998 - 12/2000   Sächsisches Staatsministerium für Wissenschaft und Kunst   **SMWK**
Blue electroluminescence from nanoscaled semiconductor structures
Dr. Wolfgang Skorupa; Tel.: (0351) 260-3612; w.skorupa@fz-rossendorf.de

28.
07/1998 - 12/2000   Sächsisches Staatsministerium für Wissenschaft und Kunst   **SMWK**
Surface layers with structures in nanometer scales used for medical implants
Dr. Edgar Richter; Tel.: (0351) 260-3326; e.richter@fz-rossendorf.de

29.
07/1998 - 12/2000   Sächsisches Staatsministerium für Wissenschaft und Kunst   **SMWK**
Preparation of TEM samples by means of focused ion beam milling
Dr. Jochen Teichert; Tel.: (0351) 260-3445; j.teichert@fz-rossendorf.de

30.
07/1998 - 12/2000   Sächsisches Staatsministerium für Wissenschaft und Kunst   **SMWK**
Optimization of Ta barrier layers for copper metallization of microelectronic devices
Prof. Dr. Egbert Wieser; Tel.: (0351) 260-3096; e.wieser@fz-rossendorf.de

31.
10/1998 - 04/2000   European Union, within the LSF Program   **EU**
Center of application of ion beams in materials research
Prof. Dr. Wolfhard Möller; Tel.: (0351) 260-2245; w.moeller@fz-rossendorf.de

32.
10/1998 - 12/2000   Deutsche Forschungsgemeinschaft   **DFG**
Ion-acoustic microscopy using focused ion beams
Dr. Lothar Bischoff; Tel.: (0351) 260-2963; l.bischoff@fz-rossendorf.de

33.
11/1998 - 12/2000   Deutsche Forschungsgemeinschaft   **DFG**
Modeling and computer simulation of amorphous hard carbon film growth by energetic
particle impact
Dr. Hans-Ulrich Jäger; Tel.: (0351) 260-3373; h.u.jaeger@fz-rossendorf.de

34.
11/1997 - 10/2001   European Union, within the TMR Network   **EU**
Synthesis, structure and properties of new carbon based hard materials
Dr. Andreas Kolitsch; Tel.: (0351) 260-3348; a.kolitsch@fz-rossendorf.de

Forschungszentrum Rossendorf

Institute of Ion Beam Physics
and Materials Research (FWI)

Postfach 51 01 19
D-01314 Dresden
Tel.: 0351 260 2245
Fax: 0351 260 3285

| DIRECTOR: Prof. Dr. W. Möller 2245 |
| DEPUTY: Prof. Dr. E. Wieser 3096 |

| NEW MATERIALS (FWIM) |
| Dr. W. Skorupa 3612 |
| Semiconductors |
| Optical Applications |
| Defect Engineering |
| Submicron Ion Beam |

| INDUSTRIAL CONTACTS (FWIK) |
| Dr. J. von Borany 3378 |

| ION IMPLANTATION (FWII) |
| Dr. E. Richter 3326 |
| Surface Properties |
| Ion Beam Assisted Deposition |
| Plasma Immersions Implantation |
| Operation of Implanters |

| MEV ACCELERATORS (FWIB) |
| Dr. M. Friedrich 3284 |
| Operation of MeV Accelerators |
| Accelerator Mass Spectrometry |

| ION BEAM ANALYSIS (FWIA) |
| Dr. R. Grötzschel 2802 |
| High Energy Ion Beam Analysis |
| Elementary Processes of |
| Ion-Surface Interaction |

| STRUCTURAL DIAGNOSTICS |
| Dr. W. Matz 3122 (FWIS) |
| Transmission Electron Microscopy |
| X-ray Diagnostics |
| Electron Spectroscopies |
| Rossendorf Beamline at ESRF |

| THEORY (FWIT) |
| Dr. M. Posselt 3279 |
| Computer Simulation |
| Reaction-Diffusion-Calculations |
| Defects |
| Precipitation |

| PREPARATION (FWIP) |
| Dr. B. Schmidt 2726 |
| PVD Coatings |
| Reactive Ion Etching |
| Wet Chemical Processing |
| Annealing |

Experimental Equipment

1. Accelerators, Ion Implanters and Ion-Assisted-Deposition

❑	van de Graaf accelerator	1,8 MeV	
❑	Tandem accelerator	5 MV	Russian
❑	Tandetron accelerator	3 MV	*HIGH VOLTAGE, NL*
❑	Ion implanter	80 kV	Own construction
❑	Ion implanter	180 kV, medium current	*SCANIBAL, FL*
❑	High current ion implanter	200 kV, high current	*DANFYSIK, DK*
❑	High energy ion implanter	500 kV	*HIGH VOLTAGE, NL*
❑	Plasma-immersion ion implantation	5-60 keV	
❑	Fine focused ion beam	50 keV, 100 nm, 10 A/cm^2	
❑	Ion beam assisted deposition		
❑	Plasma enhanced chemical vapour deposition		

2. Particle and Photon Based Analytical Techniques

❑	RBS	Rutherford backscattering	p,α: 1-6 MeV	
❑	ERDA	Elastic recoil detection analysis	35 MeV, ^{35}Cl	
❑	PIXE	Proton induced X-ray analysis	+ PIGE-option, external beam	
❑		Nuclear microprobe	MeV, > 2 μm	
❑	NRA	Nuclear reaction analysis	^{1}H (^{15}N,αγ) ^{12}C	
❑	TEM	Transmission electron microscope	300 kV	*PHILIPS, NL*
❑	STM	Scanning tunneling microscope	+ AFM-option	*DME, DK*
❑	AES	Auger electron spectroscopy	+ XPS-option	*FISONS, GB*
❑	CEMS	Mössbauer spectroscopy		
❑	XRD	X-ray diffraction		
❑	SE	Spectroscopic ellipsometry	250-1700 nm	*WOOLLAM, USA*
❑	FTIR	Fourier transform infrared spectrometry	600-7000 cm^{-1}	*NICOLET, USA*

3. Other Analytical and Measuring Techniques

❑	Dektak surface profilometer	*VEECO, USA*
❑	Micro indenter	*SHIMATSU, J*
❑	Scratch tester	*SHIMATSU, J*
❑	Spreading resistance measuring station	*SENTECH, D*
❑	Hall-effect equipment	*BIO-RAD, GB*
❑	I-U and C-U- analyzer	*KEITHLEY, USA*

4. Preparation Techniques

❑	Wet chemical etching and cleaning	including anisotropic selective KOH-etching
❑	Photolithographic patterning	5 μm-level
❑	Thermal treatment	Room Temperature - 2000°C Furnace, Flash lamp unit, Rapid thermal annealing, RF-Heating (Vacuum)
❑	Physical deposition	Sputtering DC / RF, Evaporation
❑	Dry etching	Plasma and RIE mode
❑	Bonding techniques	Anodic, Si-Si and Wire Bonding

List of Personnel

Director: Prof. W. Möller   **Deputy Director:** Prof. E. Wieser

Scientific Staff:

Permanent:

Dr. M. Betzl
Dr. L. Bischoff
Dr. J. von Borany
Dr. W. Bürger
Dr. F. Eichhorn
Dr. M. Friedrich
Dr. W. Fukarek
Dr. D. Grambole
Dr. R. Grötzschel
Dr. R. Günzel
Dr. V. Heera
Dr. K.-H. Heinig
Dr. H.-U. Jäger
Dr. A. Kolitsch
Dr. R. Kögler
Dr. U. Kreißig
Dr. W. Matz
Dr. A. Mücklich
Dr. C. Neelmeijer
Dr. D. Panknin
Dr. M.T. Pham
Dr. M. Posselt
Dr. F. Prokert
Dr. H. Reuther
Dr. E. Richter
Dr. B. Schmidt
Dr. J. Schöneich
Dr. H. Seifarth
Dr. W. Skorupa
Dr. J. Teichert
Dr. H. Tyrroff
Dr. M. Voelskow

Post Docs:

Dr. J. Brückner
Dr. T. Chevolleau
Dr. F. Fontaine
Dr. M. Klimenkov
Dr. S. Malhouitre
Dr. A. Markwitz

Projects:

W. Anwand
R. Beutner
Dr. G. Brauer
Dr. U. Brusky
Dr. M. Dobler
Dr. S. Hengst
Dr. O. Kruse
M. Mäder
E.-M. Nicht
Dr. M. Seidel

PhD Students:

K. Albe
F. Berberich
C. Fitz
T. Gebel
T. Hauschild
S. Hausmann
A. Höfgen
U. Hornauer
C. Klein
I. Mrotschek
J. Noetzel
S. Parascandola
A. Peeva
L. Rebohle
Br. Schmidt
M. Strobel
T. Telbizova

Technical Staff:

Permanent:

J. Altmann
R. Aniol
G. Anwand
I. Beatus
T. Betzl
W. Boede
K.-D. Butter

E. Christalle
K. Fukarek
W. Gäßner
B. Gebauer
H.-J. Grahl
P. Hartmann
F. Herrmann
G. Hofmann
M. Iseke
S. Klare
R. Kliemann
L. Kumpf
A. Kunz
G. Küster
D. Maul
M. Mißbach
K. Müller
F. Nötzold
W. Probst
E. Quaritsch
P. Reichel
B. Richter
M. Roch
B. Scheumann
H. Schluttig
E. Schmidt
G. Schnabel
J. Schneider
A. Scholz
C. Schulenberg
K. Thiemig
S. Turuc
A. Vetter
A. Weise
I. Winkler

Projects:

H. Felsmann
G. Grunert
A. Schneider
H. Seifert
G. Winkler